

Syracuse University

SURFACE

Dissertations - ALL

SURFACE

August 2018

Developing a New Mechanical Model for Swarm Development in *Myxococcus xanthus* & Establishing a Genotype-to-Phenotype Correlation Between Swarm Pattern Formation and Gene Homology

Fatmagul Bahar
Syracuse University

Follow this and additional works at: <https://surface.syr.edu/etd>



Part of the [Life Sciences Commons](#)

Recommended Citation

Bahar, Fatmagul, "Developing a New Mechanical Model for Swarm Development in *Myxococcus xanthus* & Establishing a Genotype-to-Phenotype Correlation Between Swarm Pattern Formation and Gene Homology" (2018). *Dissertations - ALL*. 909.

<https://surface.syr.edu/etd/909>

This Dissertation is brought to you for free and open access by the SURFACE at SURFACE. It has been accepted for inclusion in Dissertations - ALL by an authorized administrator of SURFACE. For more information, please contact surface@syr.edu.

Abstract

The primary goal of systems biologists is to understand the mechanics underlying complex, collective, self-organizing behaviors displayed by all living systems, from biofilm formation and wound healing to embryogenesis. *Myxococcus xanthus* is a soil bacterium used as a model organism to study biofilm self-organization. It has a relatively large genome and a complex life cycle that involves two distinct phases. *M. xanthus* cells can move on agar, and a few million cells will organize to form a predatory biofilm or “swarm” that grows and expands if placed on a nutrient-rich agar surface. If placed on a nutrient-poor agar surface, the same swarm will turn inward and contract, aggregating to form spore-filled multicellular fruiting bodies designed to survive periods of starvation. Extensive progress has been made in identifying genes and genetic pathways that regulate fruiting body formation. However, an accurate description of the dynamics that underlie the process of aggregation is still lacking, and there is still debate and disagreement on the subject. This dissertation provides some explanation regarding individual *M. xanthus* cell behavior during fruiting body formation, as well as the behavior of aggregates.

In the first part of this work, we show that the transition from individual cells to the formation of multicellular aggregates can be controlled through relatively small changes in *M. xanthus* cell behavior; complicated cell-to-cell signaling, stigmery (where a trace formed by a cell on an agar surface influences the movement of nearby cells that contact the trace), and cell differentiation are not required for aggregation. We propose that *M. xanthus* aggregation matches a physical phenomenon that has been characterized in non-living systems, called motility induced phase separation (MIPS). By studying non-reversing mutant cells and manipulating their velocities, we show that cell movement can be made to fall within the boundary of the phase region so that cells

succeed in forming aggregates. Alternately, cell movement can be made to fall outside the boundary of the phase region so that cells fail to form aggregates.

After the initial stages of aggregation, an *M. xanthus* swarm actively rearranges the number and relative positions of aggregates by causing some of them to move, merge, or disappear. In the second part of this work, we demonstrate that equations describing Ostwald ripening within a thin liquid film were able to predict aggregate behavior with high accuracy. Consistent with this theory, both relative aggregate size and the distance between aggregates influence the likelihood that a given aggregate will disappear. In general, in neighboring aggregates, the ones that are small and in close proximity will tend to shrink and disappear, while the larger, more isolated aggregates will likely persist and become permanent. By tracking individual cells around aggregates, we show that more cells are leaving shrinking, disappearing aggregates than entering them, while more cells are entering growing, persistent aggregates than leaving them. All of these data are in good agreement with the Ostwald ripening equations. In the last part of this work, we show that aggregation can break down in only a certain number of ways by analyzing single gene disruption of four paralogous gene families representing almost 400 genes. We found that gene families correlate with phenotype, suggesting possible redundancy. In conclusion, my dissertation data provides possible answers to some of the persistent questions regarding *M. xanthus* developmental dynamics.

Key words: *Mycococcus xanthus*, biofilm, self-organization, aggregation, aggregate fate, time lapse microcinematography, Traffic Jam Model, phase separation, Ostwald ripening, paralogous gene families.

**Developing a New Mechanical Model for Swarm Development
in *Myxococcus xanthus***

&

**Establishing a Genotype-to-Phenotype Correlation between Swarm
Pattern Formation and Gene Homology**

By

Fatmagül Bahar

B.S. Karadeniz Technical University, 2008

MPhil. Syracuse University, 2018

DISSERTATION

**Submitted in partial fulfillment of the requirements for the
degree of Doctor of Philosophy in Biology**

Syracuse University

August 2018

Copyright © Fatmagül Bahar, 2018

All Rights Reserved

ACKNOWLEDGMENTS

First, I would like to express my sincere gratitude to my advisor Prof. Roy D. Welch for the continuous support of my doctoral work and related research, for his patience, motivation, and immense knowledge. His guidance helped me in all the time of research of this thesis. His encouragement and advice on both professional and personal level helped me to succeed I could not have imagined having a better advisor and mentor for my Ph.D. study and I am so grateful to be included in his lab. Also, I would like to thank Laura Welch for being such a great feminist role model to me and also editing my documents.

I am extremely grateful for having an exceptional doctoral committee and wish to thank Prof. Anthony Garza, Prof. Dacheng Ren, Prof. Ramesh Raina, and Prof. Sandra Hewett for their support. I extend my thanks to colleagues and friends, Jinyuan Yan, Michael Bradley, John Welsh, Jessica Comstock, Linnea Ritchie for being supportive, helpful and super kind and Phil Pratt-Szeliga for his constant help and assistance over understanding computational analysis. Unforgettable great memories I have shared with you, The Welch Lab.

I further wish to thank to Biology Department at Syracuse University, Kelly Condon, Evelyn Lott (RIP), Lynn Fall, Kathrine Geraghty, Michelle Young, and Sally Hallahan. When I needed help, you were always kind and helpful to me. Many thanks to Dr. Melody Sweet for her beautiful smile and friendly conversations. I also would like to thank Prof. Jannice Friedman for her help on RStudio and statistical analysis and my collaborators in the Marchetti Lab. It has been a great experience working with you Dr. Adam Patch, Prof. M. Cristina Marchetti, and Dr. David Yllanes. Thanks to my collaborators in the Shaevitz Lab at Princeton University. I also would like to thank

Guannan Liu, Prof. Shashi Thutupalli, and Prof. Joshua Shavitz for sharing their knowledge on nematic system and phase separation.

I wish to give my greatest appreciation to my son Ali Musa Bahar and my husband Ali Adem Bahar for supporting me spiritually not only throughout my thesis but also in my life. Then I wish to thank my parents; Ahmet and Havva Altın, who did everything they could to get me to the point where I am right now and my dear brothers; Seyfullah Altın and Feyzullah Altın who were always there to support me and my only and precious sister Betül Altın.

I also want to thank Republic of Turkey Ministry of National Education, the U.S. National Science Foundation (NSF-DBI-1244295, MCB-0746066) and Syracuse University for supporting my study.

TABLE OF CONTENTS

ACKNOWLEDGMENTS	V
TABLE OF CONTENTS	VII
TABLE OF FIGURES.....	XI
Chapter 1: Introduction	1
1.1 Motivation and research questions.....	2
1.2 Motivation for developing a physical model.....	3
1.3 Contributions	4
1.4 Organization	5
1.5 References	6
Chapter 2: Background & Significance.....	7
2.1 Introduction	8
2.2 Self-Organization and pattern formation	9
2.2.1 The brief history of self-organization.....	10
2.2.2 <i>Myxococcus xanthus</i> as a model organism to study self-organization.....	12
2.2.3 Gliding motility of <i>Myxococcus xanthus</i>	18
2.2.4 <i>Myxococcus xanthus</i> Development: Complex social behavior controlled through the genome	21
2.2.4.1 Early development: becoming one.....	22
2.2.4.2 Vertical growth and maturation: stacking and symmetry breaking	25
2.3 Genetics and genomics of <i>Myxococcus xanthus</i> development.....	27
2.3.1 Contact dependent signaling coordinates developmental responses: C-signal	27
2.3.2 The Frz chemosensory system	30
2.3.3 Quorum sensing signal: A-signal	31
2.4 Physical modeling of development.....	32
2.4.1 Early description of aggregation	33
2.4.2 Traffic Jam Model.....	34
2.4.3 Simulations of <i>Myxococcus xanthus</i> development in the era of the Traffic Jam Model.....	35
2.4.4 Era of post-traffic jam model	38

2.5 Genotype to Phenotype: Genetic screens in “Post-Genomic” era	44
2.5.1 G2P in <i>Myxococcus xanthus</i>	48
2.6 Role of paralogous gene families in <i>Myxococcus xanthus</i> development	49
2.6.1 ABC transporters	50
2.6.1.1 Physiological role of biological ABC transporters	51
2.6.1.2 ABC transporters in <i>Myxococcus xanthus</i>	52
2.6.2 Signal transduction system	53
2.6.2.1 Biological function of two component signal transduction	54
2.6.2.2 Two component signal transduction system in <i>Myxococcus xanthus</i>	55
2.6.2.2.1 NTRC-like activators	56
2.6.2.3 One-component signal transduction system	59
2.6.2.4 ECF sigma factors	59
2.6.2.4.1 Biological function of ECF sigma factors	60
2.6.2.4.2 ECF sigma factors in <i>Myxococcus xanthus</i>	61
2.7 Summary	62
2.8 References	64
Chapter 3: A Motility-Induced Phase Transition Drives <i>Myxococcus xanthus</i>	
Aggregation	77
3.1 Abstract	78
3.2 Introduction	78
3.3 Material and methods	83
3.3.1 <i>Myxococcus xanthus</i> culture and development conditions	83
3.3.2 Imaging and tracking	83
3.3.3 Simulation details and parameters	85
3.4 Results	85
3.4.1 Reversing active Brownian particles	85
3.4.2 The dynamical mechanism of aggregation depends on cell density	88
3.4.3 A phase diagram for aggregation	91
3.4.4 Starving <i>Myxococcus xanthus</i> change velocity and reversal frequency to induce aggregation	94
3.5 Discussion	96

3.6 Acknowledgment.....	97
3.7 References	98
Chapter 4: Describing <i>Myxococcus xanthus</i> Aggregation Using Ostwald Ripening Equations for Thin Liquid Film	101
4.1 Abstract.....	102
4.2 Introduction	102
4.3 Material and methods	105
4.3.1 Growth and development culture conditions	105
4.3.2 Time lapse microcinematography and image processing	105
4.3.3 Dynamical model to predict aggregate behavior.....	107
4.4 Results	108
4.4.1 A quantitative comparison between Ostwald ripening and <i>Myxococcus xanthus</i> aggregation	108
4.4.2 Experimental validation of Ostwald ripening as the mechanism underlying aggregate disappearance.....	116
4.4.3 Characterizing phenotypic boundaries for an aggregation-as-Ostwald ripening analogy	118
4.5 Discussion.....	121
4.6 Acknowledgements	122
4.7 References	123
Chapter 5: Establishing A Correlation between Dynamical Changes in Developmental Phenotype and Single Gene Disruptions within Paralogous Gene Families in <i>Myxococcus xanthus</i>.....	125
5.1 Introduction	126
5.2 Material and methods	129
5.3 Results and Discussion	130
5.3.1 Identification of paralogous gene families in <i>Myxococcus xanthus</i>	131
5.3.2 Characterization of <i>Myxococcus xanthus</i> developmental phenotype.....	131
5.3.3 Correlation between gene families and phenotype	135
5.4 References	139

Chapter 6: Conclusions and Future Directions.....	141
6.1 Introduction	142
6.2 A mechanism for early aggregation.....	143
6.3 A model to predict aggregate fate.....	146
6.4 Final conclusion.....	149
6.5 References	150

TABLE OF FIGURES

Figure 2-1. Life Cycle of <i>M. xanthus</i>	14
Figure 2-2. The progression of early aggregation	23
Figure 2-3. Timeline of vertical growth and maturation	25
Figure 2-4. History of mechanical modeling of fruiting body formation in <i>M. xanthus</i>	43
Figure 3-1. Modeling <i>M. xanthus</i> cells as reversing active Brownian particles.....	82
Figure 3-2. Motility of reversing ABPs.....	87
Figure 3-3. Aggregation in <i>M. xanthus</i>	90
Figure 3-4. Phase Diagram of <i>M. xanthus</i> aggregation	93
Figure 3-5. Cell tracking over time after starvation	95
Figure 4-1. <i>M. xanthus</i> aggregation with time-lapse movie.....	109
Figure 4-2. Evolutionary algorithm work flow for <i>M. xanthus</i> development	112
Figure 4-3. Accuracy of the o-simulation of <i>M. xanthus</i> aggregation.....	113
Figure 4-4. Ostwald ripening simulation versus size threshold simulation	115
Figure 4-5. Towards/away comparison of fluorescent cells moving in and around growing and shrinking aggregates	117
Figure 4-6. Representative examples of snakes and scars.....	119
Figure 5-1. Pie chart representing annotation of 9.6 Mb <i>M. xanthus</i> genome	127
Figure 5-2. Distribution of paralogous gene families in <i>M. xanthus</i> genome	132
Figure 5-3. Phenotype categories of <i>M. xanthus</i> development	134
Figure 5-4. Pie chart of phenotype category analysis of 392 <i>M. xanthus</i> mutant strains.....	135
Figure 5-5. Distribution of developmental phenotypes based on paralogous gene families ...	137

Dedicated to my beloved husband and son,

Ali Adem and Ali Musa Bahar

Chapter 1: Introduction

1.1 Motivation and research questions

From microscale to macroscale, many living systems self-organize to form complex collective patterns. Many such patterns in nature arise from the interaction and coordination of individual cells or independent organisms, which may be several orders of magnitude smaller than the overall pattern, e.g., colonies of bacteria or fungi, swarms of insect, or starling murmuration. Another example of collective pattern formation in living systems is the development of biofilms in prokaryotes, which are nearly ubiquitous in nature. In a biofilm, bacterial cells first attach to biotic or abiotic moist surfaces, then build and embed themselves in a matrix of polysaccharides, extracellular DNA (eDNA), and proteins, where they live as a community. It is well established that bacteria in biofilms can become very tolerant to a variety of antimicrobial agents and cause serious issues for human health, such as long-lasting chronic infections in cystic fibrosis patients or instantaneous infection in patients with implants by indwelling on metal surfaces. During the multistep organization of biofilm formation, 1-15% of the bacterial genome shows significant change in gene expression profile compared to vegetative growing bacteria (Sauer, 2003).

The primary mechanisms that enable single cells to self-organize into large-scale multicellular structures is not yet well understood. We therefore chose to examine this phenomenon in *Myxococcus xanthus*, a non-pathogenic soil bacterium that forms two types of biofilm patterns, predatory swarming and developmental aggregation (Keane & Berleman, 2016). A biofilm of *M. xanthus*, which is also called a swarm, will switch between these two patterns in response to changes in nutrient conditions. The cells in an *M. xanthus* swarm under starvation conditions will synchronously gather at different points where they will self-organize into 3-dimensional multicellular aggregates called fruiting bodies. The mechanism called chemotaxis-driven

aggregation which has been found frequently enough in both prokaryotes and eukaryotes that it is often assumed to underlie the self-organization behavior. In the chemotaxis model, a diffusible attractant released from a small group of cells draws more cells into their location for individual cells temporarily sense the environment and redirect themselves toward the chemoattractant. However, these types of chemoattractants have not been observed in *M. xanthus*. Thus, as an alternative to a chemotaxis-driven aggregation model, a contact-dependent signaling model has been proposed to explain developmental aggregation in *M. xanthus*. This “traffic jam” model can simulate aggregate formation *in silico*, but it does not reproduce aggregation dynamics that resemble experimental data. We believe that the traffic jam model fails to reproduce these dynamics because it does not accurately represent aggregative development on a fundamental level. Thus, an entirely new model to explain aggregate formation required. Therefore, we adapted a model for a well-established physical phenomenon, Motility Induced Phase Separation (MIPS), to generate aggregates *in silico*. MIPS is also able to reproduce all experimentally observed aggregation dynamics at both the single cell and swarm scales.

1.2 Motivation for developing a physical model

It is very likely that self-organization in non-living systems, which obeys certain physical rules to establish a pattern, may present a base-line explanation for self-organization in biological systems, which has been already shown to follow many physical rules at the molecular level and the level of individual cells. Undoubtedly, the behavior of *M. xanthus* and swarm self-organization are controlled in part through regulations in gene expressions and complicated protein-protein interactions. Indeed, the core principles of the traffic jam model are based on experimental genetic data that explains the control of cell reversals, switching cell polarity, through cell contact

signaling (Kaiser & Welch, 2004). The problem with this kind of purely genetic model lies within its inherent flexibility: any observation that disagrees with the model can be explained by either tweaking the model's parameters or proposing a new genetic mechanism. It becomes impossible to disprove such a flexible model, but the model itself becomes increasingly improbable as it becomes increasingly complicated. The development of a dynamical data-driven mathematical model as was done herein whose core principles are based on physical phenomenon to simulate self-organization in bacteria provides a mechanism that addresses the global organization of cells, and also enables us to suggest testable genetic and behavioral hypotheses.

1.3 Contributions

1. Identification of requirements for aggregation in *M. xanthus*. Using a data-driven model, it was possible to determine sufficient or necessary requirements for aggregation. Previously introduced models, which include complicated cell-to-cell contact, slime trail, and cell differentiation (Igoshin, Kaiser, & Oster, 2004; Igoshin, Welch, Kaiser, & Oster, 2004a; Sliusarenko, Zusman, & Oster, 2007a; Sozinova, Jiang, Kaiser, & Alber, 2005), did not turn out to be necessary for development within the model. We propose a mechanism that matches with experimental data and drives aggregation via a density-dependent phase separation approach.
2. The development of a mechanism to explain aggregate dynamics. Using Ostwald ripening equations, we propose a mechanism for aggregate disappearance and are able to predict the fate of aggregates with high accuracy. These *in silico* data are supported by individual cell tracking data.

1.4 Organization

- Chapter 2: Background and Significance

This chapter first presents a review of the background of multicellularity and self-organization. It then introduces *M. xanthus* as a model organism to study pattern-formation. It continues with a literature review of fruiting body formation and proposed models for developmental aggregation in *M. xanthus*.

- Chapter 3: A Motility-Induced Phase Transition Drives *Myxococcus xanthus* Aggregation

This chapter introduces a model to uncover the mechanism of how individual cells form multicellular structures.

- Chapter 4: Describing *Myxococcus xanthus* Aggregation using Ostwald Ripening for Thin Liquid Films

This chapter presents a model to understand and predict aggregate fate during *M. xanthus* development.

- Chapter 5: Establishing A Correlation in *Myxococcus xanthus* Between Dynamical Changes in Developmental Phenotype and Single Gene Disruptions within Paralogous Gene Families

This chapter presents phenotypic characterization of large mutant library to address genotype to phenotype problem.

- Chapter 6: Conclusions and Future Directions

In this chapter, I will tie together how the two models mentioned above represent a single coherent picture of how *M. xanthus* fruiting body formation functions, including proposed future directions.

1.5 References

- Igoshin, O. A., Kaiser, D., & Oster, G. (2004). Breaking symmetry in myxobacteria. *Current Biology*, *14*(12), R459–R462.
- Igoshin, O. A., Welch, R., Kaiser, D., & Oster, G. (2004). Waves and aggregation patterns in myxobacteria. *Proceedings of the National Academy of Sciences of the United States of America*, *101*(12), 4256–4261.
- Kaiser, D., & Welch, R. (2004). Dynamics of Fruiting Body Morphogenesis. *Journal of Bacteriology*, *186*(4), 919–927.
- Keane, R., & Berleman, J. (2016). The predatory life cycle of *Myxococcus xanthus*. *Microbiology (United Kingdom)*.
- Sliusarenko, O., Zusman, D. R., & Oster, G. (2007). Aggregation during fruiting body formation in *Myxococcus xanthus* is driven by reducing cell movement. *Journal of Bacteriology*, *189*(2), 611–619.
- Sozinova, O., Jiang, Y., Kaiser, D., & Alber, M. (2005). A three-dimensional model of myxobacterial aggregation by contact-mediated interactions. *Proceedings of the National Academy of Sciences of the United States of America*, *102*(32), 11308–11312.

Chapter 2: Background & Significance

2.1 Introduction

Multicellularity, which we define as differentiated and spatially arranged cells existing as a single functional structure, is considered one of the most significant stages in the evolutionary history of living systems. The study of multicellularity and its manifestations is an essential component of understanding biological complexity, development, homeostasis, and diversity (Arias Del Angel, Escalante, Martínez-Castilla, & Benítez, 2017; Ratcliff, Denison, Borrello, & Travisano, 2012). Many essential components of multicellularity, such as adhesion, communication, motility, and apoptosis, most likely evolved in ancestral unicellular organisms (Grosberg & Strathmann, 2007).

Almost all multicellular organisms were unicellular at the beginning of their lifecycle (Grosberg & Strathmann, 1998). Multicellular organisms can be separated into two groups, based on the fate and function of the constituent cells: in the first group, multicellularity is achieved through aggregation of many metabolically or genetically diverse cells joining as one mass; in the other group, multicellularity is achieved through the clonal division of a single ancestor cell. Clonal multicellularity, once established, is usually permanent, and examples include almost all species of animals, plants, and fungi. Aggregative multicellularity tends to be more transient, with constituent cells alternating between unicellular and multicellular states depending on environmental cues. (Du, Kawabe, Schilde, Chen, & Schaap, 2015) Examples of aggregative multicellularity exist in both eukaryotes and prokaryotes, such as social amoeba and bacteria that form filaments and biofilms (Claessen, Rozen, Kuipers, Sogaard-Andersen, & van Wezel, 2014; Du et al., 2015). Bacterial biofilms represent the minimalist example of studying self-organization and pattern formation and also understanding communication, differentiation, and genetics during transition to multicellularity.

2.2 Self-organization and pattern formation

Many bacterial colonies exhibit different patterns when grown on agar that may change with changing environmental conditions, such as nutrient concentration and substrate density (Shapiro, 1995). Some of these patterns may not require much in the way of genetic instruction; the patterns can be reproduced using simulations and/or experiments with self-propelled rods, agents that move by their own motility system rather than relying on external physical forces, their formation may be the direct result of physical laws (Pipe & Grimson, 1995). This combination of genetic instructions, cellular dynamics, physical laws, and environmental sensitivity means that understanding aggregative multicellularity by microorganisms is much more than just a question of genetics.

Aggregative multicellularity is a form of self-organization, which is a fundamental property of both living and non-living systems. Self-organization occurs when small number of individuals within an initially disordered system interacts locally and gives rise to a more ordered and coordinated system. Examples exist across spatial and temporal scales, from a school of small fish to the organization of the Universe (Parrish, Viscido, & Grünbaum, 2002), flocks of birds (Hemelrijk & Hildenbrandt, 2012), cellular arrangement during embryogenesis (Wennekamp, Mesecke, Nédélec, & Hiiragi, 2013), social behavior of ants and termites (Theraulaz et al., 2002), crystal growth of chemicals (Ducastelle & Quémerais, 1997), neural networks (Hesse & Gross, 2014), aggregation in mussels (Van De Koppel et al., 2008), and the formation of fruiting bodies in organisms like *Dictyostelium discoideum* and *M. xanthus* (Hofer, Sherratt, & Maini, 1995; Pelling et al., 2006).

Self-organization is an emergent property of living systems, meaning that no “blueprint” of the final, more ordered product exists within individuals of the initial disordered population. In the life sciences, the term self-organization is used almost interchangeably with symmetry breaking and pattern formation to describe nonlinear nonequilibrium events involving groups of individuals (i.e., cells, organisms, etc.). (Wennekamp et al., 2013). It was also suggested that self-organization emerges in response to surrounding environment as an adaptive response (Gloag et al., 2013; Levine & Ben-Jacob, 2004).

2.2.1 The brief history of self-organization

Aggregative multicellularity in bacteria is a relatively recent area of investigation. The traditional study of microbiology treated bacterial populations as groups of autonomous agents. However, Costerton observed that bacteria do, in fact, connect to each other with glycocalyx or matrix (Costerton, Geesey & Cheng, 1978). In 1988, Shapiro stated that these populations are complex and communicating multicellular communities (Shapiro, 1988). For example, complex multicellular behaviors in some bacteria, such as *Myxobacteria* or *Proteus* spp. have long been recognized. However, these behaviors have always been considered as exceptions to their predominantly unicellular lifestyle (Claessen et al., 2014).

Bacterial aggregative multicellularity evolved several times with separate lineages (Lyons & Kolter, 2015). Some bacterial multicellular structures appear morphologically similar to those found in eukaryotes, even though they evolved independently (Claessen et al., 2014). Bacteria typically switch from unicellularity to multicellularity by secreting matrix polymers to link cells together as part of a stress response, resulting in a structure that is called a biofilm (Lambert,

Bergman, Zhang, Bortz, & Austin, 2014). Biofilms, represent one form of bacterial aggregative multicellularity that likely evolved as multicellular solutions in bacterial communities as a result of evolutionary survival strategies (Lyons & Kolter, 2015). Intercellular signaling, cell differentiation, and secretion of extrapolsaccharide are the some of the main components of biofilm formation (Gestel, Vlamakis, & Kolter, 2015; Von Bodman, Willey, & Diggle, 2008).

The formation of multicellular filaments, a different kind of aggregative multicellularity exhibited mostly in cyanobacteria, likely predates biofilms, and may have evolved as long as 3 billion years ago (Schirmeister, Antonelli, & Bagheri, 2011). It involves a simpler aggregation within an extracellular matrix, incomplete fission after cell division, and the sharing of periplasm or even cytoplasm. Cyanobacteria, actinomycete, chloroflexi are known examples of filament formation. Biofilms represent a more complex form of aggregative multicellularity; examples of biofilm-forming bacteria include *Bacillus*, *Proteus*, *Caulobacter*, *Pseudomonas*, and *Myxobacteria* (Lyons & Kolter, 2015).

Multicellular structures such as biofilms provide benefits that may improve an organism's survival probability, such as increased resistance to physical and chemical stresses, additional protection from predation, and an increased ability to modify surroundings and establish suitable territory (Lyons & Kolter, 2015). The costs of aggregate multicellularity include less flexibility of movement within the multicellular structure, as well as the additional energy required to produce and respond to signaling molecules, such as cAMP, or adhesive molecules, such as those found within the extracellular matrix (ECM) (Lyons & Kolter, 2015; West, Griffin, Gardner, & Diggle, 2006). This section will provide a brief review of aggregative multicellularity, a topic that has been the subject of several recent reviews (Claessen et al., 2014 and Du et al., 2015).

2.2.2 *Myxococcus xanthus* as a model organism to study self-organization

M. xanthus, which belongs to the delta branch of the phylum Proteobacteria, is a rod-shaped Gram negative bacterium that is ubiquitous in soil, as well as variety of different environments such as tree bark, animal dung, and both fresh and salt water sources. (Reichenbach, 1999). This non-pathogenic bacterium does not possess flagella and is incapable of swimming. They will grow in agitating rich liquid media, however, because the constant shaking enables the cells to stay mobile and exposed to new media where they grow and divide until all the nutrients are consumed. Otherwise, they are non-motile in liquid and tend to form a biofilm that is organized into a series of layers immediately (Kunert & Kaiser, 1982).

M. xanthus cells are not autonomous agents; they function exclusively as part of a single-species biofilm called a swarm. *M. xanthus* swarms would can be considered more self-organized than systems of autonomous agents that form patterns, such as a school of herring or a murmuration of starlings. Indeed, *M. xanthus* was one of the first model organisms exploited to study the genetics of aggregative multicellularity, and it remains one of the best characterized biofilms (Dworkin, 1996; Velicer & Vos, 2009; Zhang, Ducret, Shaeviz, & Mignot, 2012).

During their life cycle, *M. xanthus* cells within a swarm display coordinated eukaryote-like behavior (Kaiser, 2004; Zusman, Scott, Yang, & Kirby, 2007). For example, each *M. xanthus* cell moves by gliding motility, initially defined as the translocation of a cell without a propulsive outer membrane organelle, which allows a swarm to grow and expand in size on solid surfaces. Swarm expansion is induced by extracellular polymeric substance (EPS), which inhibits the reversal frequency of cells when in high local concentrations and partly enables swarm expansion (Zhou & Nan, 2017). When nutrients are limited, the cells within the swarm coordinate changes in their

movement utilizing the two systems that make up gliding motility, called ‘A’ (Adventure) and ‘S’ (Social), to transition from an outward expansion to an inward contraction. This is the first step in the execution of a synchronized multicellular developmental program (Mauriello & Zusman, 2007). Over the next 12 - 24 h, starving *M. xanthus* cells move to form mushroom-shaped aggregates that mature into fruiting bodies (Fig. 2-1); a swarm of a few million can form dozens of fruiting bodies, each of which is ~ 0.1 mm in diameter, 0.1 - 0.2 mm in height, and contains approximately $\sim 1 \times 10^5$ *M. xanthus* cells (Shimkets & Seale, 1975).

This entire process of development, from the initiation of starvation to the formation of spore-filled fruiting bodies, can take place in as little as 48 h (Curtis, Taylor, Welch, & Shimkets, 2007). It starts with the production of guanosine nucleotide in response to starvation induced ribosomal arrest (Manoil & Kaiser, 1980a), and follows through a cascade of changes in gene expression that coordinates the spatial and temporal dynamics (Kaiser & Welch, 2004). Cell division is arrested, changes in reversal frequency are synchronized, and cell fate is determined by location within the swarm: approximately 10% of the cells in the center of each fruiting body differentiate into metabolically inactive and environmentally resistant myxospores (O’Connor & Zusman, 1991); 30% of cells on the outside of any fruiting body differentiate into non-motile but metabolically active cells called peripheral rods (Fig. 2-1) (O’Connor & Zusman, 1991a; O’Connor & Zusman, 1991); and remainder undergo lysis by programmed cell death that has been attributed to a form of evolutionary altruism to increase the survival of other individuals (Wireman & Dworkin, 1977).

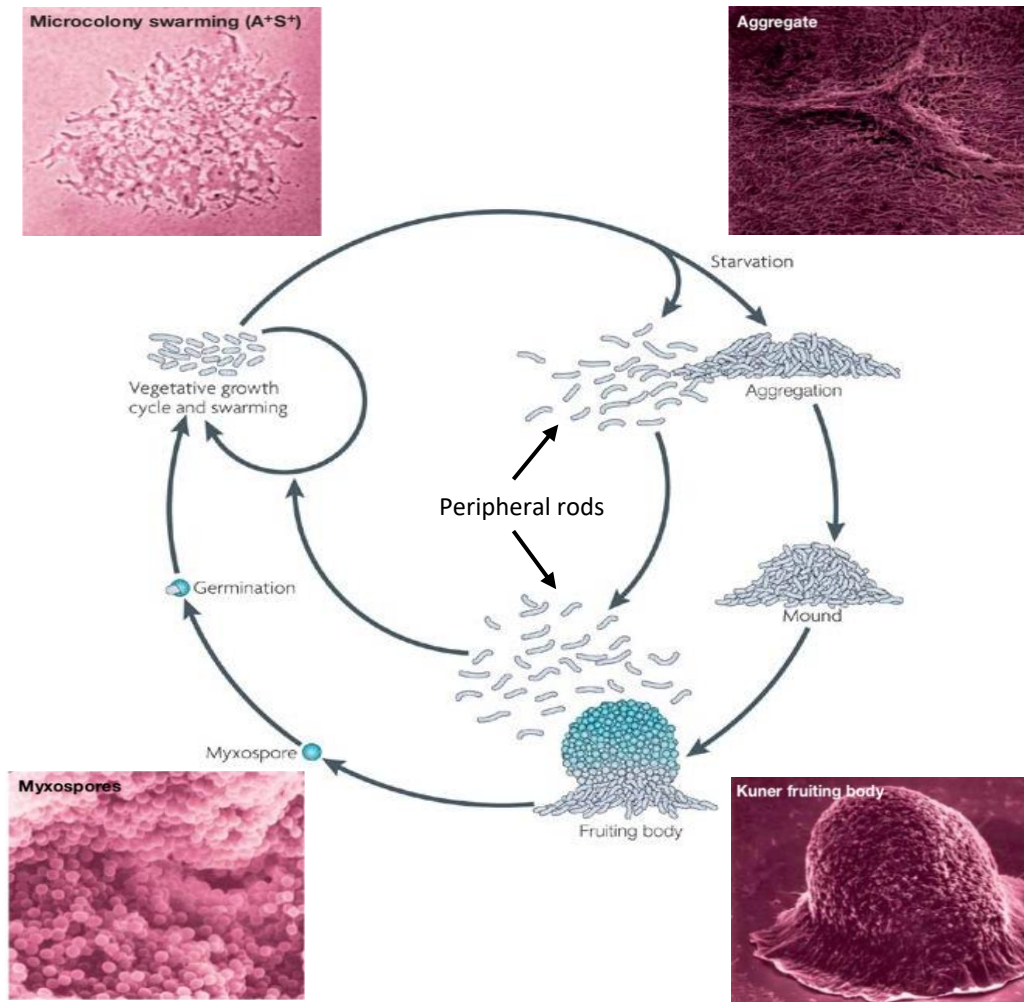


Figure 2-1. Life Cycle of *M. xanthus*. When nutrients are abundant, cells grow, divide, and expand their colony size. Under starvation conditions however, cells undergo multiple steps of highly regulated morphological change. First, after 2h of starvation, cells sense the nutrient limitation and respond by changing their behavior and coordinating their movement. In approximately 6 - 7 h, hundreds of cells form aggregation points which some of them eventually mature into fruiting bodies filled with heat-resistance myxospores. Some of the cells do not join aggregation process and swarm between fruiting bodies, which are called peripheral rods. As conditions become favorable again, cells germinate, grow, and divide (adapted and modified from Kaiser, 2003; Zusman et al., 2007)

The process of forming spores (sporulation) is also under tight genetic control and can be induced through starvation or chemical shock with glycerol. A total of 1486 genes were found to be significantly upregulated during chemically-induced sporulation, representing nearly 20% of the total genes in the *M. xanthus* genome (Müller, Treuner-Lange, Heider, Huntley, & Higgs, 2010). Sporulation requires (i) remodeling of cell envelope (Müller, Schink, Hoiczky, Cserti, & Higgs, 2012), (ii) formation of two-chromosome DNA complement (Tzeng & Singer, 2005), and (iii) synthesis of lipid composition such as 1-O-alkylglycerol, monoacylglycerol and diacylglycerol (Muñoz-Dorado, Marcos-Torres, García-Bravo, Moraleda-Muñoz & Pérez, 2016a; Ring et al., 2006).

The genetic control of peripheral rod formation is comparatively unknown, but it has been speculated that their purpose is to stay active to search for new food sources (O'Connor & Zusman, 1991). During development, cells secrete ECM as a cellular cohesion. It is composed of small amounts of lipids and extracellular DNA, protein, and EPS which contains at least five monosaccharides; galactose, glucosamine, glucose, rhamnose, and xylose (Kearns, Bonner, Smith, & Shimkets, 2002; Behmlander & Dworkin, 1994). EPS has long been thought to play role in S-motility by triggering the retraction of *M. xanthus* type 4 pili (T4P) (Li et al., 2003), and a more recent study argues that EPS may also be essential for *M. xanthus* cells to forage by A-motility (Zhou & Nan, 2017). Several studies have demonstrated that the Dif chemosensory system is involved in production and regulation of ECM (Yang, Geng, Xu, Kaplan, & Shi, 1998), as well as several genes involved in the coordination of development. For example, a strain of *M. xanthus* with a deletion mutation covering the gene *nla24*, one of the NtrC-like activators that coordinate gene expression during development, exhibits a decrease of exopolysaccharides in ECM and no change in levels of FibA, a protein involved in the production of fibrils that function in cell

movement through ECM. Deletion of genes for NtrC-like activators do not always downregulate exopolysaccharides; a *nla19* deletion mutant strain actually exhibits an increased accumulation of exopolysaccharides in ECM content (Caberoy, Welch, Jakobsen, Slater, & Garza, 2003; Lancero et al., 2004).

Carbon (such as pyruvate), nitrogen, phosphate, and amino acid limitation triggers aggregation and development, but purine and pyrimidine starvation do not induce developmental response (Dworkin, 1963). It was shown that limitation of these nutrients induces a stringent response (Manoil & Kaiser, 1980b) which causes accumulation of (p)ppGpp like in most other gram-negative bacteria (Singer & Kaiser, 1995). Elevation of (p)ppGpp is both necessary and sufficient for the initiation of early developmental gene expression and thus fruiting body formation (Shimkets, 1999). For example, mutant strains with a deletion of *relA*, which encodes for a ribosome-dependent (p)ppGpp synthetase, fail to aggregate and sporulate (Diodati et al., 2006; Manoil & Kaiser, 1980b). When nutrients become available, myxospores germinate and join the vegetative growth cycle again, but the signals and underlying genetics controlling germination are not as well understood. The study done in the Velicer lab showed that the laboratory strain of *M. xanthus* can lose its ability to aggregate if it is subjected to vegetative growth for 1000 generations. Yet it recovers development after four alternating starvation and growth cycles, which indicates that the *M. xanthus* genome can readily evolve to reacquire the ability to self-organize (Velicer et al., 2006).

M. xanthus is a predatory bacterium that must compete with other living systems in the soil. Indeed, 8% of its genome encodes for secondary metabolites, many of which are involved in killing or disabling competitive microbes (Meiser, Bode, & Müller, 2006). There are 18 gene clusters

responsible for production of nonribosomal peptide synthetase and polyketide antibiotics such as myxovirescins (macrocyclic), myxalamides (polene), myxochelins (siderophores), myxochromides (cyclic oligopeptides with an unsaturated polyketide chain), and DKXanthenes (DKX- gives the yellowish color to swarms, and is also essential for sporulation) (Konovalova, Petters, & Sogaard-Andersen, 2010; Meiser et al., 2006).

M. xanthus prey on other eukaryotic and prokaryotic microorganism as a group by secreting antibiotics and digestive enzymes. Because an individual cell is unable to produce sufficient quantities of these secondary metabolites to kill prey effectively, it requires a large population (Rosenberg, Keller, & Dworkin, 1977). This is colloquially referred to as the “wolf-pack” phenomenon (Berleman & Kirby, 2009). Predation initiates after contact with prey cells. Ordinarily, predation experiments are done in the laboratory on agar, when a small swarm of *M. xanthus* is spotted near a colony of prey bacteria and allowed to expand, but researchers have also investigated the role of *M. xanthus* within the natural microbial food web by labelling *E. coli* with ¹³C and putting it back on topsoil. *M. xanthus* was found to be a major group that fed on the labelled *E. coli* (Lueders, Kindler, Miltner, Friedrich, & Kaestner, 2006), demonstrating the significant predatory role *M. xanthus* plays within the soil microbial food web.

Fruiting body development and predatory swarming are the two best characterized examples of aggregative multicellularity in *M. xanthus*. Both development and swarming require a set of complicated self-organizing behaviors that can sometimes be observed as patterns within the swarm. One of these patterns is called rippling, which can appear across a swarm during both development and predation, and superficially resembles ripples on the surface of water (Berleman, Chumley, Cheung, & Kirby, 2006). The mechanism underlying the traveling bands observed

during rippling is fundamentally different from the spiral and concentric bands formed by *D. discoideum*, which are closer to those observed in Belousov-Zhabotinsky chemical wave systems (Siegert & Weijer, 1995; Zhang et al., 2012; Siegert & Weijer, 1995; H. Zhang et al., 2012). This difference can be observed at both the single-cell and population scale; *D. discoideum* wave fronts are annihilated when they collide, but *M. xanthus* ripples reflect off one another, and appear as though they are passing through each other (Igoshin, Welch, Kaiser, & Oster, 2004a).

Rippling may be observed before aggregation or between aggregates during development, as well as during predation when *M. xanthus* cells are on top of prey bacteria. Its role in both processes is not well understood, but it has been suggested that rippling occurs during predation to maximize the efficiency of nutrient acquisition (Berleman et al., 2006).

2.2.3 Gliding motility of *Myxococcus xanthus*

M. xanthus cells move 2 - 4 μm per minute on a 1% agar surface, which is slow when compared to many other bacteria. For example, *Candidatus ovabacter* with ~400 flagella swims at the rate of ~1 mm per second (Fenchel & Thar, 2004), *E. coli* with ~8 flagella swims at the rate of ~30 μm per second (Swiecicki, Sliusarenko, & Weibel, 2013), and *Flavobacterium johnsoniae* glides at up to 10 μm per second (Braun, Khubbar, Saffarini, & McBride, 2005).

Motility: *M. xanthus* utilizes two distinct motility systems to move on a solid surface, as mentioned above. These two systems are A (Adventurous) and S (Social).

A-Motility: A-motility was named to indicate independent cell movement. A-motility can operate within single cells, as well as in large groups of cells (Hodgkin & Kaiser, 1979a, 1979b). There

have been many hypotheses suggested for how A-motility generates force, but two incompatible models currently exist: the slime gun model and the focal adhesion complex model (Sliusarenko, Zusman, & Oster, 2007c). Although neither has been proven, at present the focal adhesion complex model is generally considered to be more plausible and better supported by experimental evidence.

The slime gun model is built on the observation that *M. xanthus* cells leave a trail of “slime” behind them. The descriptive term “slime” was first used because of its appearance; its composition was analyzed, and it has been identified as absorbent mucopolysaccharide. It was then shown that slime was secreted at either end of *M. xanthus* cells from nozzle-like organelles. The slime gun motility model is based on the idea that, upon secretion from the lagging end an *M. xanthus* cell, the slime absorbed water from the agar substrate and expanded, thereby pushing the cell forward from the leading end (Wolgemuth, Hoiczky, Kaiser, & Oster, 2002). At present, there is no evidence to indicate that slime absorption would provide sufficient mechanical force to move a cell forward.

The focal adhesion model requires the A-filament-forming coiled-coil protein, AglZ (Yang et al., 2004). Mignot et al., showed that AglZ is localized along the cell body and when cells move, it “remains at fixed positions relative to the substratum.” The A-motility system works best on dry and hard surface with 1.0 – 2.0 % agar (Shi & Zusman, 1993). It was found that AglZ interacts with mutual gliding A (MglA), the only protein known to be required for both motility systems, and the chemotaxis-like protein FrzCD. It was suggested that AglZ negatively regulates gliding motility through the Frz pathway that controls the rate of cell reversals (Mauriello, Nan, & Zusman, 2009; Nan et al., 2011; Yang et al., 2004). Compared to Wild-Type *M. xanthus*, any cells carrying the mutant version of one of the A-motility genes *agl*, *cgl*, or *agm* are unable to glide as individual cells and shows reduced spreading speed. Therefore, the function of all these genes are required

for gliding in A-motility (Spormann, 1999). Despite all these above-mentioned studies, the complete mechanism of A-motility still remains elusive.

S-motility: S-motility is better understood than A-motility; it is a type of motility that requires groups of cells. To function, S-motility requires that cells within the group be no more than one cell length apart (Hodgkin & Kaiser, 1979a, 1979b). S-motility uses T4P, which are molecular machines localized at the leading pole of the cell that function as a type of winch (Hong Sun, Zusman, & Shi, 2000; Wu & Kaiser, 1995). It is very similar to twitching motility, a crawling movement, first described in *Pseudomonas aeruginosa*. The role of T4P in S-motility force generation can be explained in three steps: (i) extension of T4P from the leading cell pole, (ii) attachment to a surface, and (iii) retraction (Konovalova et al., 2010). Extraction and retraction of pili create enough force to pull a cell forward. It has been shown that EPS and lipopolysaccharide O-antigen are required for S motility as triggers for the retraction of pili (Arnold & Shimkets, 1988; Bowden & Kaplan, 1998). S-motility works best on moist and soft surfaces of between 0.3 and 0.5% agar (Shi & Zusman, 1993). Cells with a deletion mutation in a social motility gene, *pil*, *sgl*, *tgl* or *eps*, show reduced swarm expansion with a mounded core compare to Wild-Type colony (Arnold & Shimkets, 1988).

One of the major subunits of T4P is PilA which is localized at the leading pole of cells. PilA is secreted through PilQ channel which requires lipoprotein Tgl for its assembly, while PilC, PilB, and PilT, which have ATPase activity, are involved in extraction/retraction of pili (Jakovljevic, Leonardy, Hoppert, & Sogaard-Andersen, 2008; Mauriello & Zusman, 2007). It was also reported that *dif* mutants are defective in ECM fibril biogenesis which is crucial for the attachment of T4P for S motility (Yang et al., 2000).

Control and regulation of these motility systems are largely independent of each other (Hodgkin & Kaiser, 1979a, 1979b) and their activities appear to be coordinated so that they generate force in the same direction (Kaiser & Crosby, 1983). Evolving two functionally different motility systems may also enable *M. xanthus* cells to move on a greater variety of surfaces (Shi & Zusman, 1993). Both systems appear to be almost entirely genetically separate with *nla24* and *mglA* being the only genes thus far found to be required for both motility systems (Lancero et al, 2004; Zusman et al., 2007). Individual *M. xanthus* cells lacking both A- and S-motility (A-S-) do not move at all on agar, and A-S- swarms expand at less than one-eighth of the rate of an A+S+ colony. A-S- swarm expansion is not due to cell movement, as it is in A+S+ swarms, rather it is due simply to cell growth and division, where new and larger cells push out the boundary of the swarm (Kaiser & Crosby, 1983). The rate of Wild-Type swarm expansion on 1% agar is 1.6 $\mu\text{m}/\text{min}$; when compared to mutant strains lacking either A-motility or S-motility (0.6 and 0.4 $\mu\text{m}/\text{min}$, respectively), the combined expansion rate of A- and S-motility is 1.5X greater than the sum of their independent expansion rates (Kaiser & Crosby, 1983). This result has been interpreted to mean that A-motility and S-motility systems work cooperatively to move cells forward and swarms outward (Shi & Zusman, 1993).

2.2.4 *Myxococcus xanthus* development: Complex social behavior controlled through the genome

M. xanthus development displays discrete stages that are spatially and temporally separated through a regulated pattern of gene expression. Expression studies indicate that development involves the regulation of more than 2000 genes, which corresponds to approximately 30% of *M. xanthus* genome (Giglio, Caberoy, Suen, Kaiser, & Garza, 2011; Müller, Treuner-Lange, Heider,

Huntley & Higgs, 2010). I will summarize how these changes in expression direct cell behavior and self-organization during development.

2.2.4.1 Early development: becoming one

Early development can be described as events happening from the time cells are spotted on starvation agar to the time when cells build aggregates, which covers approximately the first 6 h of fruiting body formation (Fig. 2-2). In order for early development to occur, individual cells must recognize that they are starving, which is controlled through the intercellular accumulation of (p)ppGpp and recognize that they are in a population of starving cells that is large enough to form fruiting bodies, which is achieved through quorum sensing. This recognition should ultimately initiate development that leads to the coordinated movement of cells and the start of aggregation (Garza et al., 1998).

Within a developing swarm, cells organize themselves into long continuous streams, and it has been repeatedly suggested that streams (Fig. 2-2) drive the initiation of aggregates. The first evidence to support this hypothesis came from Scanning electron microscopy (SEM) images of developing swarms on agar (Shimkets & Seale, 1975). The swarm cells were described as oriented uniformly with respect to one another and streaming with their longitudinal axis towards to aggregate center. Later, SEM images were taken at different stages of fruiting body formation that were developed on submerged culture, which is designed to induce aggregation on a glass surface under a layer of liquid to eliminate artifacts coming from agar surface (Kuner & Kaiser, 1982).

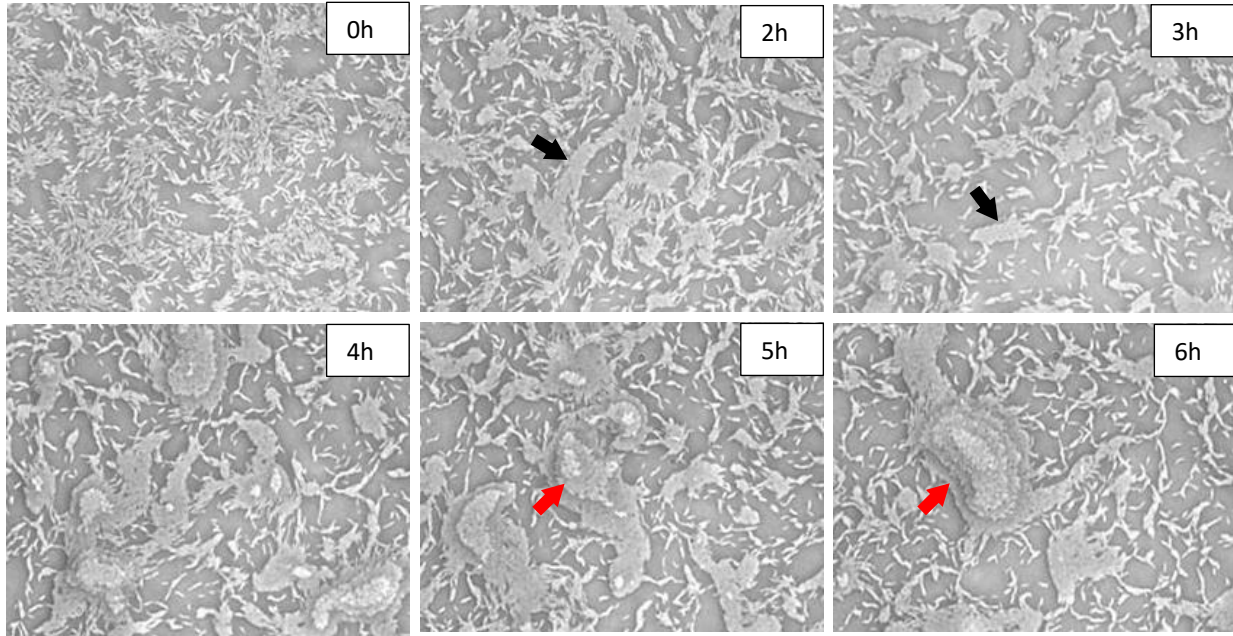


Figure 2-2. The progression of early aggregation. Six microcinematography images selected from a time-lapse image stack. Elapsed time is indicated in the upper right corner of each frame (0, 2, 3, 4, 5 and 6 h). Images were taken by phase contrast microscopy under 200X total magnification. Black arrows show streaming cells (2 h and 3 h timepoints) and red arrows represent initiation of aggregation (at 5 h and 6 h)

Once again, the images showed streaming of *M. xanthus* cells gathering from 3 different angles pointed towards to aggregation center (Shimkets & Seale, 1975).

Thutupalli et al. (Thutupalli, Sun, Bunyak, Palaniappan, & Shaevitz, 2015) proposed that changes in cell movement during *M. xanthus* development are akin to changes in the movement of molecules during a phase transition from an isotropic gas-like phase (initial starving cells) to a nematic-liquid-phase (streaming cells) to viscoelastic-solid-like phase (aggregates and fruiting bodies). Automated individual cell tracking during first four hours of starvation revealed dynamics

of early aggregation cell behavior. Images taken every 10 s gave very precise motility measurements, since *M. xanthus* cells move approximately 1.5 μm in 10 s. Randomly oriented cells glide over agar surface for the first one-hour to search for food and find neighboring cells to initiate aggregation, which is called the “exploratory phase.” Collisions and slime trails force cells into local alignment, which orients them in the same net direction. After about an hour, these locally aligned cells transiently join together in streams by joining other aligned cell groups during what is called the “streaming phase”. Tracking of the non-reversing ΔfrzE cells showed that cells stay in exploratory phase during the tracking period without forming streams. Therefore, they conclude that reversal is required for streaming (Thutupalli et al., 2015).

Wild-Type *M. xanthus* cells show a greater tendency to join streaming cells than remain at the swarm edge, and streams form in areas where the highest number cells had moved across. In contrast, a non-reversing mutant glided over the surface without showing favorability toward streams. The ordered nematic-liquid-like phase, where rod-shaped organic molecules self-align in a direction along their long axis (Marchetti et al., 2013), kept streams together once they had formed (Thutupalli et al., 2015). O’Connor suggested that large spiral patterns of cells drive the aggregate centers based on their interpretation of SEM data (O’Connor & Zusman, 1989). These spiral monolayers of cells are tightly coherent. Several hours of spinning leads to the terrace formation which eventually give rise to mounds. They further suggested that these spiral movement happens not only at the level of agar surface, but also at the z-axis which is perpendicular to the substratum within the mound which eventually becomes fruiting body (O’Connor & Zusman, 1989).

2.2.4.2 Vertical growth and maturation: stacking and symmetry breaking

In the period between 6 and 24 h, developing *M. xanthus* aggregates ‘mature’ (Fig. 2-3). They become taller and denser, and their outer surface becomes more stable and defined as they transition into spore-filled fruiting bodies. Maturation begins when aggregates start appearing, and ends when spore-filled fruiting bodies are completed (Curtis et al., 2007; Konovalova et al., 2010).

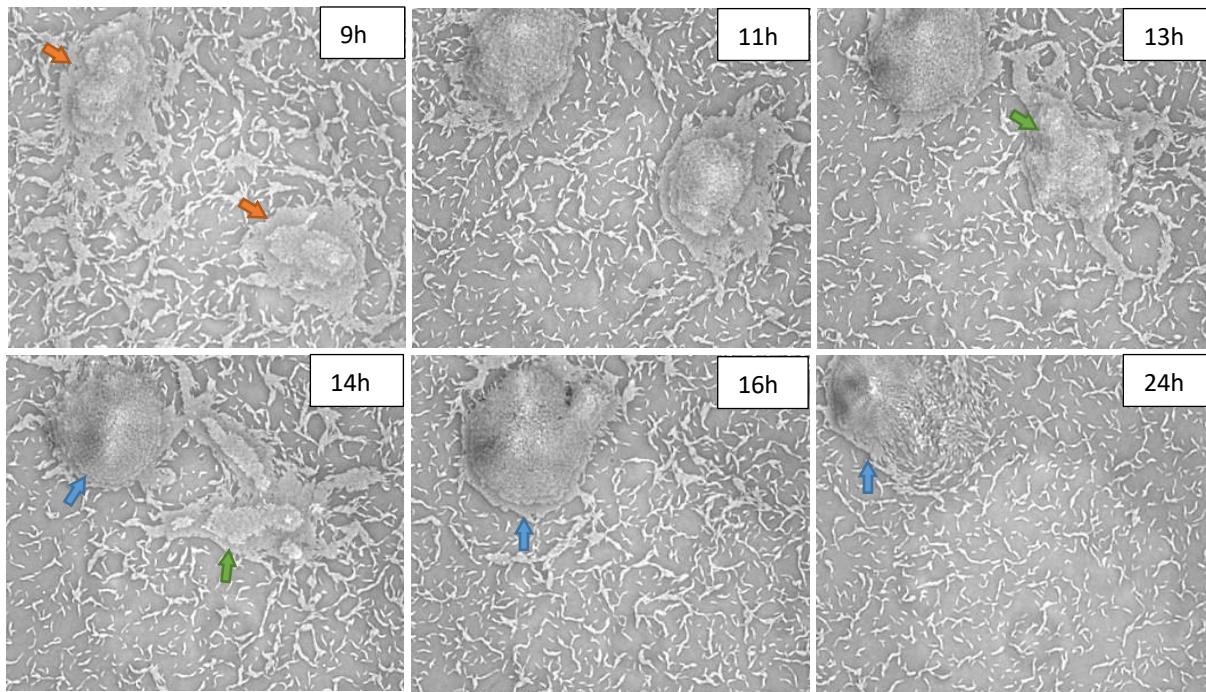


Figure 2-3. Timeline of vertical growth and maturation. Six microcinematography images selected from a time-lapse image stack that shows the progression of fruiting body formation. Elapsed time is indicated in the upper right corner of each frame (9, 11, 13, 14, 16 and 24 h). Images were taken by phase contrast microscopy under 200X total magnification. Orange arrows (at 9 h) indicate tier formation on growing aggregates. Green arrow (at 13 and 14 h) represents moving and disappearing aggregate and blue arrows (at 14, 16 and 24 h) show growing and maturing aggregate into fruiting body

Aggregates have been described as pyramids composed of concentric layers as illustrated in Fig. 2-3 at the 9 h timepoint (Shimkets & Seale, 1975), and Curtis et al. suggested a conceptual model to explain how these tiered layers form (Curtis et al., 2007). After approximately 6 h of starvation, developing swarm cells appear to move faster in streams. Two or three streams coming from opposing directions will sometimes intersect, and the collision will cause one of the streams to elevate vertically on the top of the other streaming cells. Further collisions will lead cells to stream along this vertical plane and then realign horizontally over the streaming cells below them. This creates first tier. The surface of the first (bottom) tier will increase as more streaming cells are pushed upward to join it. Other tiers form as more streaming cells climb on top of the previous tiers. Up to 9 tiers were observed before the process slowed and the ECM covered the maturing fruiting body (Curtis et al., 2007). It was also suggested that cells can move from one layer to another (Shi, Ngok, & Zusman, 1996a). Aggregates first appear elongated but become increasingly circular after approximately 12 h. The cells within an aggregate do not always remain in that aggregate, and all aggregates do not share the same fate. Some aggregates appear to steadily grow in size until they mature, some grow for a period and then shrink and disappear (Fig. 2-3), and some move and merge with other nearby aggregates. Very rarely, an early elongated aggregate will split into 2 or 3 aggregates that mature separately into fruiting bodies (Xie, Zhang, Shimkets, & Igoshin, 2011; Zhang et al., 2011). As each stable aggregate grows in size and matures, a thin skirt around the base becomes visible after approximately 60 h (Kuner & Kaiser, 1982).

The start of sporulation correlates with the time when aggregates round up, and stop moving, merging and disappearing (O'Connor & Zusman, 1989). The spatial arrangement of cell density and movement within and around the nascent fruiting body is demonstrably variable. Whereas cells in the inner domain of a fruiting body form less organized and denser areas with no cell

movement, which indicates the transition to spores, the cells in the outer domain of the fruiting body form more ordered and less dense areas, with concentric clockwise and counterclockwise movement (Kaiser & Welch, 2004; Sager & Kaiser, 1993). Further, it was shown that spores are first formed at the outer domain of fruiting bodies and then pushed inward by neighboring motile cells. As more cells differentiate into spores, more cells will be pushed into the inner domain, so that the oldest spores will fill the inner domain, and the newest spores will surround them as the outer domain (Sager & Kaiser, 1993). Confocal laser scanning microscopy images revealed that spore formation begins at the top layer, and then moves to the lower layers (Lux, Li, Lu, & Shi, 2004). Infra-red optical coherence tomography images showed that, rather than a homogenous inner spore domain, fruiting bodies are not uniform, but consist of distributed high spore concentration regions and low spore concentration regions (Harvey et al., 2012).

2.3 Genetics and genomics of *Myxococcus xanthus* development

The expression of many genes is highly regulated during the *M. xanthus* life cycle. In this section we will focus on the genes that have been characterized with respect to *M. xanthus* development.

2.3.1 Contact dependent signaling coordinates developmental responses: C-signal

One of the most extensively studied signaling proteins in *M. xanthus* is C-signal, 17-kDa (p17), a cell surface associated protein encoded by *csgA* (Kim & Kaiser, 1990a, 1990b). The *CsgA* gene codes for a 25kDa (p25) protein, which has homology to a short-chain alcohol dehydrogenase (SCAD) (Kruse, Lobedanz, Berthelsen, & Søgaard-Andersen, 2001; Lee, Lee, Mendez, & Shimkets, 1995). *CsgA* protein has two conserved sequence motifs: an N-terminal coenzyme binding motif and C-terminal active site motif which are also found of SCADs (Persson, Krook,

& Jörnvall, 1991). PopC protein with protease activity is required for cleavage of p25 to generate the precursor of the C-signal, p17 (Lobedanz & Søgaaard-Andersen, 2003; Rolbetzki, Ammon, Jakovljevic, Konovalova, & Søgaaard-Andersen, 2008). It is still unclear if p25 has SCAD activity, or only functions as a precursor for p17. p25 is detected in vegetative cells, and it is only cleaved to generate p17 during starvation (Konovalova et al., 2010; Kruse et al., 2001). Studies show that development can be rescued by exogenous p17. It has been suggested that non-diffusible C-signal transmission requires cell-to-cell contact between p17 and a p17-receptor on a neighboring cell. However, no such a receptor has been identified yet (Konovalova et al., 2010).

The DNA binding response regulator FruA, which has an N-terminal receiver domain and a C-terminal DNA binding domain, is in the center of C-signal transduction pathway (Ellehaug, Norregaard, & Søgaaard-Andersen, 1998). Transcription and accumulation of FruA depends on A- and E- signals, intercellular signal that is expressed during development, but is independent of C-signal. It was found that C-signal regulates FruA activity at the post-translational level by triggering phosphorylation. Phosphorylation of FruA leads to its interaction with downstream targets, which initiates two signal transduction pathways (Dale Kaiser, 2004). In the Frz pathway, the activation or suppression of *frzE* through the methylation of FrzCD results in rippling or aggregation, respectively. The second pathway covers the *devRS* locus related to sporulation (Ellehaug et al., 1998), and can explain why some mutant strains only aggregate or sporulate (Morrison & Zusman, 1979). Mutant strains with deletions of *fruA*, whose protein expression is first detected at 6 h (Ellehaug et al., 1998), results in an abnormal aggregation phenotype and fails to mature into fruiting bodies or sporulate (Ellehaug et al., 1998; Horiuchi, Taoka, Isobe, Komano, & Inouye, 2002). MrpC protein induces *fruA* transcription by directly binding to its

promoter (Ueki & Inouye, 2003). MrpC, which shows sequence similarity to cyclic AMP receptor protein in *E. coli*, is essential for aggregation and sporulation (Sun & Shi, 2001).

The regulation of the *dev* operon in response to extracellular C signaling is important, although exactly how this operon affects aggregate formation is not completely understood (Campbell et al., 2015). The operon includes eight genes, and three of them (*devTRS*) are known to be involved in the development process with negative auto-regulated expression. Mutant strains with deletions of *devTRS* are able to aggregate, but fail to sporulate (Boysen, Ellehaug, Julien, & Sjøgaard-Andersen, 2002; Thony-Meyer & Kaiser, 1993; Viswanathan, Murphy, Julien, Garza, & Kroos, 2007).

The special significance of cell-to-cell contact was first suggested when researchers observed that A⁻S⁻ motility deficient cells were arrested mid-aggregation, which is similar to a *csgA* mutant strain (Kaiser, 2004; Kroos, Hartzell, Stephens, & Kaiser, 1988). To test if C-signaling occurs only between aligned cells, Kim & Kaiser designed an experiment in which non-swarming cells were mechanically forced to align end-to-end (Kim & Kaiser, 1990). They used a fine-grained aluminum oxide sandpaper to produce narrow grooves in agar which were in the range of 5 to 10 μm in diameter. Microscopic images showed that *M. xanthus* cells within the grooves were oriented with their long axis parallel to the axis of the groove, expressed C-signal, and sporulated if they are incubated for a long enough period. Non-aligned cells outside the grooves failed to express C-signal and to sporulate, (Kim&Kaiser, 1990; Kaiser, 2004), thus it was suggested that C-signal is necessary for sporulation, and its expression is induced during cell-to-cell collision.

It has been proposed that C-signal has three essential roles in the *M. xanthus* life cycle: (i) rippling, (ii) aggregate formation, and (iii) sporulation. Within these three stages, C-signal works in a

threshold dependent manner; rippling is triggered at low thresholds, aggregation is triggered at intermediate thresholds, and sporulation is triggered at high thresholds (Kim & Kaiser, 1991; Kruse et al., 2001; Li, Lee, & Shimkets, 1992). The importance of C-signal during fruiting body formation becomes evident after 6 h of starvation. When *csgA*, responsible for C-signal synthesis of *M. xanthus*, is mutated, the gene expression profile of the whole genome changes dramatically (Kroos & Kaiser, 1987). These mutant strains were found to be defective in both aggregation and sporulation, although their phenotype can be rescued by the addition of purified exogenous C-signal (Kim & Kaiser, 1990a).

Individual cell tracking of Wild-Type and *csgA* mutants of *M. xanthus* at different time points during development (0, 3, 6, 9, 12, and 15 h), revealed dissimilar behaviors. Whereas gliding speed and gliding interval (i.e., the time period between when cell movement starts and stops) were increased with respect to Wild-Type cells, reversal frequency and number of stops per minute were decreased. Motility did not show any change for *csgA* mutant cells. It was proposed that C-signal regulates motility parameters to direct longer net distance travelled per minute during aggregation, which ultimately leads to fruiting body formation (Jelsbak & Sogaard-Andersen, 1999; Jelsbak & Sogaard-Andersen, 2000, 2003). The Frz signal transduction system, which is involved in reversal frequency, is known to be regulated by C-signal (Sogaard-Andersen & Kaiser, 1996).

2.3.2 The Frz chemosensory system

M. xanthus cells rarely make U-turns, they mostly reverse, changing their polarity so that the head becomes the tail and tail becomes the head (Kaiser, 2003). Wild-Type cells reverse at intervals of 8 min on average (Kaiser & Zusman, 2016). In 1982, Zusman created a Tn5 insertion mutant collection to identify mutant strains with defective developmental phenotypes, and he discovered

a tight cluster of seven genes (Zusman, 1982). Under starvation conditions, these mutants are not able to aggregate into fruiting bodies. Instead they form filamentous structures. Therefore, he names these genes as “frizzy” (*frz*) genes (Zusman, 1982). Microscopy analysis showed that frizzy mutants are defective in controlling cell reversal. *frzA-C*, *-E* and *-F* mutants reverse much less frequently, approximately once every 2 h. On the other hand, mutant strains missing *frzCD*, a cytoplasmic protein, reverse very frequently, about once every 2.2 min (Blackhart & Zusman, 1985). Methylated FrzCD is known to activate the autophosphorylation of FrzE (McCleary, McBride, & Zusman, 1990), which triggers a change in the direction of movement.

Reversal frequency becomes very important during rippling and fruiting body formation. In order for a cell to reverse, its head and a tail, where the S- and A-machinery are located respectively, must switch simultaneously by disassembling at the old leading and lagging poles and reassembling at the new leading and lagging poles, which takes about a minute in Wild-Type cells (Spormann & Kaiser, 1995; Spormann & Kaiser, 1999). After cell division, both daughter cells are motile, and old motility engines are preserved by daughter cells and new engine str synthesized at the division of the daughter cells. (Igoshin, Mogilner, Welch, Kaiser, & Oster, 2001; Igoshin, Welch, Kaiser, & Oster, 2004b; Sliusarenko, Neu, Zusman, & Oster, 2006; Stevens & S gaard-Andersen, 2005; Welch & Kaiser, 2001b, 2001a).

2.3.3 Quorum sensing signal: A-signal

A-signal is a quorum sensing signal which functions as a cell density indicator in starving cells to measure whether the number of cells present is sufficient to successfully complete aggregation (Plamann, Li, Cantwell, & Mayor, 1995). Each cell produces A-signal, which consists of amino acids and peptides, and development proceeds after the level of A-signal reaches concentrations

greater than 10 μM (Kuspa, Plamann, & Kaiser, 1992; Plamann, Kuspa, & Kaiser, 1992). Even though *asg* mutant strains, which are missing the genes required for A-signaling, cannot generate extracellular signals, they can still respond to it (Kaplan & Plamann, 1996). In addition, *asg* mutants fail to aggregate, but their development can be rescued by the addition of exogenous A-signal. This quorum sensing signal becomes important for development after 2 h of starvation (Kuspa, Kroos, & Kaiser, 1986). AsgABCDE proteins function together in the same signal transduction pathway, and *asgB* is found to be essential for growth (Plamann, Davis, Cantwell, & Mayor, 1994). The expression of the gene 4521, requires both starvation and A-signal to initiate the expression of other early developmental genes (Keseler & Kaiser, 1995).

2.4 Physical modeling of development

A great deal of biochemical, genetic, and image data has been collected regarding *M. xanthus* cell behavior, cell-to-cell interactions, and the genes that are important during development. Despite all of this research, however, significant gaps exist in our understanding, and some data are inconsistent or contradictory. Uncovering what is sufficient and necessary to drive an *M. xanthus* swarm into a self-organized state requires more information to make a complete coherent story.

Models designed around one particular set of conceptual, mathematical, and algorithmic assumptions are powerful ways to make predictions that can then be experimentally tested (Brodland, 2015). Therefore, models can help us gain insight into the mechanisms underlying an observed process. Flexibility in changing the initial parameters or properties of individuals in a model may lead to changes in the results, which can be used to propose testable hypotheses

(Brodland, 2004). Powerful models include all observed dynamics in the system, from a single cell to a cluster or multiple clusters (Zhang et al., 2011).

2.4.1 Early description of aggregation

When starved, the social amoeba *D. discoideum* executes a multicellular development process that is superficially similar to *M. xanthus* development (Dao, Kessin, & Ennis, 2000). Small clusters of *D. discoideum* cells begin to secrete cAMP as a chemoattractant in response to nutrient limitation as a means to initiate aggregation and fruiting body formation (Maree & Hogeweg, 2001). Each fruiting body is composed of a stalk, where programmed cell death (PCD) occurs, and a cap where spore formation takes place (Murata & Ohnishi, 1980). The swarm-scale similarities in aggregation and fruiting body formation, and the discovery of genes that encode for chemotaxis proteins in *M. xanthus*, led to the hypothesis that *M. xanthus* cells may also coordinate their movement due to a chemical like cAMP that is released by cells to trigger fruiting body formation (McBride, Weinberg, & Zusman, 1989). This hypothesis was widely accepted for a while, (Kearns & Shimkets, 1998; Kearns et al., 2001; Lonski, Heromin, & Ingraham, 1977; McBride et al., 1989; Parish, Wedgwood, & Herries, 1976; Shi, Kohler, & Zusman, 1993; Shi et al., 1996); however, after much effort, no chemoattractant has been identified, and feasible alternative hypotheses have been proposed.

The first proposed model for *M. xanthus* aggregation was conceptual, and involved contact-dependent signaling leading to aggregation through the organization of cell behavior and the regulation of gene expression (Jelsbak & Sogaard-Andersen, 1999; Jelsbak & Sogaard-Andersen, 2002, 2003; Sozinova, Jiang, Kaiser, & Alber, 2006). An SEM time series representing the formation of a fruiting body was used as the basis of an initial hypothesis for how aggregation

might start. In 1982, Kuner et al employed submerged culture methods to get clearer SEM pictures of *M. xanthus* development; they placed cells on a petri dish filled with growth medium and let them settle on the bottom and grow overnight. The cells formed a swarm at the bottom, and strongly adhered to each other. After 24 h, the rich liquid media was gently aspirated without disturbing the swarm, and then distilled water was added as a replacement. This initiated starvation and led the swarm cells to aggregate. The authors argued that the image of the swarm taken at 7 h post starvation showed streaming coming from three different angles, intersecting and forming a denser pitch area at the point of intersection. From these data, the traffic jam model was conceived as a means of explaining the mechanism of aggregation (Kuner & Kaiser, 1982).

2.4.2 Traffic Jam Model

The Traffic Jam Model (TJM) was first proposed (published) in 2003 by Dale Kaiser (Kaiser & Welch, 2004) based on the aforementioned SEM images and time-lapse image stacks of rippling at the edge of a swarm, where aggregation occurs at the edge of the colony at the points where ripples intersect. The principle idea of TJM has three essential components (i) cells jam within an initiating swarm because of intersecting traffic, (ii) cell fate changes within a traffic jam, and (iii) a traffic jam is at the center of each aggregate and, consequently, each fruiting body. The authors draw an analogy between crowded motor cars in a traffic jam where they are coming from different directions to an intersection, and starving cells streaming on agar or in submerged culture. According to TJM, when starving cells glide over the surface, they form streaming lines of cells that are almost perfectly aligned side by side along their long axes; the authors refer to these as cellular domains. Streaming cells from different domains contact each other at points of intersection. These contacts, which the authors refer to as collisions, cause cells at intersection

points to stop moving, and this triggers a change in cell fate so that cells become permanently non-motile. Because of differences in orientation between colliding cells from intersecting domains, the now non-motile cells at intersection points form elevated ridges akin to traffic jams; it is at these points where aggregation begins. As motile cells from different parts of the swarm come into contact with the non-motile cells of each traffic jam, they also stop, change cell fate to become non-motile, and join the growing aggregate. After approximately 12 h, cells within the aggregates start moving again, circling clockwise and counterclockwise (Sager & Kaiser, 1993). This lifts a movement blockage, and aggregates become circular shape and mature to become fruiting bodies (Kaiser & Welch, 2004).

2.4.3 Simulations of *Myxococcus xanthus* development in the era of the Traffic Jam Model

Following publication of the initial traffic jam conceptual model, there were several attempts at algorithmic models of *M. xanthus* development that were based on the concept of a traffic jam. Each took a ‘bottom-up’ approach, meaning they focused on describing behavior at the scale of individual cells, and then tested the model’s ability to form patterns that matched experimental results at the scale of an entire swarm. Each of these models were designed around one of two different scaffolds; each was either an agent-based or a cellular automaton-based model (Igoshin, Mogilner, Welch, Kaiser, & Oster, 2001; Sliusarenko et al., 2007a; Sozinova et al., 2005). An algorithm for an agent-based model describes the dimensions, behaviors, and interactions of an ‘agent’ (i.e., an *M. xanthus* cell), and then describes the conditions of the area (size, shape, boundaries, etc.) in which the agents exist and interact. Alternatively, an algorithm for a cellular automaton describes an area as a lattice of connected cells (not living cells, but rather shapes such

as squares, hexagons, cubes, etc.), the states that can exist for each cell, and the rules by which a cell can transition from one state to another. These rules usually depend upon the states of nearby cells (Lett, Silber, & Barret, 1999).

The first agent based model was published in 2004 by Igoshin et al. to explain both rippling and aggregation (Igoshin, Goldbeter, Kaiser, & Oster, 2004). The model relies entirely on the traffic jam conceptual model and attempts to explain individual cell behavior through contact dependent C-signaling. The speed and reversal frequency of the agents was set based on experimental microscopy tracking data. The direction of each agent was not set at random; attempts were made to include the following of slime trails. For example, if a cell agent bends to the left and then immediately reverses, it bends to the right so that it stays on the slime trail it just made. When the agents collide, they exchange C-signal, and the history of each agent's collisions was important. More collisions led to more C-signal accumulation, which led to even more collisions and cell alignments. In order to succeed in modeling the formation of aggregates, the reversal frequency was continuously adjusted down to promote the formation of streams. Agents again changed their fate to become non-motile at regions of high density where traffic jams occurred. With this set of rules, the model was able to form clusters of cells, but they lacked several observable properties of real aggregates (Igoshin et al., 2004).

In 2006, a second agent based model was presented by Sliusarenko et al., which represented a modified version of the previous model (Sliusarenko et al., 2007a). There were several significant differences in the underlying set of rules. C-signal was excluded from the model and a random walk, where the movement of a cell is random and independent from its previous actions and environment, was introduced. Experimental cell data revealed that cells decrease their velocity

when they enter at the high-density regions, but reversal frequency doesn't change with cell density within the swarm. From these data, the authors hypothesized that there is a density threshold where cells adjust their speed, and these behaviors were incorporated into agents of the new model. To accomplish this, the reversal rate of each agent was determined independently, but the velocity changed with the local agent density. As a result, reducing cell velocity is sufficient to initiate aggregation. The authors also demonstrated that streams can be formed by pure steric alignment, rather than requiring C-signal. Streams were found to be non-essential for aggregation because the authors were able to simulate aggregation without streaming cells (Sliusarenko, Zusman, & Oster, 2007b).

Sozinova et al. proposed an alternative model using a cellular automata to simulate fruiting body formation (Sozinova et al., 2005). This cellular automaton model was created using a 3-dimensional lattice, which allowed for the simulation of aggregates in 3-dimensions; the above described agent-based models exist in 2-dimensions. The reorientation probability of each cell was calculated in each time step based on its nearest neighbors' orientation on a 3-dimensional hexagonal lattice, where each cell has 12 nearest neighbors and 12 possible orientations. Cells are not allowed to reverse but can turn by 60 degrees. This model also built upon the traffic jam model by incorporating C-signaling through cell-to-cell contact. C-signal becomes important after the initial jamming of cells; when the cell density increases, it triggers more cell-to-cell contact and therefore the accumulation of more C-signal. That eventually leads to streaming of cells. When streaming cells come in contact with jammed cells, they circulate around them, which leads to the transformation of elongated aggregates to symmetrically circular aggregates. Later in development, the initial nucleus of cells that started the traffic jam dissolve, which results in a 3-dimensional ring of streaming cells. This is significantly different than previous models, in that

cells allowed to climb over each other and down the other side. Some results of this model were inconsistent with experimental observations. In particular, the authors had to introduce traffic jam ‘regions’ in order to trigger aggregation, and streaming cells treated these regions as obstructions. Also, non-reversing 3-dimensional cells were able to simulate aggregation with same set of rules as reversing cells and there are limitations with this model.

A year later, the same research group improved their cellular automaton model by incorporating slime deposition and slime following (Sozinova et al., 2006). In the more recent model, non-reversing cells deposit slime only from one pole of their body and, as more slime is secreted on each location, it forms a slime trail which triggers cells to adjust their orientation to align with the slime trail; the next move of each cell was calculated based on the probabilities of all possible reorientations of the cell along with slime deposition at the particular location. This model can simulate aggregation, and it is able to replicate circulating movements within the aggregates that increases the probability of cell-to-cell contact. More contact means more C-signal accumulation, which then triggers sporulation. Since spores are non-motile, they are pushed to the inner domain/middle of the aggregate by moving neighboring cells. Therefore, the authors conclude that the inner domain is filled with the first differentiated cells and outer domain is filled with spores that differentiated later in the development (Sozinova et al., 2006).

2.4.4 Era of post-traffic jam model

Even though the algorithmic models succeeded in simulating aggregation, they failed to capture and address many of the observed swarm dynamics, including aggregate fate, shape and size. In 2011, Zhang et al. (Zhang et al., 2011) quantified aggregation dynamics by generating Wild-Type time-lapse movies and carefully analyzing each aggregate in the images. They showed that traffic

jam model does not coincide with experimental data with respect to aggregate (i) size and (ii) number, and (iii) distribution.

- (i) The rapid appearance of aggregates begins approximately 7 h into development. It quickly reaches a maximum, and then the number of aggregates actually decreases following a brief stationary phase. Between 10 to 20 h, this decrease in the aggregate number slows down and stops, at which point sporulation is initiated, and aggregates mature into fruiting bodies. The decrease in aggregate number is mostly due to aggregates shrinking and disappearing, but sometimes two or more aggregates will merge into one, and very occasionally one large aggregate will split into two or three. This dynamic quick increase, plateau, and decrease of aggregates does not match with any form of the TJM, which all display a gradual increase in aggregate number with no decrease.
- (ii) Aggregate size increases with time up to 15 h and then shrinks, which may be caused by the fact that aggregates start growing upward instead of outward when they mature. Aggregates in all TJM simulations grow throughout development.
- (iii) The spatial distribution of aggregates is random at the beginning of development and ordered during the later stages of development. This is caused by the rearrangement of aggregates due to their disappearing, merging, splitting, and moving. Aggregates in TJM simulations are in an ordered distribution throughout the process. (Zhang et al., 2011).

During development, *M. xanthus* aggregates have different fates, but this did not occur in any of the TJM simulations, and Zhang et al described these features but did not attempt to address how and why they happen. To begin to address this, Xie et al designed an automated feature extraction method to identify and characterize each aggregate on images of Wild-Type development with approximately 160 fruiting bodies in the field of view. Mainly, 33 features such as area, orientation, solidity, distance to the nearest neighbors, and sum of area of neighbors were determined by applying high-throughput statistical analysis to try and determine which of these features would correlate to differences in aggregate fate. The authors found that aggregate dispersal is highly correlated with aggregate size, in that aggregates smaller than $6000 \mu\text{m}^2$ are more likely to disappear and aggregates larger than this threshold are more likely to persist. Distance to nearest neighbor had only slight correlation with the probability of an aggregate merging with another; if two aggregates are separated from each other by approximately $150 \mu\text{m}$, there is 28% chance that they will end up merging. The splitting of one aggregate into two is a rare event, so the authors hypothesized that extremely elongated aggregates may have an increased probability of splitting (Xie et al., 2011).

Since the underlying assumptions of TJM could not be reconciled with experimental observations of *M. xanthus* aggregation, a new explanation was needed. A biophysical agent-based model based on mechanical cell-alignment was proposed for flexible self-propelled agents (aka *M. xanthus* cells) (Balagam & Igoshin, 2015). Although pure steric interaction of non-reversing agents was able to simulate clusters, the inclusion of cell reversals to the model disrupted the clusters, which suggested that mechanical alignment was not sufficient to induce aggregation. The authors dismissed the possibility of a chemoattractant, since none has been found despite considerable effort, and instead proposed new rules to establish clustering, such as a cohesion factor to stick

cells together. However, these were not enough to drive cluster formation. The authors then included slime trail deposition and following, which led to mesh-like clustering. A high slime effectiveness factor was sufficient for reversing self-propelled agents to form clusters because a high factor prevented cells from escaping the slime trails, so they had no choice but follow the slime trail when they were on it. This model successfully produces clusters at low density, but (i) it fails to simulate agents at high density, and (ii) rather than incorporating experimental cell tracking data, which are increased cell speed and decreased reversal, as shown in (Jelsbak & Sogaard-Andersen, 1999; Shi, Ngok, & Zusman, 1996b), other somewhat arbitrary features were introduced into the model to produce clustering (Balagam & Igoshin, 2015).

Cotter et al. (Cotter, Schüttler, Igoshin, & Shimkets, 2017), simulated fruiting body formation based on individual cell tracking data within developing swarms and growing aggregates. In this simulation, they left out the cell-to-cell signaling, slime trails, and cell fate change. They found that four key concepts are necessary for fruiting body formation: (i) a decreased cell motility inside aggregates, (ii) a biased walk towards aggregate centers, (iii) an alignment with the neighboring cells, and (iv) a radial reorientation of position based on the nearest aggregate center. These simulations indicated that a density-dependent velocity decrease does not drive aggregation. Instead, the system stays at a steady state with respect to velocity. The authors hypothesize that one or more external stimuli are necessary to direct cell movement toward a point for aggregation (Cotter et al., 2017).

These simulations function as the foundation for the most recent agent-based model, which returns to the concept of chemotaxis to explain the cell behavior mechanism (Zhang, Igoshin, Cotter, & Shimkets, 2018). The authors initially tested whether TJM with different properties were able to

reproduce fruiting body formation, as was suggested in early TJM models. First, agents were designed to slow down at the region of high cell density and jam up when they collide to form aggregates. Aggregation time is far longer than what is observed in experiments without local agent alignment. Second, they included active agent alignment into the model to see if it could speed up the process. As a result, clusters formed earlier, but did not represent the features of aggregates, such as their circular shape or different cell fate. Third, adding slime trail into the model helped to form streams but, failed to form normal size aggregates. It was concluded that there must be biased walk towards aggregate centers, which could be caused either by cell contact signaling or a chemotaxis through a diffusible signal. To test both of these possibilities, the authors introduced aggregates into the middle of a simulation domain to see if more active agents moved toward aggregates through the accumulation of C-signal and found that it did not reinforce aggregation. Next, agents within aggregates were simulated to secrete a chemoattractant which diffuses and decays with time, and which drives more agents into aggregates. This represents the first chemotaxis model to describe *M. xanthus* fruiting body formation (Zhang et al., 2018). The summary of models can be found in Fig 2-4.

Although, the models that have been proposed so far have been successfully generated clusters, they all incorporate different components into the simulations such as cell-to-cell contact, slime trail, and lastly chemoattractant in order to simulate aggregation and yet either they fail to replicate all the processes through or positive stimuli needed to be discovered. Therefore, how *M. xanthus* cells establish organization of cells into aggregates still remains elusive.

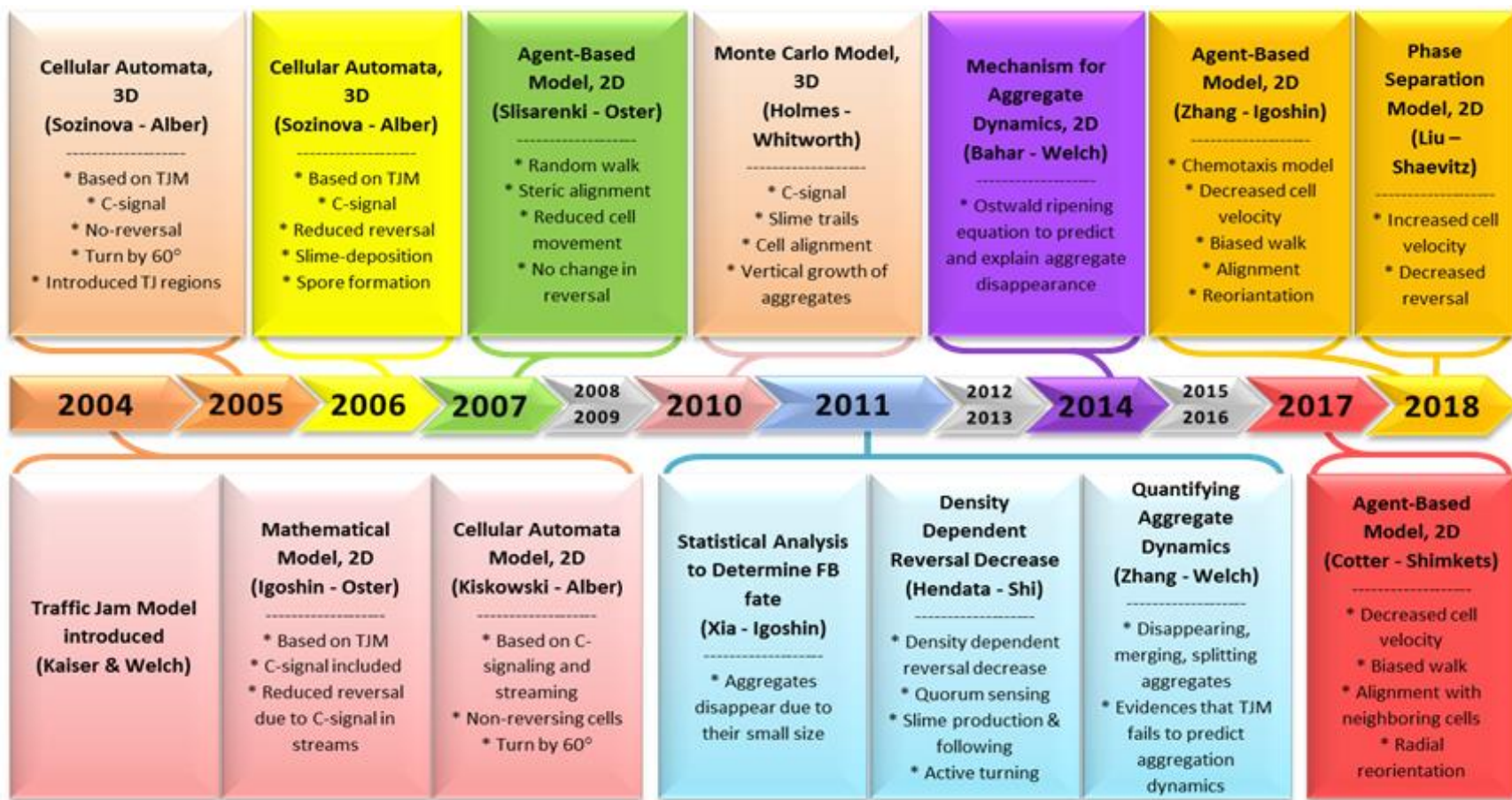


Figure 2-4. History of mechanical modeling of fruiting body formation in *M. xanthus*. Each colored arrow box represents different year starting from 2004 where the very first model was proposed to current date - 2018. Each rectangular box that matches with the color of the year gives the information about the modeling papers; starts with descriptive title, then first and corresponding author of the papers and followed by components of the models. Gray arrow boxes represent the years when no paper was published on modeling

2.5 Genotype to Phenotype: Genetic screens in “Post-Genomic” era

Genome sequencing has become a powerful tool to identify protein coding genes. Knowledge about a putative gene sequence leads to identification by sequence-based homology to uncover the components of pathways and cellular structures. One of the fundamental goals of geneticists is to understand function and regulation of gene products. Creating mutations in genes of interest and studying related phenotypic changes is the most common way to gain insight into function of a gene under specific conditions (Thompson et al., 2013).

Phenotype may be the combination of genotype and environment, but exactly how this manifests in a developing system remains an unanswered fundamental biological question. The answer seems deceptively obvious as long as you focus on the central dogma of DNA to RNA, and RNA to protein (Crick, 1958). The difficulty, of course, is that almost all proteins are involved in at least one cellular structure, process, or pathway that is likely controlled by multiple overlapping regulatory mechanisms. Some proteins are extremely interactive (i.e., master regulators), some are essential, and some have redundancies or are part of decaying pathways and are therefore disposable. In even a small genome, the number of possible interactions is nearly infinite, which makes predicting the phenotypic result of mutation, based on sequence analysis alone, akin to predicting the weather. Researchers can observe patterns and make very broad short-term predictions based on changes in sequence data, but the accuracy of those predictions will decrease sharply as we move farther away from the immediate impact of those changes.

Through high-throughput data sets and systems-level analyses, researchers are now creating maps that purport to reveal how organisms function at the molecular level, but the model based on the Central Dogma that underlies these maps remains unchanged. The application of Occam’s razor

still leads to the conclusion that an organism can be considered the product of all genes and all interactions between genes in the absence of environmental variation. Systems-level maps are an attempt to show how these interactions create pathways that drive metabolism, maintain homeostasis, and guide replication (Papin, Price, Wiback, Fell, & Palsson, 2003; Schilling, Schuster, Palsson, & Heinrich, 1999). Mutation can alter an organism's phenotype because it redirects or prematurely disrupts one or more of these pathways, and so if the maps are detailed and complete, they can be used to predict the phenotypic effects of individual mutations.

Of course, a living system is more complicated than a map showing its genes and their molecular interaction partners, and it seems likely that this conceptualization was adopted because it is similar to a computer network or the Internet. However, even if this kind of oversimplified map was sufficient to predict changes in phenotype based on changes in genotype, the number of variables would still be overwhelming for at least the following three reasons; first, pathways are neither static nor isolated and the effect of mutation may alter the course of one or more pathways by breaking or creating new connections to other pathways; second, the effects of a mutation on phenotype may arise from an indirect rather than a direct effect, and the map would show only the first level of "cause and effect" between a mutation and a change in phenotype; third, a mutation may cause multiple direct and indirect effects on multiple pathways and the change in phenotype does not reflect one or even a few changes on the map. In other words, the molecular interactions that connect a mutation through an interaction map to a change in phenotype are not stable, comprehensive, or symmetrical; and each of these three confounding factors impacts the others. Therefore, the whole "genes and their interactions" concept is insufficient for addressing the problem of linking a mutation to phenotypic change combined with the fact that there are still many genes with unknown functions.

Ongoing improvements in genome sequencing, transcriptomics, and image acquisition and analysis mean that it will soon be possible and easier to reliably match a genome to a transcription profile and a phenotype. Genome sequences of thousands of bacteria have been revealed already, along with a smaller assortment of higher organisms, including human (Blattner, 1997; Consortium, 2004; Mewes et al., 1997). Although many researchers have focused on predicting an organism's protein functions and interactions based on its genome sequence (Bork et al., 1998; Jensen, Gupta, Staerfeldt, & Brunak, 2003; Marcotte et al., 1999; Sur & Taipale, 2016), accuracy still remains low. The problem has become so persistent that it has acquired its own name: "genotype to phenotype" (G2P) problem (Webb, Thorisson, & Brookes, 2011).

Despite recent advances in the genetic field, the problem of G2P is still a real challenge because the number of variables is enormous and most of the data are the static representation of dynamic processes. Some of these variables can be eliminated through careful experimental design. For example, many of the environmental variables that shape phenotype can be held constant by studying the effect of genes on phenotype in a well-defined and stable environment.

A second problem in establishing the phenotype to genotype relationship is our incomplete understanding of the genome. It is estimated that in any given organism the function of only 50% of genes can be predicted with a reasonable confidence (Kolker et al., 2004). The remaining genes are deemed either "conserved hypotheticals," which are homologs to the genes with unknown function, or as "hypotheticals", which have been predicted to be open reading frames with no homologs in any database. For even the most comprehensively understood model organism, *E. coli*, the functions of some of the genes are still not known, and assigning essential genes is still complicated (Goodall et al., 2018). With a less well-studied organism like *M. xanthus*, the problem is worse, with 43.2% of the predicted ORFs in the genome still annotated as hypothetical as of

2006 (Unpublished data from Garza,s lab). It is estimated that characterizing all the hypothetical genes using current methods will take decades (Kolker et al., 2004). This means that, without having complete knowledge and understanding on either genome or phenotype separately, working on understanding the relation between is quite a challenge.

The G2P problem is not a new concept. In fact, the entire field of developmental biology is focused on defining the relationship between genotype and phenotype. The difference between developmental biology and the type of G2P study we are proposing is that developmental biology aims at understanding the role of each genetic element during the process of development, while G2P aims at predicting the phenotypic effects of genetic alterations, regardless of whether that phenotype is considered “normal” or “Wild-Type”.

In traditional screens, through thousands of mutant strains you would only wind up characterizing a few of the “extreme” cases. New technologies have changed both screening and selection studies, such that phenotypic screens are now routinely performed on model organisms using high-throughput methods (Alfred et al., 2012; Friedman & Perrimon, 2004). This significantly increases the number of mutant strains that can be carefully characterized, and the amount of data being collected, but it doesn't necessarily add value unless the analysis of data is also expanded. Many of these studies collect data on various functions of cell growth, division and morphology by observing phenotypic characters such as growth curve and morphology analysis by microscopy (Gönczy et al., 2000; Harada et al., 2005; Hartman & Tippery, 2004; Ohya et al., 2005; Sönnichsen et al., 2005; Weiss, Delproposto, & Giroux, 2004).

Microscopy, in particular, is one of the most powerful and informative technologies used to collect phenotypic data at the cellular level (Wählby et al., 2012), and advances in technology and

reductions in cost have made the collection of microscopic time-lapse image data amenable to high-throughput analysis. In a representative study, Sawai and his colleagues (2007) performed a screen on approximately 2000 *D. discoïdium* mutant strains, focusing specifically on the multicellular self-organizing process of fruiting body formation called development, and collecting an assortment of quantitative phenotypic data that included time lapse microscopy. However, despite collecting this large amount of data, the authors reported only 4% of mutant strains had a phenotype that deviated from Wild-Type enough to be characterized as “mutant” (Sawai, Guan, Kuspa, & Cox, 2007). In other words, the authors are stating that, after characterizing approximately 2000 mutant strains, 96% of them show a phenotype indistinguishable from the Wild-Type. An alternative explanation is that the authors collected a plethora of data, but their analysis did not include enough of the relevant variables to distinguish “mutant” from “Wild-Type” with respect to the development phenotype.

2.5.1 G2P in *Myxococcus xanthus*

Thanks to genome sequencing technology, now we know sequences of almost all the open reading frames of a given organism. By using bioinformatic tools, homolog genes were sequenced and identified in *M. xanthus*. (Caberoy et al., 2003; K. M. Giglio et al., 2011; Lancero et al., 2004). Garza and his research group have been working on the characterization of NtrC-like activators, which are found to be necessary mostly for development. In 2014, Yan et al. carefully characterized another set of homolog gene, ABC Transporters, based on different traits, such as motility, aggregation, and sporulation. Although these studies have provided a great deal of understanding on the effects of particular genes during development, comprehensive analysis on aggregation as a dynamic process has not been understood well.

One of the fundamental questions about *M. xanthus* development is how many different ways formation of fruiting bodies can be genetically altered with respect to phenotype. All studies on transcription profiling of *M. xanthus* shows that mRNA levels for a significant fraction of the genes change during *M. xanthus* development (Zusman et al., 2007), indicating that there are hundreds, or thousands of genes involved in the process. This can be interpreted as either development can be altered in many ways through genetic mutations, or mutant strains that affect the development can be clustered according to phenotype. To address this question, in chapter 5, we performed a thorough phenotypic analysis by systematically characterizing the effect of 400 different individual gene disruptions on developmental phenotype using time-lapse microcinematography. For this purpose, we recorded time-lapse images of development for each single-gene mutated strains. We proceeded systematically, by studying only one protein family at a time, to further test if there is a relationship between sequence homology and changes in developmental phenotype after disruption.

2.6 Role of paralogous gene families in *Myxococcus xanthus* development

Genome annotation is important for understanding organisms' genomic makeup. Sequence similarity search is the basic of genome annotation which can help to identify characterization of protein families and evolutionary relationships. The proteins that show statistically significant sequence similarities is defined as homologous, mostly carrying similar structure and function (Gonzalez & Pearson, 2010). However, there are cases that homologous proteins function differently. Therefore, homology does not always correlates with the function (Saier Jr., 1996). There are several paralogous protein groups in *M. xanthus* that one or more members are found to have important functions in *M. xanthus* complex life cycle.

2.6.1 ABC transporters

One of the essential features of all living organisms is to transport organic and inorganic molecules across cellular membrane to provide vital compounds for the cell and remove unnecessary/toxic materials for its survival (Wilkins, 2015). In order for cells to overcome transportation of a variety of different molecules, they have evolved to take advantage of large numbers of transporter genes in their genome. For example, ATP binding cassette or ABC transporters is one of the largest transport superfamily.

ABC transporters are ubiquitous in both prokaryotes and eukaryotes. In fact, ABC transporter forms the largest proportion of protein families found in bacteria and archaea which represent 1 to 3% of genome (Tomii & Kanehisa, 1998). Humans also encode ABC transporters (Wilkins, 2015). Mutation in different ABC transporters can cause a variety of diseases such as cystic fibrosis with nonfunctional chloride ion channels (Collins, 1992; Mendoza & Thomas, 2007), rare autosomal disease sitosterolemia (Plösch et al., 2004), cardiovascular disease (Schumacher & Benndorf, 2017), Tangier Disease (Rust et al., 1999), Stargardt disease (Allikmets et al., 1997), and age-related macular degeneration (H. Sun, Molday, & Nathans, 1999). In case of over-expression of an ABC transporter, ABCB1, anticancer drug resistance becomes a major challenge during chemotherapy (Gottesman & Ambudkar, 2001; Fletcher, Haber, Henderson, & Norris, 2010; Sun, Patel, Kumar, & Chen, 2012). Since they play important roles in health-related issues, ABC transporters have been a widely studied protein family.

ABC transporters have a specific structure that consists of at least four domains: two in the membrane and two in the cytoplasm. Two hydrophobic transmembrane domains (TMD) are embedded in the membrane bilayer and their variety of sequence and structure indicates the

diversity of translocated substrates. Other two water-soluble ABC domains are nucleotide-binding domains (NBDs) located in cytoplasm and consists of highly conservative motifs (Biemans-Oldehinkel, Doeven, & Poolman, 2006; Rees, Johnson, & Lewinson, 2009). ATP hydrolysis is catalyzed by NBDs, whereas the translocation of the substrate is facilitated by TMDs. ABC transporters can be both exporters and importers, but importers have only been found in prokaryotes, while exporters are in all kingdoms to this date. In bacteria, there is a third group of ABC transporters, which are involved in translation of mRNA and DNA repair- (several non-transport-related processes) (Locher, 2016). Conserved coupling mechanism may allow both ABC importers and exporters to convert ATP binding and hydrolysis to a change in conformation which facilitates active transport. In most cases, ABC importers require substrate binding protein (SBP) found in periplasm or anchored to the outer membrane in G⁺ bacteria and archaea via a lipid-anchor or a transmembrane peptide.

Importers are divided into two classes; Type I and Type II. They have a distinct transmembrane domain with different helicase architecture. First, the crystal structure of Type I importer, putative molybdate transporter, was shown in *Archaeoglobus fulgidus* (Locher, 2016). Larger group of Type II crystal structure was first revealed in *E. coli* vitamin B12 transport BtuCD (Locher, Lee, & Rees, 2002). ABC efflux pumps which consist of 12 transmembrane helicases are less complex compared to ABC uptake system. Substrate binding protein are not required for their function, but they increase affinity of transporters for their substrate (Biemans-Oldehinkel et al., 2006).

2.6.1.1 Physiological role of biological ABC transporters

ABC transporters utilize the power from ATP hydrolysis to translocate substrates across the cell membrane. Importers facilitate the uptake of a wide range of different nutrients such as,

carbohydrates (Schneider, 2001), organic and inorganic ions, amino acids (Hosie & Poole, 2001), peptides (Detmers, Lanfermeijer, & Poolman, 2001), metals (Claverys, 2001), and vitamins (Erkens, Majsnerowska, Ter Beek, & Slotboom, 2012). Pathogens such as *Mycobacterium tuberculosis* (Rodriguez & Smith, 2006) and *Streptococcus pneumoniae* (Brown, Gilliland, & Holden, 2001) utilize an ABC iron uptake system for their virulence effect. Some other examples are vitamin B12 importer BtuCD and maltose importer MalFGM in *E. coli*. ABC transporters are also responsible for a large range of substrate export, such as small peptides and nonprotein substrates. ABC transporters are also important in membrane synthesis; LolCDE complex translocates lipoproteins from the inner membrane onto the outer membrane after sorting (Ito, Kanamaru, Taniguchi, Miyamoto, & Tokuda, 2006).

2.6.1.2 ABC transporters in *Myxococcus xanthus*

ABC transporters were found to be important in motility, fruiting body formation and sporulation of *M. xanthus*. RfbAB, which is encoded in the *sasA* locus, is the first ABC transporter that was characterized in *M. xanthus*; its absence causes defective fruiting body formation and reduced sporulation. RfbA is predicted to provide a channel structure and RfbB couples hydrolyze ATP for transportation (Guo, Bowden, Pershad, & Kaplan, 1996). Later, the Zusman group found that *abcA* is important in fruiting body formation. Mutation in *abcA* results in frz-like aggregates. Yeast two-hybrid system analysis showed that *frzZ* interacts with *abcA* suggesting a connection in the same signaling pathway. Mixing experiments rescued abnormal phenotype of defected *abcA*, so researchers hypothesized that AbcA protein may export a molecule that drives an autochemotactic process for aggregation (Ward, Mok, Astling, Lew, & Zusman, 1998). Mutation in *pilH*, which encodes an exporter required for type IV pilus biogenesis, results in a significant reduction in

extracellular pili, S motility defect, delayed and elongated fruiting body formation, and a 3-fold increase in sporulation.

Some spores are known to be located outside of fruiting bodies (Wu, Wu, Cheng, & Kaiser, 1998). The *mac-1* has significant sequence similarities to a macrolide antibiotic transport gene encoding a protein with transport function in *M. xanthus*; *mac-1* deficient cells are able to form mounds but fail to develop into fruiting bodies or to form viable spores. Therefore, it has been suggested that this gene may be responsible for transportation of a molecule required for sporulation (Kimura, Yamanishi, Tokumasu, Terasaka, & Yoshinobu, 2001). In the development stage, there are many other important genes and operons. For example, in *pstSCAB* operon, the phosphate importer is located downstream of a response regulator, *phoP4*, which is required for development. *phoP4* deletion downregulates the transcription of *pstSCAB* (Pham et al., 2006).

A mutation library was created for detailed characterization of all ABC transporters by Jinyuan Yan (Yan, Bradley, Friedman, & Welch, 2014). They analyzed the phenotypic effects of ABC transporters during (i) growth including assays on soft agar (0.4%) and hard agar (1.5%), (ii) fruiting body formation including timing, grayness, circularity, number and average size of aggregates, and (iii) sporulation. It was found that 12 of 191 transporter genes are essential for growth and 86% of mutant strains showed statistically significant deviation from the Wild-Type. Although the expression profile did correlate with phenotype, sequence-based data did not co-cluster with phenotype.

2.6.2 Signal transduction system

In order to survive, all living cells have evolved to sense and communicate with their environment and with neighboring cells and to adjust their metabolism and behavior in response. These

adjustments can vary from the regulation of the *lac* (lactose) operon to more complex regulatory mechanisms that include cellular responses to external signals transmitted through the cytoplasmic membrane followed by activating intercellular signal transduction (Galperin, 2005). Comparative genome analysis provided evidence that proteobacteria and cyanobacteria have more signal transduction proteins than G (+) or archaea of the same genome size, and bacterial parasites with a stable environment have fewer sensory transduction systems (Galperin, 2004; Galperin, Nikolskaya, & Koonin, 2001). There are three known bacterial signaling systems: one component systems, two component systems, and ECF sigma factors (Staroń et al., 2009; Ulrich, Koonin, & Zhulin, 2005).

2.6.2.1 Biological function of two component signal transduction

Two component transduction systems feature signal transmission between two conserved components, a membrane-bound histidine kinase and DNA-binding response regulator (RR). Mostly histidine kinase is responsible for sensing specific environmental cues, such as nutrients, temperature, quorum sensing, antibiotics, pH, chemoattractants, etc. These cues trigger autophosphorylation at a conserved histidine residue of the kinase, followed by phosphate transfer to the aspartate residue on the response regulator. This activates the response regulator, which leads to a conformational change to carry out specific functions such as DNA-binding or catalyzing biochemical reactions (Stock, Robinson, & Goudreau, 2000).

Histidine protein kinases are found in Bacteria, Archaea and Eukarya, but are thought to be completely missing in the animal kingdom (Drosophila, 2000; International Human Genome Sequencing Consortium, Human, & Sequencing, 2001; The *C. elegans* Sequencing Consortium, 1998). Recent studies showed that histidine phosphorylation exists in mammals as well (Attwood,

2013; Besant, Tan, & Attwood, 2003). The sequence analysis of 348 histidine kinase domain revealed that sensor histidine kinases consist of two signaling components, highly conserved cytoplasmic C-terminal kinase core and a more diverse periplasmic N-terminal sensing domain (Thorsten W Grebe & Stock, 1999). There are a few kinases that are missing a sensing domain such as chemoreceptor CheA (T W Grebe & Stock, 1998) and nitrogen-regulatory NtrB (Jiang, Peliska, & Ninfa, 1998). In order for autophosphorylation to occur, ATP binds to catalytic ATP-binding domain (CA) of kinase core and then phosphorylates the His residue in histidine phosphotransfer domain (DHP) of the kinase core, which is formed by two long helices (Casino, Miguel-Romero, & Marina, 2014).

Response regulators' role comes in after autophosphorylation of histidine kinases regulate output of the responses. The RRs are composed of a conserved N-terminal receiver domain, also called regulatory domain, and a variable C-terminal effector domain(s). The receiver domain catalyzes the phosphotransfer reaction to one of its 3 aspartic acid residues. This phosphorylation causes conformational changes in the effector domain, which regulates its activity. The diversity of effector domains allows them to have a wide range of responses, including regulation of flagellar rotation (Aldridge & Jenal, 1999), plant pathogen defense (Argueso et al., 2012), biosynthesis of secondary messengers, cyclic-di-GMP signaling (Ryan, 2013), and DNA binding. DNA-binding effector domains constitute 63% of response regulators, so they are transcriptional regulators (Gao & Stock, 2009) that control gene expression in response to environmental stimuli.

2.6.2.2 Two component signal transduction system in *Myxococcus xanthus*

M. xanthus has one of the largest prokaryotic genomes, which reflects the complexity of its life cycle: 9.14 Mb with 7,380 ORFs (Goldman et al., 2006). It encodes 272 Two Component System

(TCS) proteins which covers 3.5% of its genome. This is the highest reported number for TCS proteins in an organism so far. 21 of these are part of Che-like system; chemotaxis-like signal transduction cascade, while 118 encodes histidine protein kinases, 119 are response regulators and 14 of them are histidine-like genes which contains only a HisKA domain or a HATPase_c domain. They are not all organized as paired genes; some of them are orphans, some are complex gene clusters. 35 of TCS proteins are reported to be important in fruiting body formation and sporulation. Microarray analysis on 213 TCS genes revealed that 63 genes showed altered expression during development (X. Shi et al., 2008). CheY family with 49 members and NtrC family with 53 members represents the two largest groups of response regulators in *M. xanthus*.

2.6.2.2.1 NtrC-like activators

Nitrogen Regulatory Protein C (NtrC) is one of the many enhancer proteins found in prokaryotes. NtrB - NtrC are part of a two-component system and control the expression of genes for nitrogen assimilation in response to nitrogen limitations. While NtrB acts as histidine kinase, NtrC functions as a response regulator (Zimmer et al., 2000). NtrC is one of the best characterized response regulators that also acts as an enhancer binding protein (EBP) (North, Weiss, Suzuki, Flashner, & Kustu, 1996; Wedel & Kustu, 1995). Transcription starts when bacterial polymerase core enzyme binds to a sigma factor which defines the promoter specification. Sigma factors are divided into two groups based on their characteristic molecular weight: sigma 54 and sigma 70. Bacterial enhancer binding proteins (bEBPs) are required for sigma 54 dependent transcription, which is different from transcription initiation mediated by sigma 70-like sigma factors. NtrC has ATPase activity for isomerization of closed complex, otherwise transcription would be kinetically and thermodynamically unfavorable (Popham, Szeto, Keener, & Kustu, 1989).

Sigma 54 activators are found in larger numbers in delta proteobacteria compared to other bacterial genomes, which indicates that these activators play important roles in these bacteria (Karlin, Brocchieri, Mrazek, & Kaiser, 2006), giving them the advantage of being able to regulate transcription based on various environmental changes.

To date, none of the sigma 54 activators are reported to be crucial for growth in any prokaryotic organisms other than *M. xanthus* (Keseler & Kaiser, 1997). It was predicted that there are 53 sigma 54 dependent enhancer binding proteins (NtrC-like activators or nla) in *M. xanthus* genome (Goldman et al., 2006). Expression analysis suggested that they are essential for all stages of development, but more appear to be expressed during the early stages of development rather than later stage of fruiting body formation (Caberoy et al., 2003).

The *M. xanthus* genome is predicted to contain 53 EBPs, and expression data showed that six EBP genes are upregulated during development including *pilR*, *sasR*, *spdR*, MXAN_5041, MXAN_2902, and MXAN_4240 (Jakobsen et al., 2004). PilR is the very first identified sigma 54 activator that is required in pili formation and S-motility. Mutation of *pilR* causes delayed aggregation and S-motility defect. Both PilR, response regulator, and PilS, histidine kinase function, form two-component signal transduction system together to regulate *pilA* expression (Wu & Kaiser, 1995). While SasR is suggested to function in the A-signal pathway (Guo, Wu, & Kaplan, 2000), SpdR negatively regulates A- and B- signaling and shows varying phenotypes depending on the nutritional conditions of the substrate (Hager, Tse, & Gill, 2001). RpoN was found to be vital for cell growth, since targeted mutagenesis on *rpoN* failed to produce viable cells (Keseler & Kaiser, 1997).

In order to detect new sigma 54 activators, Tn5 insertion was introduced to the ATP binding regions in the *M. xanthus* chromosomal DNA. 5 out of 8 mutants were found to diverge from Wild-Type in aggregation, and 3 of them failed to sporulate (Gorski & Kaiser, 1998). Garza and his research group did extensive studies on identifying and characterizing more response regulators and their role in development (Caberoy et al., 2003; Diodati et al., 2006; Garza et al., 1998; Giglio et al., 2011; Krista M. Giglio, Eisenstatt, & Garza, 2010; Lancero et al., 2004; Sarwar & Garza, 2015). While *nla1*, *nla19*, and *nla23* mutants aggregate later than Wild-Type and showed S-motility defects, the *nla24* mutant was not able to aggregate or sporulate and showed A- and S-motility defects. Moreover, *nla24* mutants failed to differentiate into spores when the cells were treated with glycerol, which indicates that it is also essential for sporulation. *nla4*, *nla6*, *nla18* and *nla28* mutants passed the motility test, but showed late aggregation and failed to sporulate. 20 out of 28, including 8 sigma factors mentioned above, did not demonstrate any difference from Wild-Type with standard motility, aggregation and sporulation assays (Caberoy et al., 2003). FruA production, involved in C-signaling pathway, was found to be abolished in the cells carrying the *nla18* mutation. Additionally, they showed defects in accumulation of (p)ppGpp and production of A- signal, which are both necessary for early development. Later, in 2009, Giglio et al. characterized eleven more EBPs, six of which were defective in fruiting body formation (Krista M. Giglio, Eisenstatt, & Garza, 2010). The mutants of MXAN_0172, MXAN_0603, MXAN_4261, MXAN_5879, and MXAN_7143 showed deviation from Wild-Type aggregates with characteristics shapes.

Another gene important in the *M. xanthus* life cycle is MXAN_4196. Mutation in MXAN_4196 results in A-motility deficiency, fruiting body formation failure, and lack of viable spores. Nla6 and Nla28 were found to be crucially important for sporulation and controlling the expression of

genes prior to aggregation. ActB, sigma 54 regulator, was also found to be involved in gene expression during sporulation (Sarwar & Garza, 2015).

2.6.2.3 One-component signal transduction system

For a long time, two-component systems have been accepted as the most abundant signaling pathways in bacteria and archaea. Bioinformatic analysis of 145 prokaryotic genomes revealed that majority of signal transduction systems were composed of a single protein, making One-Component Systems (OCS) more prevalent (Ulrich et al., 2005). These proteins contain input and output domains but lack a phosphotransfer domain. Analysis of over 25,000 OCS protein sequences showed that they do contain an HTH domain, which is a characteristic of DNA binding motif, but missing a transmembrane domain, indicating that they are cytosolic proteins (Ulrich et al., 2005).

To date, there has not been any characterization or analysis done in One Component Signaling System in *M. xanthus*.

2.6.2.4 ECF sigma factors

Another type of signal transduction system and transcriptional regulator is extracytoplasmic function (ECF) sigma factors. Bacterial cells constantly monitor external conditions to survive in a changing environment and adjust their response accordingly. This adjustment can be initiated by sigma factors (Missiakas & Raina, 1998).

There are many proteins responsible for transcriptional initiation in eukaryotes. However, sigma factors are an essential part of promoter selectivity for transcription in prokaryotes. The basal gene

expression level is controlled by housekeeping sigma factors (Taniguchi & Wendisch, 2015). Additionally, most bacteria encode alternative sigma factors. Bacteria with complex genomes have multiple sigma factors, including: *Bacillus subtilis* with 7 ECF sigma factors (Souza et al., 2014), *P. aeruginosa* with 19 ECF sigma factors (Potvin, Sanschagrín, & Levesque, 2008), *Streptomyces coelicolor* with 50 ECF sigma factors (Heimann, 2002), and *M. xanthus* with 38 ECF sigma factors (Goldman et al., 2006).

2.6.2.4.1 Biological function of ECF sigma factors

The architecture of “core enzyme” (E) RNA polymerase (RNAP) consists of five subunits, $\beta\beta'\alpha 2\omega$. In order for this core enzyme to bind a specific promoter, it requires a sigma factor; together they form holoenzyme, $E\sigma$. Sigma factor in the bacterial RNAP holoenzyme recognizes and binds to a promoter. The holoenzyme forms a “closed” complex (RP_c) with the DNA and then unwinds the DNA at the -10 consensus. Holoenzyme with unwound DNA forms the “open” complex (RP_o), then sigma factor is released. This leads RNAP core enzyme to move along the DNA (Paget, 2015; Saecker, Record, & Dehaseth, 2011).

One of the large and diverse subfamilies of sigma factors is ECF sigma factor, which contains sigma 2 and sigma 4 regions. Some of ECF sigma factors autoregulate their own expression. Others are co-transcribed with anti-sigma factors, which regulate the sigma factor activity. Anti-sigma factors are located in the membrane, with an extracytoplasmic sensory domain and an intracellular inhibitory domain (Brooks & Buchanan, 2008; Heimann, 2002; Missiakas & Raina, 1998; Staroń et al., 2009). Molecular analysis suggests that they respond to extracytoplasmic stimuli, which is how they got their name. These sigma factors function in ferric citrate transport in *E. coli* (Mahren & Braun, 2003), metal ion efflux in *Cupriavidus necator*, (formerly known as *Alcaligenes*

europus) (Schmidt & Schlegel, 1994), alginate secretion in *P. aeruginosa* (Schurr, Yu, Martinez-Salazar, Boucher, & Deretic, 1996), oxidative stress response in *P. syringae* (Butcher et al., 2017), and synthesis of carotenoids in *M. xanthus* (Fontes, Galbis-Martínez, & Murillo, 2003).

2.6.2.4.2 ECF sigma factors in *Myxococcus xanthus*

It was predicted that the *M. xanthus* genome encodes for 38 ECF sigma 70 factors (Goldman et al., 2006), yet only three of them have been characterized. *M. xanthus* cells response to blue light by synthesizing carotenoids to protect themselves from cellular damage caused by photo-excited molecules. One of the characterized ECF sigma factors in *M. xanthus* is CarQ. *carQ*, *carR* and *carS* are grouped at the same operon under the control of a light-inducible promoter. CarR acts as an anti-sigma factor; in the dark, it physically interacts with CarQ to prevents transcription activation. On the other hand, CarQ is released under light conditions (Browning, Whitworth, & Hodgson, 2003; Martinez-Argudo, Ruiz-Vázquez, & Murillo, 1998).

It was also found that RpoE1, an ECF sigma factor, plays a role in transcriptional regulation of genes involved in motility during both vegetative growth and development. For example, RpoE1 mutation results in density depended developmental defect (Ward, Lew, Treuner-Lange, & Zusman, 1998).

A recently discovered ECF sigma factor, CorE, is responsible for regulation of copper detoxification in *M. xanthus*. C terminus of the CorE (for copper-regulated ECF σ factor) has a Cys-rich domain which is important for activation and inactivation of the protein. When Copper is present, expression of *corE* peaks at 2 h and activates the expression of *copB* (Gómez-Santos,

Pérez, Sánchez-Sutil, Moraleda-Muñoz, & Muñoz-Dorado, 2011; Muñoz-Dorado, Gómez-Santos, & Pérez, 2012).

2.7 Summary

Self-organization in biology can be explained as a strategic way to survive under stress conditions, establish territory, or obtain food in a more efficient way. In the case of biofilms, self-organization strategies provide resilience for bacterial populations, and understanding behavior at the population level becomes important. Cell behavior, gene expression, and cell-to-cell interactions change during biofilm formation in order to optimize outcomes for the swarm. One of the challenges developmental biologists face is to make use of the wealth of information from experimental data and observations to understand the behavior of individual cells within multicellular structures to illuminate the connection between genome and phenotype.

To understand the basics of self-organization and pattern formation in *M. xanthus*, several models have been suggested so far. However, we still lack comprehensive explanation for multicellular organization from the point, where (p)ppGpp accumulates to initiate development, to the point, where aggregates are formed simultaneously on the agar surface. After aggregate formation, maturation proceeds until the fruiting bodies are filled with spores. During the maturation process, aggregates rearrange themselves by disappearing, merging, splitting, or moving to reach a final stable state. It has been suggested that the size of an aggregate is the only driving factor for its eventual fate (Xie et al., 2011). However, how rearrangement is regulated still remains unanswered.

Our work has tested a mechanism addressing both aspects of fruiting body formation. In order to improve our model and define the boundaries of aggregation, we generated a time-lapse microcinematography library from the phenotypic data pool of 400 insertion mutants. The integration of biological, computational, and physical approaches led us to a comprehensive explanation of aggregation in *M. xanthus* that could not be established by any one of them alone.

2.8 References

- Arias Del Angel, J. A., Escalante, A. E., Martínez-Castilla, L. P., & Benítez, M. (2017). An Evo-Devo Perspective on Multicellular Development of Myxobacteria. *Journal of Experimental Zoology Part B: Molecular and Developmental Evolution*.
- Arnold, J. W., & Shimkets, L. J. (1988). Cell surface properties correlated with cohesion in *Myxococcus xanthus*. *Journal of Bacteriology*, 170(12), 5771–5777.
- Balagam, R., & Igoshin, O. A. (2015). Mechanism for Collective Cell Alignment in *Myxococcus xanthus* Bacteria. *PLoS Computational Biology*.
- Behmlander, R. M., & Dworkin, M. (1994). Biochemical and structural analyses of the extracellular matrix fibrils of *Myxococcus xanthus*. *Journal of Bacteriology*, 176(20), 6295–6303.
- Berleman, J. E., Chumley, T., Cheung, P., & Kirby, J. R. (2006). Rippling is a predatory behavior in *Myxococcus xanthus*. *Journal of Bacteriology*, 188(16), 5888–5895.
- Berleman, J. E., & Kirby, J. R. (2009). Deciphering the hunting strategy of a bacterial wolfpack. *FEMS Microbiology Reviews*.
- Blackhart, B. D., & Zusman, D. R. (1985). “Frizzy” genes of *Myxococcus xanthus* are involved in control of frequency of reversal of gliding motility. *Proceedings of the National Academy of Sciences*, 82(24), 8767–8770.
- Bowden, M. G., & Kaplan, H. B. (1998). The *Myxococcus xanthus* lipopolysaccharide O-antigen is required for social motility and multicellular development. *Molecular Microbiology*, 30(2), 275–284.
- Boysen, A., Ellehauge, E., Julien, B., & Sjøgaard-Andersen, L. (2002). The DevT protein stimulates synthesis of FruA, a signal transduction protein required for fruiting body morphogenesis in *Myxococcus xanthus*. *Journal of Bacteriology*.
- Braun, T. F., Khubbar, M. K., Saffarini, D. A., & McBride, M. J. (2005). Flavobacterium johnsoniae gliding motility genes identified by mariner mutagenesis. *Journal of Bacteriology*, 187(20), 6943–6952.
- Brodland, G. W. (2004). Computational modeling of cell sorting, tissue engulfment, and related phenomena: A review. *Applied Mechanics Reviews*, 57(1), 47.
- Brodland, G. W. (2015). How computational models can help unlock biological systems. *Seminars in Cell and Developmental Biology*.
- Caberoy, N. B., Welch, R. D., Jakobsen, J. S., Slater, S. C., & Garza, A. G. (2003). Global Mutational Analysis of NtrC-Like Activators in *Myxococcus xanthus* : Identifying Activator Mutants Defective for Motility and Fruiting Body Development, 185(20), 6083–6094.

- Campbell, A., Viswanathan, P., Barrett, T., Son, B., Saha, S., & Kroos, L. (2015). Combinatorial regulation of the dev operon by MrpC2 and FruA during *Myxococcus xanthus* development. *Journal of Bacteriology*.
- Claessen, D., Rozen, D. E., Kuipers, O. P., Sogaard-Andersen, L., & van Wezel, G. P. (2014). Bacterial solutions to multicellularity: a tale of biofilms, filaments and fruiting bodies. *Nat Rev Microbiol*, 12(2), 115–124.
- Cotter, C. R., Schüttler, H.-B., Igoshin, O. A., & Shimkets, L. J. (2017). Data-driven modeling reveals cell behaviors controlling self-organization during *Myxococcus xanthus* development. *Proceedings of the National Academy of Sciences*, 114(23), E4592–E4601.
- Curtis, P. D., Taylor, R. G., Welch, R. D., & Shimkets, L. J. (2007). Spatial organization of *Myxococcus xanthus* during fruiting body formation. *Journal of Bacteriology*, 189(24), 9126–9130.
- Dao, D. N., Kessin, R. H., & Ennis, H. L. (2000). Developmental cheating and the evolutionary biology of Dictyostelium and Myxococcus. *Microbiology*, 146(7), 1505–1512.
- Diodati, M. E., Ossa, F., Caberoy, N. B., Jose, I. R., Hiraiwa, W., Igo, M. M., ... Garza, A. G. (2006). Nla18, a key regulatory protein required for normal growth and development of *Myxococcus xanthus*. *J Bacteriol*.
- Du, Q., Kawabe, Y., Schilde, C., Chen, Z. H., & Schaap, P. (2015). The Evolution of Aggregative Multicellularity and Cell-Cell Communication in the Dictyostelia. *Journal of Molecular Biology*, 427(23), 3722–3733.
- Ducastelle, F., & Quémerais, P. (1997). Chemical self-organization during crystal growth. *Physical Review Letters*, 78(1), 102–105.
- Dworkin, M. (1963). Nutritional Regulation of Morphogenesis in *Myxococcus xanthus*. *J Bacteriol*, 86(March), 67–72.
- Dworkin, M. (1996). Recent advances in the social and developmental biology of the myxobacteria. *Microbiological Reviews*, 60(1), 70–102.
- Ellehaug, E., Norregaard, M., & Sogaard-Andersen, L. (1998). The FruA signal transduction protein provides a checkpoint for the temporal co-ordination of intercellular signals in *Myxococcus xanthus* development. *Molecular Microbiology*, 30(4), 807–817.
- Fenchel, T., & Thar, R. (2004). “Candidatus Ovobacter propellens”: A large conspicuous prokaryote with an unusual motility behaviour. *FEMS Microbiology Ecology*, 48(2), 231–238.
- Garza, A. G., Pollack, J. S., Harris, B. Z., Lee, A., Keseler, I. M., Licking, E. F., & Singer, M. (1998). SdeK is required for early fruiting body development in *Myxococcus xanthus*. *Journal of Bacteriology*.
- Gestel, J. V. a N., Vlamakis, H., & Kolter, R. (2015). Division of Labor in Biofilms : the Ecology of Cell Differentiation. *Microbiology Spectrum*.

- Giglio, K. M., Caberoy, N., Suen, G., Kaiser, D., & Garza, A. G. (2011). A cascade of coregulating enhancer binding proteins initiates and propagates a multicellular developmental program. *Proceedings of the National Academy of Sciences*, *108*(32), E431–E439.
- Giglio, K. M., Eisenstatt, J., & Garza, A. G. (2010). Identification of enhancer binding proteins important for *Myxococcus xanthus* development. *Journal of Bacteriology*.
- Gloag, E. S., Javed, M. A., Wang, H., Gee, M. L., Wade, S. A., Turnbull, L., & Whitchurch, C. B. (2013). Stigmergy: A key driver of self-organization in bacterial biofilms. *Communicative and Integrative Biology*, *6*(6).
- Goldman, B. S., Nierman, W. C., Kaiser, D., Slater, S. C., Durkin, A. S., Eisen, J. A., ... Kaplan, H. B. (2006). Evolution of sensory complexity recorded in a myxobacterial genome. *Proceedings of the National Academy of Sciences*, *103*(41), 15200–15205.
- Goodall, E. C. A., Robinson, A., Johnston, I. G., Jabbari, S., Turner, K. A., Cunningham, A. F., ... Henderson, I. R. (2018). The essential genome of *Escherichia coli* K-12. *MBio*.
- Grosberg, R. K., & Strathmann, R. R. (1998). One cell, two cell, red cell, blue cell: The persistence of a unicellular stage in multicellular life histories. *Trends in Ecology and Evolution*.
- Harvey, C. W., Du, H., Xu, Z., Kaiser, D., Aranson, I., & Alber, M. (2012). Interconnected Cavernous Structure of Bacterial Fruiting Bodies. *PLoS Computational Biology*, *8*(12).
- Heimann, J. D. (2002). *The extracytoplasmic function (ECF) sigma factors*. *Advances in Microbial Physiology* (Vol. 46).
- Hemelrijk, C. K., & Hildenbrandt, H. (2012). Schools of fish and flocks of birds: Their shape and internal structure by self-organization. *Interface Focus*.
- Hesse, J., & Gross, T. (2014). Self-organized criticality as a fundamental property of neural systems. *Frontiers in Systems Neuroscience*, *8*.
- Hodgkin, J., & Kaiser, D. (1979a). Genetics of gliding motility in *Myxococcus xanthus* (Myxobacterales): Genes controlling movement of single cells. *MGG Molecular & General Genetics*, *171*(2), 167–176.
- Hodgkin, J., & Kaiser, D. (1979b). Genetics of gliding motility in *Myxococcus xanthus* (Myxobacterales): Two gene systems control movement. *MGG Molecular & General Genetics*, *171*(2), 177–191.
- Hofer, T., Sherratt, J. A., & Maini, P. K. (1995). *Dictyostelium discoideum*: Cellular self-organization in an excitable biological medium. *Proceedings of the Royal Society B: Biological Sciences*, *259*(1356), 249–257.
- Horiuchi, T., Taoka, M., Isobe, T., Komano, T., & Inouye, S. (2002). Role of fruA and csgA genes in gene expression during development of *Myxococcus xanthus*. Analysis by two-dimensional gel electrophoresis. *Journal of Biological Chemistry*, *277*(30).

- Igoshin, O. A., Mogilner, A., Welch, R. D., Kaiser, D., & Oster, G. (2001). Pattern formation and traveling waves in myxobacteria : Theory and modeling, *98*(26), 14913–14918.
- Igoshin, O. A., Welch, R., Kaiser, D., & Oster, G. (2004). Waves and aggregation patterns in myxobacteria. *Proceedings of the National Academy of Sciences of the United States of America*, *101*(12), 4256–4261.
- Igoshin, O. A., Welch, R., Kaiser, D., & Oster, G. (2004b). Waves and aggregation patterns in myxobacteria.
- Igoshin, O. a, Goldbeter, A., Kaiser, D., & Oster, G. (2004). A biochemical oscillator explains several aspects of *Myxococcus xanthus* behavior during development. *Proceedings of the National Academy of Sciences of the United States of America*, *101*(44), 15760–15765.
- Jakovljevic, V., Leonardy, S., Hoppert, M., & Søgaaard-Andersen, L. (2008). PilB and PilT are ATPases acting antagonistically in type IV pilus function in *Myxococcus xanthus*. *Journal of Bacteriology*, *190*(7), 2411–2421.
- Jelsbak, L., & Sogaard-Andersen, L. (1999). The cell surface-associated intercellular C-signal induces behavioral changes in individual *Myxococcus xanthus* cells during fruiting body morphogenesis. *Proc Natl Acad Sci U S A*, *96*(9), 5031–5036.
- Jelsbak, L., & Søgaaard-Andersen, L. (2000). Pattern formation: Fruiting body morphogenesis in *Myxococcus xanthus*. *Current Opinion in Microbiology*, *3*(6), 637–642.
- Jelsbak, L., & Søgaaard-Andersen, L. (2002). Pattern formation by a cell surface-associated morphogen in *Myxococcus xanthus*. *Proceedings of the National Academy of Sciences of the United States of America*, *99*(Track II), 2032–2037.
- Jelsbak, L., & Søgaaard-Andersen, L. (2003). Cell behavior and cell-cell communication during fruiting body morphogenesis in *Myxococcus xanthus*. In *Journal of Microbiological Methods* (Vol. 55, pp. 829–839).
- Kaimer, C., & Zusman, D. R. (2016). Regulation of cell reversal frequency in *Myxococcus xanthus* requires the balanced activity of CheY-like domains in FrzE and FrzZ. *Molecular Microbiology*.
- Kaiser, D. (2003). Coupling cell movement to multicellular development in myxobacteria. *Nature Reviews Microbiology*, *1*(1), 45–54.
- Kaiser, D. (2004). Signaling in myxobacteria. *Annual Review of Microbiology*, *58*(1), 75–98.
- Kaiser, D., & Crosby, C. (1983). Cell movements and its coordination in swarms of *Myxococcus xanthus*. *Cell Motil.*, *3*, 227–245.
- Kaiser, D., & Welch, R. (2004). Dynamics of Fruiting Body Morphogenesis Dynamics of Fruiting Body Morphogenesis, *186*(4).
- Kaiser, D., & Welch, R. (2004). Dynamics of Fruiting Body Morphogenesis. *Journal of Bacteriology*, *186*(4), 919–927.

- Kaplan, H. B., & Plamann, L. (1996). A *Myxococcus xanthus* cell density-sensing system required for multicellular development. *FEMS Microbiology Letters*.
- Kearns, D. B., & Shimkets, L. J. (1998). Chemotaxis in a gliding bacterium. *Proceedings of the National Academy of Sciences*, 95(20), 11957–11962.
- Kearns, D. B., Venot, a, Bonner, P. J., Stevens, B., Boons, G. J., & Shimkets, L. J. (2001). Identification of a developmental chemoattractant in *Myxococcus xanthus* through metabolic engineering. *Proceedings of the National Academy of Sciences of the United States of America*, 98(24), 13990–13994.
- Keseler, I. M., & Kaiser, D. (1995). An early A-signal-dependent gene in *Myxococcus xanthus* has a σ^{54} -like promoter. *Journal of Bacteriology*, 177(16), 4638–4644.
- Kim, S. K., & Kaiser, a D. (1990a). C-factor: A cell-cell signaling protein required for fruiting body morphogenesis of *M. xanthus*. *Cell*, 61, 19–26.
- Kim, S. K., & Kaiser, D. (1990b). Purification and properties of *Myxococcus xanthus* C-factor, an intercellular signaling protein. *Proceedings of the National Academy of Sciences of the United States of America*, 87(10), 3635–3639.
- Kim, S. K., & Kaiser, D. (1991). C-factor has distinct aggregation and sporulation thresholds during *Myxococcus* development. *Journal of Bacteriology*, 173(5), 1722–1728.
- Konovalova, A., Petters, T., & Sjøgaard-Andersen, L. (2010). Extracellular biology of *Myxococcus xanthus*. *FEMS Microbiology Reviews*.
- Kroos, L., Hartzell, P., Stephens, K., & Kaiser, D. (1988). A link between cell movement and gene expression argues that motility is required for cell-cell signaling during fruiting body development, (1978), 1677–1685.
- Kroos, L., & Kaiser, D. (1987). Expression of many developmentally regulated genes in *Myxococcus* depends on a sequence of cell interactions. *Genes & Development*, 1(8), 840–854.
- Kruse, T., Lobedanz, S., Berthelsen, N. M. S., & Sjøgaard-Andersen, L. (2001). C-signal: A cell surface-associated morphogen that induces and co-ordinates multicellular fruiting body morphogenesis and sporulation in *Myxococcus xanthus*. *Molecular Microbiology*, 40(1), 156–168.
- Kuner, J. M., & Kaiser, D. (1982). Fruiting body morphogenesis in submerged cultures of *Myxococcus xanthus*. *Journal of Bacteriology*, 151(1), 458–461.
- Kunert, J. M., & Kaiser, D. (1982). Fruiting body morphogenesis in submerged cultures of *Myxococcus xanthus*. Fruiting Body Morphogenesis in Submerged Cultures of *Myxococcus xanthus*, 151(1), 458–461.
- Kuspa, A., Kroos, L., & Kaiser, D. (1986). Intercellular signaling is required for developmental gene expression in *Myxococcus xanthus*. *Dev Biol*, 117(1), 267–276.

- Kuspa, A., Plamann, L., & Kaiser, D. (1992). Identification of heat-stable A-factor from *Myxococcus xanthus*. *Journal of Bacteriology*, *174*(10), 3319–3326.
- Lambert, G., Bergman, A., Zhang, Q., Bortz, D., & Austin, R. (2014). Physics of biofilms: The initial stages of biofilm formation and dynamics. *New Journal of Physics*.
- Lancero, H., Caberoy, N. B., Castaneda, S., Li, Y., Lu, A., Dutton, D., ... Garza, A. G. (2004). Characterization of a *Myxococcus xanthus* mutant that is defective for adventurous motility and social motility. *Microbiology*, *150*(12), 4085–4093.
- Lee, B. U., Lee, K., Mendez, J., & Shimkets, L. J. (1995). A tactile sensory system of *Myxococcus xanthus* involves an extracellular NAD(P)⁺-containing protein. *Genes and Development*, *9*(23), 2964–2973.
- Lett, C., Silber, C., & Barret, N. (1999). Comparison of a cellular automata network and an individual-based model for the simulation of forest dynamics. *Ecological Modelling*, *121*(2–3), 277–293.
- Levine, H., & Ben-Jacob, E. (2004). Physical schemata underlying biological pattern formation - Examples, issues and strategies. *Physical Biology*.
- Li, S., Lee, B. U., & Shimkets, L. J. (1992). csgA expression entrains *Myxococcus xanthus* development. *Genes and Development*, *6*(3), 401–410.
- Li, Y., Sun, H., Ma, X., Lu, A., Lux, R., Zusman, D., & Shi, W. (2003). Extracellular polysaccharides mediate pilus retraction during social motility of *Myxococcus xanthus*. *Proceedings of the National Academy of Sciences*, *100*(9), 5443–5448.
- Lobedanz, S., & Søgaard-Andersen, L. (2003). Identification of the C-signal, a contact-dependent morphogen coordinating multiple developmental responses in *Myxococcus xanthus*. *Genes and Development*, *17*(17), 2151–2161.
- Lonski, J., Heromin, R., & Ingraham, D. (1977). A quantitative assay to study cell movement in the myxobacteria. *Journal of Cell Science*, *25*, 173–178.
- Lueders, T., Kindler, R., Miltner, A., Friedrich, M. W., & Kaestner, M. (2006). Identification of bacterial micropredators distinctively active in a soil microbial food web. *Applied and Environmental Microbiology*, *72*(8), 5342–5348.
- Lux, R., Li, Y., Lu, A., & Shi, W. (2004). Detailed three-dimensional analysis of structural features of *Myxococcus xanthus* fruiting bodies using confocal laser scanning microscopy. *Biofilms*, *1*(4), 293–303.
- Lyons, N. A., & Kolter, R. (2015). On the evolution of bacterial multicellularity. *Current Opinion in Microbiology*.
- Manoil, C., & Kaiser, D. (1980a). Accumulation of guanosine tetraphosphate and guanosine pentaphosphate in *Myxococcus xanthus* during starvation and myxospore formation. *Journal of Bacteriology*, *141*(1), 297–304.

- Manoil, C., & Kaiser, D. (1980b). Guanosine pentaphosphate and guanosine tetraphosphate accumulation and induction of *Myxococcus xanthus* fruiting body development. *Journal of Bacteriology*, *141*(1), 305–315.
- Marchetti, M. C., Joanny, J. F., Ramaswamy, S., Liverpool, T. B., Prost, J., Rao, M., & Simha, R. A. (2013). Hydrodynamics of soft active matter. *Reviews of Modern Physics*, *85*(3), 1143–1189.
- Maree, A. F. M., & Hogeweg, P. (2001). How amoeboids self-organize into a fruiting body: Multicellular coordination in *Dictyostelium discoideum*. *Proceedings of the National Academy of Sciences*.
- Mauriello, E. M. F., Nan, B., & Zusman, D. R. (2009). AglZ regulates adventurous (A-) motility in *Myxococcus xanthus* through its interaction with the cytoplasmic receptor, FrzCD. *Molecular Microbiology*, *72*(4), 964–977.
- Mauriello, E. M., & Zusman, D. R. (2007). Polarity of motility systems in *Myxococcus xanthus*. *Current Opinion in Microbiology*.
- McBride, M. J., Weinberg, R. a, & Zusman, D. R. (1989). “Frizzy” aggregation genes of the gliding bacterium *Myxococcus xanthus* show sequence similarities to the chemotaxis genes of enteric bacteria. *Proceedings of the National Academy of Sciences of the United States of America*, *86*(2), 424–428.
- McCleary, W. R., McBride, M. J., & Zusman, D. R. (1990). Developmental sensory transduction in *Myxococcus xanthus* involves methylation and demethylation of FrzCD. *Journal of Bacteriology*, *172*(9), 4877–4887.
- Meiser, P., Bode, H. B., & Müller, R. (2006). The unique DKxanthene secondary metabolite family from the myxobacterium *Myxococcus xanthus* is required for developmental sporulation. *Proceedings of the National Academy of Sciences of the United States of America*, *103*(50), 19128–19133.
- Mignot, T., Merlie, J. P., & Zusman, D. R. (2005). Regulated pole-to-pole oscillations of a bacterial gliding motility protein. *Science*, *310*(5749), 855–857.
- Missiakas, D., & Raina, S. (1998). The extracytoplasmic function sigma factors: role and regulation. *Molecular Microbiology*, *28*(6), 1059–1066.
- Morrison, C. E., & Zusman, D. R. (1979). *Myxococcus xanthus* mutants with temperature-sensitive, stage-specific defects: Evidence for independent pathways in development. *Journal of Bacteriology*, *140*(3), 1036–1042.
- Muñoz-Dorado, J., Marcos-Torres, F. J., García-Bravo, E., Moraleda-Muñoz, A., & Pérez, J. (2016). Myxobacteria: Moving, killing, feeding, and surviving together. *Frontiers in Microbiology*, *7*(MAY), 1–18.
- Müller, F. D., Schink, C. W., Hoiczky, E., Cserti, E., & Higgs, P. I. (2012). Spore formation in *Myxococcus xanthus* is tied to cytoskeleton functions and polysaccharide spore coat deposition. *Molecular Microbiology*, *83*(3), 486–505.

- Müller, F. D., Treuner-Lange, A., Heider, J., Huntley, S. M., & Higgs, P. I. (2010). Global transcriptome analysis of spore formation in *Myxococcus xanthus* reveals a locus necessary for cell differentiation. *BMC Genomics*, *11*(1).
- Murata, Y., & Ohnishi, T. (1980). Dictyostelium discoideum fruiting bodies observed by scanning electron microscopy. *Journal of Bacteriology*, *141*(2), 956–958.
- Nan, B., Chen, J., Neu, J. C., Berry, R. M., Oster, G., & Zusman, D. R. (2011). Myxobacteria gliding motility requires cytoskeleton rotation powered by proton motive force. *Proceedings of the National Academy of Sciences*, *108*(6), 2498–2503.
- O'Connor, K. A., & Zusman, D. R. (1989). Patterns of cellular interactions during fruiting-body formation in *Myxococcus xanthus*. *Journal of Bacteriology*, *171*(11), 6013–6024.
- O'Connor, K. A., & Zusman, D. R. (1991). Development in *Myxococcus xanthus* involves differentiation into two cell types, peripheral rods and spores. *Journal of Bacteriology*, *173*(11), 3318–3333.
- Parish, J. H., Wedgwood, K. R., & Herries, D. G. (1976). Morphogenesis in *Myxococcus xanthus* and *Myxococcus virescens* (Myxobacterales). *Archives of Microbiology*, *107*(3), 343–351.
- Parrish, J. K., Viscido, S. V., & Grünbaum, D. (2002). Self-organized fish schools: An examination of emergent properties. In *Biological Bulletin* (Vol. 202, pp. 296–305).
- Pelling, A. E., Li, Y., Cross, S. E., Castaneda, S., Shi, W., & Gimzewski, J. K. (2006). Self-organized and highly ordered domain structures within swarms of *Myxococcus xanthus*. *Cell Motility and the Cytoskeleton*, *63*(3), 141–148.
- PERSSON, B., KROOK, M., & JÖRNVALL, H. (1991). Characteristics of short-chain alcohol dehydrogenases and related enzymes. *European Journal of Biochemistry*, *200*(2), 537–543.
- Pipe, L. Z., & Grimson, M. J. (1995). Computer Simulations of Bacterial-Colony Formation.
- Plamann, L., Davis, J. M., Cantwell, B., & Mayor, J. (1994). Evidence that asgB encodes a DNA-binding protein essential for growth and development of *Myxococcus xanthus*. *J Bacteriol*, *176*(7), 2013–2020.
- Plamann, L., Kuspa, A., & Kaiser, D. (1992). Proteins that rescue A-signal-defective mutants of *Myxococcus xanthus*. *Journal of Bacteriology*, *174*(10), 3311–3318.
- Plamann, L., Li, Y., Cantwell, B., & Mayor, J. (1995). The *Myxococcus xanthus* asgA gene encodes a novel signal transduction protein required for multicellular development. *J Bacteriol*, *177*(8), 2014–2020.
- Potvin, E., Sanschagrin, F., & Levesque, R. C. (2008). Sigma factors in *Pseudomonas aeruginosa*. *FEMS Microbiology Reviews*.
- Ratcliff, W. C., Denison, R. F., Borrello, M., & Travisano, M. (2012). Experimental evolution of multicellularity. *Proceedings of the National Academy of Sciences*, *109*(5), 1595–1600.
- Reichenbach, H. (1999). The ecology of the myxobacteria. *Environmental Microbiology*.

- Ring, M. W., Schwär, G., Thiel, V., Dickschat, J. S., Kroppenstedt, R. M., Schulz, S., & Bode, H. B. (2006). Novel iso-branched ether lipids as specific markers of developmental sporulation in the myxobacterium *Myxococcus xanthus*. *Journal of Biological Chemistry*, 281(48), 36691–36700.
- Rolbetzki, A., Ammon, M., Jakovljevic, V., Konovalova, A., & Søggaard-Andersen, L. (2008). Regulated Secretion of a Protease Activates Intercellular Signaling during Fruiting Body Formation in *M. xanthus*. *Developmental Cell*, 15(4), 627–634.
- Rosenberg, E., Keller, K. H., & Dworkin, M. (1977). Cell density-dependent growth of *Myxococcus xanthus* on casein. *Journal of Bacteriology*, 129(2), 770–777.
- Sager, B., & Kaiser, D. (1993). Two cell-density domains within the *Myxococcus xanthus* fruiting body. *Proceedings of the National Academy of Sciences of the United States of America*, 90(8), 3690–3694.
- Sager, B., & Kaiser, D. (1993). Spatial restriction of cellular differentiation. *Genes and Development*, 7(9), 1645–1653.
- Sarwar, Z., & Garza, A. G. (2015). Two-component signal transduction systems that regulate the temporal and spatial expression of *Myxococcus xanthus* sporulation genes. *Journal of Bacteriology*. <https://doi.org/10.1128/JB.00474-15>
- Schirrmeister, B. E., Antonelli, A., & Bagheri, H. C. (2011). The origin of multicellularity in cyanobacteria. *BMC Evolutionary Biology*, 11(1).
- Shapiro, J. a. (1988). Bacteria as Multicellular Organisms. *Scientific American*, 258(6), 82–89.
- Shapiro, J. A. (1995). The significances of bacterial colony patterns. *BioEssays*.
- Shi, W., Kohler, T., & Zusman, D. R. (1993). Chemotaxis plays a role in the social behaviour of *Myxococcus xanthus*. *Mol Microbiol*, 9(3), 601–611.
- Shi, W., Ngok, F. K., & Zusman, D. R. (1996a). Cell density regulates cellular reversal frequency in *Myxococcus xanthus*. *Proceedings of the National Academy of Sciences of the United States of America*, 93(9), 4142–4146.
- Shi, W., Ngok, F. K., & Zusman, D. R. (1996b). Cell density regulates cellular reversal frequency in *Myxococcus xanthus*. *Proceedings of the National Academy of Sciences of the United States of America*, 93(9), 4142–4146.
- Shi, W., & Zusman, D. R. (1993). The two motility systems of *Myxococcus xanthus* show different selective advantages on various surfaces. *Proceedings of the National Academy of Sciences of the United States of America*, 90(8), 3378–3382.
- Shimkets, L. J. (1999). Intercellular Signaling During Fruiting-Body Development of *Myxococcus xanthus*. *Annual Review of Microbiology*, 53(1), 525–549.

- Shimkets, L., & Seale, T. W. (1975). Fruiting body formation and myxospore differentiation and germination in *Myxococcus xanthus* viewed by scanning electron microscopy. *Journal of Bacteriology*, 121(2), 711–720.
- Siegert, F., & Weijer, C. J. (1995). Spiral and concentric waves organize multicellular Dictyostelium mounds. *Current Biology*, 5(8), 937–943.
- Singer, M., & Kaiser, D. (1995). Ectopic production of guanosine penta- and tetraphosphate can initiate early developmental gene expression in *Myxococcus xanthus*. *Genes and Development*, 9(13), 1633–1644.
- Sliusarenko, O., Neu, J., Zusman, D. R., & Oster, G. (2006). Accordion waves in *Myxococcus xanthus*, 103(5).
- Sliusarenko, O., Zusman, D. R., & Oster, G. (2007a). Aggregation during fruiting body formation in *Myxococcus xanthus* is driven by reducing cell movement. *Journal of Bacteriology*, 189(2), 611–619.
- Sliusarenko, O., Zusman, D. R., & Oster, G. (2007b). Aggregation during Fruiting Body Formation in *Myxococcus xanthus* Is Driven by Reducing Cell Movement □ †, 189(2), 611–619.
- Sliusarenko, O., Zusman, D. R., & Oster, G. (2007c). The motors powering A-motility in *Myxococcus xanthus* are distributed along the cell body. *Journal of Bacteriology*, 189(21), 7920–7921.
- Søgaard-Andersen, L., & Kaiser, D. (1996). C factor, a cell-surface-associated intercellular signaling protein, stimulates the cytoplasmic Frz signal transduction system in *Myxococcus xanthus*. *Proceedings of the National Academy of Sciences of the United States of America*, 93(7), 2675–2679.
- Souza, B. M., de Castro, T. L. P., de Carvalho, R. D. O., Seyffert, N., Silva, A., Miyoshi, A., & Azevedo, V. (2014). σ ECF factors of gram-positive bacteria: A focus on *Bacillus subtilis* and the CMNR group. *Virulence*.
- Sozinova, O., Jiang, Y., Kaiser, D., & Alber, M. (2005). A three-dimensional model of myxobacterial aggregation by contact-mediated interactions. *Proceedings of the National Academy of Sciences of the United States of America*, 102(32), 11308–11312.
- Sozinova, O., Jiang, Y., Kaiser, D., & Alber, M. (2006). A three-dimensional model of myxobacterial fruiting-body formation. *Proceedings of the National Academy of Sciences of the United States of America*, 103(46), 17255–17259.
- Spormann, A. M. (1999). Gliding motility in bacteria: insights from studies of *Myxococcus xanthus*. *Microbiology and Molecular Biology Reviews : MMBR*.
- Spormann, A. M., & Kaiser, A. D. (1995). Gliding movements in *Myxococcus xanthus*. *Journal of Bacteriology*, 177(20), 5846–5852.

- Spormann, A. M., & Kaiser, D. (1999). Gliding mutants of *Myxococcus xanthus* with high reversal frequencies and small displacements. *Journal of Bacteriology*, 181(8), 2593–2601.
- Stevens, A., & Søgaard-Andersen, L. (2005). Making waves: Pattern formation by a cell-surface-associated signal. *Trends in Microbiology*.
- Sun, H., & Shi, W. (2001). Genetic studies of *mrp*, a locus essential for cellular aggregation and sporulation of *Myxococcus xanthus*. *Journal of Bacteriology*, 183(16), 4786–4795.
- Sun, H., Zusman, D. R., & Shi, W. (2000). Type IV pilus of *Myxococcus xanthus* is a motility apparatus controlled by the *frz* chemosensory system. *Current Biology*, 10(18), 1143–1146.
- Swiecicki, J. M., Sliusarenko, O., & Weibel, D. B. (2013). From swimming to swarming: *Escherichia coli* cell motility in two-dimensions. *Integrative Biology (United Kingdom)*, 5(12), 1490–1494.
- Taniguchi, H., & Wendisch, V. F. (2015). Exploring the role of sigma factor gene expression on production by *Corynebacterium glutamicum*: Sigma factor H and FMN as example. *Frontiers in Microbiology*.
- Theraulaz, G., Bonabeau, E., Nicolis, S. C., Solé, R. V., Fourcassié, V., Blanco, S., ... Deneubourg, J.-L. (2002). Spatial patterns in ant colonies. *Proceedings of the National Academy of Sciences of the United States of America*, 99(15), 9645–9649.
- Thompson, O., Edgley, M., Strasbourger, P., Flibotte, S., Ewing, B., Adair, R., ... Waterston, R. H. (2013). The million mutation project: A new approach to genetics in *Caenorhabditis elegans*. *Genome Research*.
- Thony-Meyer, L., & Kaiser, D. (1993). *devRS*, an autoregulated and essential genetic locus for fruiting body development in *Myxococcus xanthus*. *Journal of Bacteriology*, 175(22), 7450–7462.
- Thutupalli, S., Sun, M., Bunyak, F., Palaniappan, K., & Shaevez, J. W. (2015). Directional reversals enable *Myxococcus xanthus* cells to produce collective one-dimensional streams during fruiting-body formation. *Journal of the Royal Society Interface*, 12(109).
- Tzeng, L., & Singer, M. (2005). DNA replication during sporulation in *Myxococcus xanthus* fruiting bodies. *Proceedings of the National Academy of Sciences of the United States of America*, 102(40), 14428–14433.
- Ueki, T., & Inouye, S. (2003). Identification of an activator protein required for the induction of *fruA*, a gene essential for fruiting body development in *Myxococcus xanthus*. *Proceedings of the National Academy of Sciences*, 100(15), 8782–8787.
- Van De Koppel, J., Gascoigne, J. C., Theraulaz, G., Rietkerk, M., Mooij, W. M., & Herman, P. M. J. (2008). Experimental evidence for spatial self-organization and its emergent effects in mussel bed ecosystems. *Science*, 322(5902), 739–742.

- Velicer, G. J., Raddatz, G., Keller, H., Deiss, S., Lanz, C., Dinkelacker, I., & Schuster, S. C. (2006). Comprehensive mutation identification in an evolved bacterial cooperators and its cheating ancestor. *Proceedings of the National Academy of Sciences*, *103*(21), 8107–8112.
- Velicer, G. J., & Vos, M. (2009). Sociobiology of the Myxobacteria. *Annual Review of Microbiology*, *63*(1), 599–623.
- Viswanathan, P., Murphy, K., Julien, B., Garza, A. G., & Kroos, L. (2007). Regulation of dev, an operon that includes genes essential for *Myxococcus xanthus* development and CRISPR-associated genes and repeats. *Journal of Bacteriology*.
- Von Bodman, S. B., Willey, J. M., & Diggle, S. P. (2008). Cell-cell communication in bacteria: United we stand. In *Journal of Bacteriology*.
- Webb, A. J., Thorisson, G. A., & Brookes, A. J. (2011). An informatics project and online “Knowledge Centre” supporting modern genotype-to-phenotype research. *Human Mutation*.
- Welch, R., & Kaiser, D. (2001a). Cell behavior in traveling wave patterns of myxobacteria. *Proceedings of the National Academy of Sciences of the United States of America*, *98*(26), 14907–14912. h
- Welch, R., & Kaiser, D. (2001b). Cell behavior in traveling wave patterns of myxobacteria.
- Wennekamp, S., Mesecke, S., Nédélec, F., & Hiiragi, T. (2013). A self-organization framework for symmetry breaking in the mammalian embryo. *Nature Reviews Molecular Cell Biology*.
- West, S. A., Griffin, A. S., Gardner, A., & Diggle, S. P. (2006). Social evolution theory for microorganisms. *Nature Reviews Microbiology*.
- Wolgemuth, C., Hoiczky, E., Kaiser, D., & Oster, G. (2002). How myxobacteria glide. *Current Biology*, *12*(5), 369–377.
- Wu, S. S., & Kaiser, D. (1995). Genetic and functional evidence that Type IV pili are required for social gliding motility in *Myxococcus xanthus*. *Molecular Microbiology*, *18*(3), 547–558.
- Xie, C., Zhang, H., Shimkets, L. J., & Igoshin, O. A. (2011). Statistical image analysis reveals features affecting fates of *Myxococcus xanthus* developmental aggregates. *Proceedings of the National Academy of Sciences*, *108*(14), 5915–5920.
- Yang, R., Bartle, S., Otto, R., Stassinopoulos, A., Rogers, M., Plamann, L., & Hartzell, P. (2004). AglZ is a filament-forming coiled-coil protein required for adventurous gliding motility of *Myxococcus xanthus*. *Journal of Bacteriology*, *186*(18), 6168–6178.
- Yang, Z., Geng, Y., Xu, D., Kaplan, H. B., & Shi, W. (1998). A new set of chemotaxis homologues is essential for *Myxococcus xanthus* social motility. *Molecular Microbiology*, *30*(5), 1123–1130.
- Yang, Z., Ma, X., Tong, L., Kaplan, H. B., Shimkets, L. J., & Shi, W. (2000). *Myxococcus xanthus* dif genes are required for biogenesis of cell surface fibrils essential for social gliding motility. *Journal of Bacteriology*, *182*(20), 5793–5798.

- Zhang, H., Angus, S., Tran, M., Xie, C., Igoshin, O. A., & Welch, R. D. (2011). Quantifying aggregation dynamics during *Myxococcus xanthus* development. *Journal of Bacteriology*, *193*(19), 5164–5170.
- Zhang, H., Vaksman, Z., Litwin, D. B., Shi, P., Kaplan, H. B., & Igoshin, O. A. (2012). The Mechanistic Basis of *Myxococcus xanthus* Rippling Behavior and Its Physiological Role during Predation. *PLoS Computational Biology*, *8*(9).
- Zhang, Y., Ducret, A., Shaevitz, J., & Mignot, T. (2012). From individual cell motility to collective behaviors: Insights from a prokaryote, *Myxococcus xanthus*. *FEMS Microbiology Reviews*.
- Zhang, Z., Igoshin, O. A., Cotter, C. R., & Shimkets, L. J. (2018). Agent-Based Modeling Reveals Possible Mechanisms for Observed Aggregation Cell Behaviors in *Myxococcus xanthus*, 1–41.
- Zhou, T., & Nan, B. (2017). Exopolysaccharides promote *Myxococcus xanthus* social motility by inhibiting cellular reversals. *Molecular Microbiology*, *103*(4), 729–743.
- Zusman, D. R. (1982). “Frizzy” mutants: A new class of aggregation-defective developmental mutants of *Myxococcus xanthus*. *Journal of Bacteriology*, *150*(3), 1430–1437.
- Zusman, D. R., Scott, A. E., Yang, Z., & Kirby, J. R. (2007). Chemosensory pathways, motility and development in *Myxococcus xanthus*. *Nature Reviews Microbiology*.

Chapter 3: A Motility-Induced Phase Transition Drives

***Myxococcus xanthus* Aggregation**

This chapter has been submitted as below with some modifications. Majority of experimental data was done by me. Guannan Liu*, Adam Patch*, Fatmagül Bahar*, David Yllanes, Roy D. Welch, M. Cristina Marchetti, Shashi Thutupalli, and Joshua W. Shaevitz. A motility-induced phase transition drives *Myxococcus xanthus* aggregation. Physical Review Letters 2018.

* These authors contributed equally to this work.

3.1 Abstract

A hallmark of living systems is their ability to generate complex spatial patterns at the molecular, cellular, and multicellular levels. Many such systems rely on coupled biochemical and genetic signaling mechanisms that can produce large-scale organization. Long-range order and patterning can also emerge, however, through purely mechanical interactions. Here, we study starvation-induced fruiting body (FB) formation in gliding *Myxococcus xanthus* bacteria and show that these cells induce a dewetting phase separation by tuning their motility over time. By experimentally controlling the density and speed of gliding cells, tracking individual cells in large populations, and performing numerical simulations of moving particles, we show that FB formation can be understood with a single-phase diagram in terms of cell density and a dimensionless Péclet number that encompasses the key cell motility parameters of speed and reversal frequency. We further track changes in motility that naturally occur upon starvation and show that a reduction of the reversal frequency and an increase in gliding speed change the Péclet number to favor FB formation. Thus, *M. xanthus* evolved to take advantage of an active-matter phase transition that can be controlled through changes in motility at the individual cell level without complex feedback and chemical communication between cells to change population-level behavior.

3.2 Introduction

Unicellular organisms such as bacteria and amoeba are sometimes capable of spontaneously organizing into complex multicellular structures (Dormann, Vasiev, & Weijer, 2002; Laub & Loomis, 1998). A striking example of such collective behavior is the starvation-induced organization of the rod-shaped, soil-dwelling bacterium *M. xanthus* into macroscopic,

multicellular droplets known as “fruiting bodies” (Zusman, Scott, Yang, & Kirby, 2007). When nutrients are scarce, starving *M. xanthus* cells undergo a multicellular process of self-organization during which cells move to form dome-shaped droplets comprising hundreds of thousands of cells. A subset of cells at the center of each droplet differentiate to form metabolically quiescent spores that can survive long periods of starvation (Konovalova, Petters, & Sørensen, 2010; Shimkets, 1990; Zusman et al., 2007).

Superficially, the striking phenotypic similarity between FB formation in the amoeba *D. discoideum* and *M. xanthus* has led to the longstanding hypothesis that *M. xanthus* FB formation is driven by long-range chemical signaling mechanisms as it is in the amoeba. However, despite decades of research, the links between spatial chemical cues and the direct mechanisms of FB formation remain unclear. Although *M. xanthus* cells are known to employ chemical communication to initiate FB formation (termed A-signaling) (Kuspa, Plamann, & Kaiser, 1992), to potentially synchronize reversal frequency (termed C- signaling) (Lobedanz & Sørensen, 2003; Shimkets & Rafiee, 1990), and to communicate through the production of mucopolysaccharide “slime trails” that other cells can sense and follow (Burchard, 1982), a quantitative understanding of the mechanisms that drive aggregation has remained elusive.

Both the biochemical and mechanical aspects of multicellular organization are driven by the dissipation of chemical energy keeping the system far from equilibrium. Efforts to understand collective behavior in far from equilibrium systems from generic interactions between individuals in large ensembles have led to statistical approaches predicting broadly applicable organizational principles, phase transitions, and scaling laws (Cates, Marenduzzo, Pagonabarraga, & Tailleur, 2010; Marchetti et al., 2013; Ramaswamy, 2010). In the past decade, hydrodynamic theories have

been developed (Marchetti et al., 2013) to understand the large-scale, long-time behavior of a wide class of active systems, defined as out of equilibrium systems comprised of individual units each consuming and dissipating energy. Active matter theories (Ramaswamy, 2010) have been successfully applied to such diverse phenomena as bird and animal flocks (Cavagna & Giardina, 2014), tissue-level changes during embryogenesis (Popović et al., 2017), collective cell migration in wound healing (Banerjee, Utuje, & Marchetti, 2015), pattern formation in motile microorganisms (Cates et al., 2010), the assembly of the mitotic spindle (Brugués & Needleman, 2014), and synthetic active systems (Bricard, Caussin, Desreumaux, Dauchot, & Bartolo, 2013).

Perhaps the most remarkable properties of systems comprised of self-propelled units are their ability to spontaneously generate flows (Ramaswamy, 2010) and to phase separate into dense and dilute phases even in the absence of attractive interactions (Fily & Marchetti, 2012). As a consequence of the breaking of detailed balance at the microscale, populations of motile individuals can undergo spontaneous aggregation without the need for additional signaling mechanisms or cohesive forces between individual units (Liu et al., 2013).

Phase separation arises when the time for self-propelled units to reorient their direction of motion after a collision exceeds the mean free time between collisions, giving rise to the formation of long-lived clusters of particles. This phenomenon, which does not have a counter-part in passive systems where the constituents move via random thermal excitations, has been termed motility-induced phase separation (MIPS) (Cates & Tailleur, 2015; Fily, Henkes, & Marchetti, 2014; Fily & Marchetti, 2012; Cristina Marchetti, Fily, Henkes, Patch, & Yllanes, 2016; Redner, Baskaran, & Hagan, 2013). The dynamics of the phase separation process is controlled by the initial density

of the units and can be quantified in terms of the non-dimensional inverse rotational Péclet number, the ratio of particle size ℓ_c to the persistence length ℓ_p ,

$$\text{Pe}_r^{-1} = \ell_c/\ell_p = \ell_c D_r/v_0 \quad (1)$$

where v_0 is the self-propulsion speed and D_r is the rotational diffusion coefficient of cells. Starting from a homogeneous dilute system, increasing density or decreasing the inverse Péclet number will favor first the nucleation of short-lived clusters and then spontaneous spinodal decomposition into bulk phase separated gas and condensed states. Data obtained in systems of varying motility and rotational diffusion rate can be organized into a phase diagram controlled entirely by Pe_r^{-1} and the density.

By examining the spatial density profile of aggregating cells combined with single-cell tracking and active-particle simulation, we show that the dynamical mechanism underlying *M. xanthus* aggregation is a MIPS process. At low cell density, the aggregation occurs via a nucleation-and-growth process whereby small aggregates appear asynchronously and grow steadily as development proceeds. At high cell density, the dynamics resemble a spontaneous spinodal-like process, with phase separation occurring everywhere at once, resulting in a connected network of allantoid aggregates that then resolve into circular aggregates during development (Fig. 3-1). We control the motility properties of gliding cells using a mutant strain and chemical perturbations to show that when scaled in terms of an effective Péclet number constructed by independent measures of *M. xanthus* motility parameters, the experimental data can be organized into a phase diagram that shows striking quantitative correspondence to that of active Brownian particles. Additionally, the observed kinetics of aggregate growth agree quantitatively with that of MIPS coarsening. We

conclude that, when starved, *M. xanthus* cells dynamically regulate their motility properties to traverse phase space and position the population in a region of low effective inverse Péclet number where spontaneous phase separation occurs.

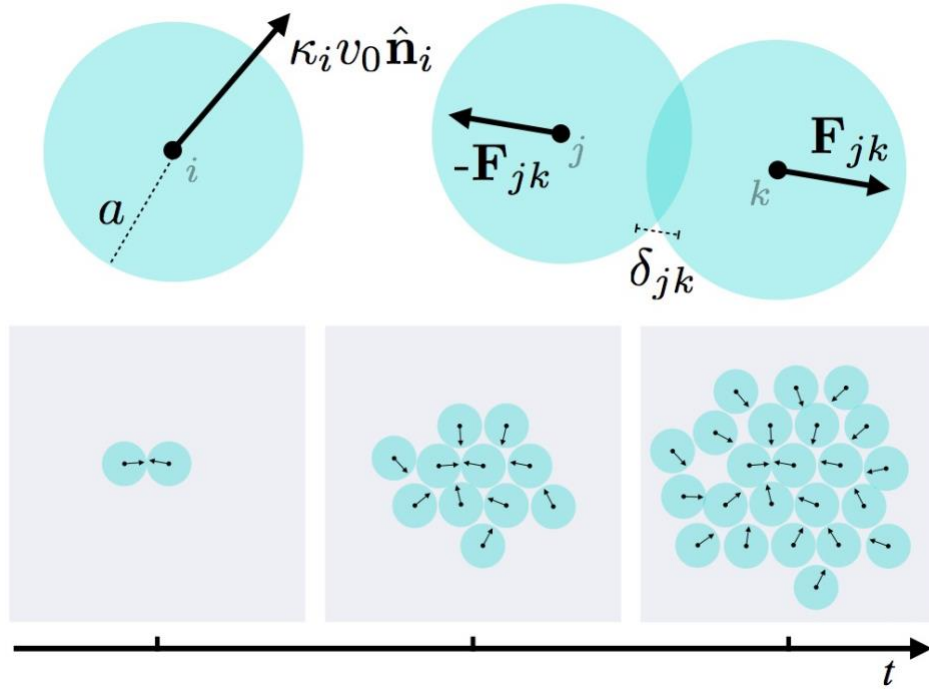


Figure 3-1. Modeling *M. xanthus* cells as reversing active Brownian particles. Schematic of our minimal ABP model. A single particle has radius α and moves with velocity $v_0 n_i$. The direction of self-propulsion is continuously affected by a white noise with variance proportional to D_r and directional reversals at times given by a Poisson process with frequency f_{rev} . These two parameters can be combined into an effective rotational diffusion coefficient: $D_r^{\text{eff}} = D_r + 2f_{\text{rev}}$. In addition, there is a spring-like repulsive interaction force \mathbf{F}_{ij} between each pair of particles. High-density clusters nucleate when colliding particles are caged by their surrounding neighbors before being able to reorient

3.3 Material and methods

3.3.1 *Myxococcus xanthus* culture and development conditions

Liquid cultures of Wild-Type *M. xanthus* strain DK1622 and $\Delta frzE$ were grown at 32°C in agitating CTTYE medium (1.0% Casitone, 0.5% yeast extract, 10.0 mM Tris-HCl at pH 8.0, 1.0 mM KH_2PO_4 , and 8.0 mM $MgSO_4$). Kanamycin (40 µg/ml) was added only to liquid cultures of $\Delta frzE$. Starvation assays were performed using non-nutritive Tris phosphate medium (TPM) agarose (10.0 mM Tris-HCl at pH 7.6, 1.0 mM KH_2PO_4 , 8.0 mM $MgSO_4$, and 1.5% agarose). To induce development, growing cells were harvested from liquid culture at mid-log phase and resuspended to a final concentration of various densities in TPM: 5×10^8 , 1.5×10^9 , 2.5×10^9 , 5×10^9 , 2.5×10^{10} cells/ml. 10 µl spots were plated on a TPM agarose slide complex and allowed to dry as described previously (Curtis, Taylor, Welch, & Shimkets, 2007). To modulate velocity, cells suspensions and TPM agarose was treated with nigericin sodium salt at concentrations of 0, 1, 2, 4, and 10 µM.

3.3.2 Imaging and tracking

Cells were imaged at 20X and 100X magnification to record the behavior of both single cells and aggregates. For 100X magnification, cells were imaged on a modified Nikon TE2000 inverted microscope with an oil-immersion objective (NA 1.49). To capture an enlarged 110 x 110 µm field of view, we used a tiling strategy and imaged a 3 x 3 grid of 100X fields. Details of this imaging and auto-focusing strategy were reported previously (Thutupalli, Sun, Bunyak, Palaniappan, & Shaevitz, 2015). Images were recorded at a frame rate of 10 s. Cell tracking using bright field images was performed using our previously published BCTracker algorithm (Thutupalli et al., 2015).

For high cell density fluorescence cell tracking, a 1:400 mixture of Alexa Fluor 594 carboxylic acid succinimidyl ester labeled DK1622 or $\Delta frzE$ cells to non-labeled cells was used to record the behavior of individual cells in large groups. To stain cells, cells were grown to mid-log, harvested by centrifugation and resuspended in MC7 buffer. 2 μ l of dye (10 mg/ml, dissolved in DMSO) and 5 μ l of 1M NaHCO₂ was added to 100 μ l of cells and shaken vigorously at 100 RPM for 1 h in the dark at room temperature. Cells were then pelleted by centrifugation, washed 3 times in TPM and microscopically examined. Fluorescent microscopy images were taken at a rate of one frame per min for the first 15 min in each hour to minimize the amount of laser exposure for cells. Experiments lasted 11 h. Fluorescent cells were tracked using a particle tracking algorithm developed by Crocker, Grier and Weeks (Crocker & Grier, 1996). In our analysis, a cell is counted as actively moving if during each tracked hour it glides with a mean speed greater than 0.5 μ m/min. A reversal event is defined as occurring when the velocity vector between two successive time points changes sign.

To calculate the rotational diffusion constant, we tracked 50 $\Delta frzE$ cells and observed their motion for at least 35 μ m. The diffusion constant was then calculated from the decay of the velocity temporal autocorrelation function and assumed to be the same for all experiments. To measure the length-scale growth displayed in Fig. 3-1, we imaged Wild-Type *M. xanthus* (1×10^{11} cells/ml) on a 20X magnification home-built bright field microscope at frame rate every 10 s for 24 h.

At higher densities, it is experimentally difficult to break up cell clumps that have formed in the liquid culture. Thus, at the beginning of a movie we sometimes see isolated aggregates that are not fruiting bodies, and which very quickly dissolve as cells migrate out of them. We start our analysis from the point where the initial visible aggregates have dissolved.

3.3.3 Simulation details and parameters

We simulated (Dormann et al., 2002) using a standard Brownian Dynamics algorithm in an $L \times L$ box with periodic boundary conditions. In all cases, we use $k = \mu = 1$ so the interaction timescale $\tau_D = (\mu k)^{-1}$ sets the unit time and we use the particle radius a as the unit of length ($\alpha = 1$). To prevent particles from passing through each other, we set $v_0 = (\alpha \mu k)/100$. We fix the packing fraction $\phi = N\pi a^2/L^2$, which sets the total number of particles, N . The rotational diffusion D_r and the reversal frequency f_{rev} are varied to obtain the desired Pe_r^{-1} .

For each set of parameters, we average over 10 – 100 runs and use a jackknife method (Stenhammar, Tiribocchi, Allen, Marenduzzo, & Cates, 2013) to estimate statistical errors. In order to compute the length scale $L(t)$ and its coarsening exponent (Fig. 3-1) we used a large system size with $L = 1000$, $Pe_r^{-1} = 0.01$ and a packing fraction of $\phi = 0.5$ ($N = 159,154$ particles), averaging over 100 independent runs. The same box size was used to generate the movies and snapshots for phase diagram. For other quantities we did not need such a large system size. The phase diagram was computed on systems with $L = 200$ (10 runs for each set of parameters).

3.4 Results

3.4.1 Reversing active Brownian particles

M. xanthus cells move by gliding on solid surfaces using both tank-tread-like transport motors and the retraction of extruded filaments called pili. It has been shown that these cells can modulate their speed in a seemingly continuous manner (Balagam et al., 2014; Hodgkin & Kaiser, 1979). While cells do not appear to have the ability to steer in 2-dimensions during gliding, they are able to reverse the direction of all the transport motors quickly, causing them to move in the opposite

direction. These “reversals” typically occur every several minutes, and cells modify the reversal frequency in different situations (Blackhart & Zusman, 1985; Thutupalli et al., 2015; Wu, Kaiser, Jiang, & Alber, 2009).

Previous numerical work on reversing active particles has typically used systems of self-propelled rods (Peruani et al., 2012). In this paper, we modify instead a well-established minimal model (Fily & Marchetti, 2012; Marchetti et al., 2016) of active Brownian particles (ABPs) by adding reversals (Fig. 3-1). Each reversing ABP is modeled as a disk of radius a , with dynamics governed by overdamped Langevin equations of motion,

$$\dot{\mathbf{r}}_i = v_0 \kappa_i(t) \hat{\mathbf{n}}_i + \mu \sum_j \mathbf{F}_{ij}, \quad \dot{\theta}_i = \sqrt{2D_r} \eta_i(t) \quad (2)$$

where \mathbf{r}_i and $\mathbf{n}_i = (\cos \theta_i, \sin \theta_i)$ are the position and orientation of the i^{th} disk. (Dormann et al., 2002) describes the velocity of the i^{th} particle as a function of its self-propulsion and steric interactions. The direction of self-propulsion is up-dated stochastically according to a random torque $\eta_i(t)$ of unit variance. In (Dormann et al., 2002), we have modified the standard ABP model by incorporating reversals through a function $\kappa_i(t)$, which takes the values ± 1 , changing sign at times given by a Poisson process with a mean reversal frequency f_{rev} . The force \mathbf{F}_{ij} is purely repulsive and represents an excluded-volume interaction. We use a harmonic potential, with $\mathbf{F}_{ij} = k(2a - r_{ij}) \hat{\mathbf{r}}_{ij}$ for $r < 2a$ and $\mathbf{F}_{ij} = 0$ otherwise, where $\hat{\mathbf{r}}_{ij} = \mathbf{r}_i - \mathbf{r}_j / |\mathbf{r}_i - \mathbf{r}_j|$.

Since we want to investigate the role of motility in aggregation, we do not describe motility in terms of molecular mechanisms, such as chemical signaling, and ignore other physical mechanisms such as attraction, alignment, and torque generation due to the elongated cell shape,

and complex interactions with the substrate. Instead, particles only interact through repulsive forces and independently adjust their direction of self-propulsion.

Introducing a reversal frequency adds a new timescale to the ABPs, the effects of which can be included in an effective rotational diffusion via

$$D_r^{\text{eff}} = D_r + 2f_{\text{rev}} \quad (3)$$

Hence, particles travel with an orientational persistence time $\tau_r = 1/D_r^{\text{eff}}$ and their random paths have a persistence length $\ell_p = v_0\tau_r$. We can demonstrate this by measuring the mean squared displacement (MSD) for individual ABPs with different reversal frequencies (Fig. 3.2).

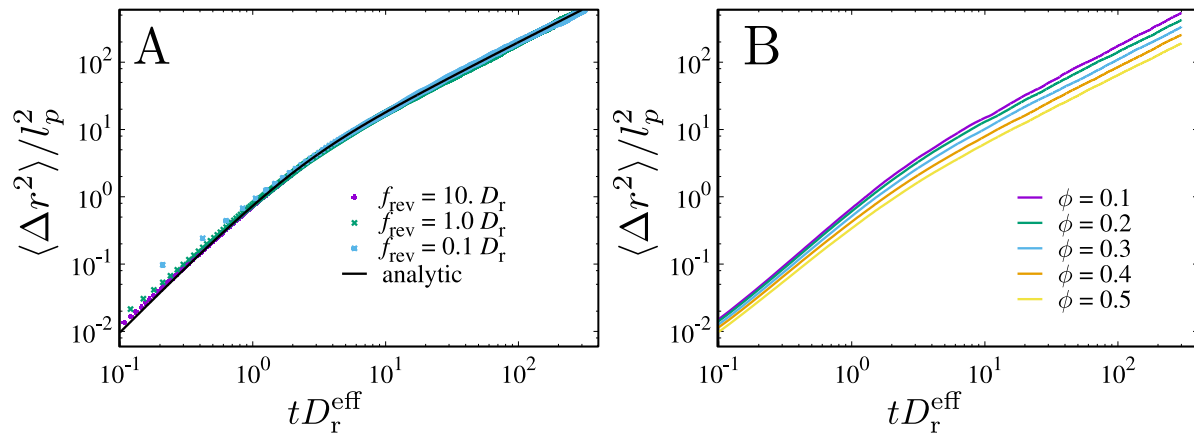


Figure 3-2. Motility of reversing ABPs. (A) Mean square displacement (MSD) versus time for single particles, plotted for various reversal frequencies. The data for different reversal frequencies collapse when time is scaled by the reorientation time $\tau_r^{-1} = D_r^{\text{eff}}$. (B) MSD for finite densities in the case $D_r = f_{\text{rev}}$. The more frequent collisions and eventual caging reduce the particles' displacement, but the crossover from ballistic to diffusive motion is still controlled by D_r^{eff}

In agreement with our calculations, we find that the crossover between ballistic and diffusive motion occurs at precisely τ_r for all f_{rev} . Interestingly, this property holds for finite particle densities as well. Therefore, the effective diffusion coefficient, D_r^{eff} , is the appropriate parameter to use in (Laub & Loomis, 1998) for calculating the inverse Péclet number for reversing ABPs.

3.4.2 The dynamical mechanism of aggregation depends on cell density

We first investigated the effects of different cell densities on *M. xanthus* aggregation. In our experiments, we spotted a drop of bacterial liquid culture of known density onto a minimal media agar substrate. We then recorded time-lapse, bright-field images of the plate such that pixel intensity is indicative of local cell density, with low intensities (darker regions) corresponding to high cell density. Though there are non-linear effects, e.g., halos formed around large aggregates and issues of saturation, we focus on large structures formed in these movies which are largely insensitive to these issues.

We first observed that when the spotting cell density is very low (5×10^8 cells/ml), cells exhibit no large-scale pattern formation. Over the first few hours, cells largely move independently, reversing frequently and with minimal cell-to-cell contact and interactions. After a sufficient amount of time, typically 6 – 8 h, we observed the formation of spatially stable streams that exist mostly as monolayers of cells (as opposed to the many hundreds of layers that exist in the fruiting body) as reported in Thutupalli et al. (Thutupalli et al., 2015). At this low density, starving cells do not aggregate to form fruiting bodies regardless of observation time. Similarly, very dilute simulations of ABPs do not aggregate.

As we increased the density to 1.5×10^9 cells/ml, we observed the random formation of aggregates in both space and time which then grow (Fig. 3-3A). In a field of view of 3 mm by 2.5 mm, approximately 10 aggregation sites can be typically observed, although in some cases as few as 2 form. These features of random appearance and growth over both space and time are indicative of a nucleation and growth process, familiar from many precipitation and crystallization processes (Gasser, Weeks, Schofield, Pusey, & Weitz, 2001). ABPs at low density also aggregate via a nucleation and growth mechanism.

When we further increased the initial culture density to 1×10^{10} cells/ml and above, we observed that *M. xanthus* forms aggregates via a different dynamical mechanism (Fig. 3-3B). Rather than the spatially random nucleation and slow growth of individual fruiting bodies that occur stochastically in time, we observed that high density cultures spontaneously and immediately aggregate over the entire field of view. Within the first 6 h after plating, we observed the formation of a global instability and small, mesh-like structures. As the mesh coarsens over time, small aggregates appear that are connected by less dense layers of cells. Finally, a subset of these aggregates grows in time and turn into round fruiting bodies. This kind of spontaneous phase separation is called spinodal decomposition and classically arises when microscopic fluctuations in the local density are inherently unstable with no energy barrier separating the mixed and more favorable phase-separated regimes.

A quantitative treatment of the distinction between the spinodal decomposition and nucleation and growth reveals that we do observe these two regimes in both experiments and simulations. However, due to the difficulty of this type of analysis, we do not attempt to distinguish these them in the following and simply refer to a configuration as either homogeneous or phase-separated.

A hallmark of spinodal decomposition is a well-defined length scale of the phase-separated domains that increases with time as a power-law as the domains grow in a self-similarity manner (Bray, 1994). We found that at high inoculation densities, a single dominant length scale emerges in the organization of the bacterial domains (Fig. 3-3C) and grows in time as a power law with an exponent $\alpha = 0.30 \pm 0.02$ (Fig. 3-3D).

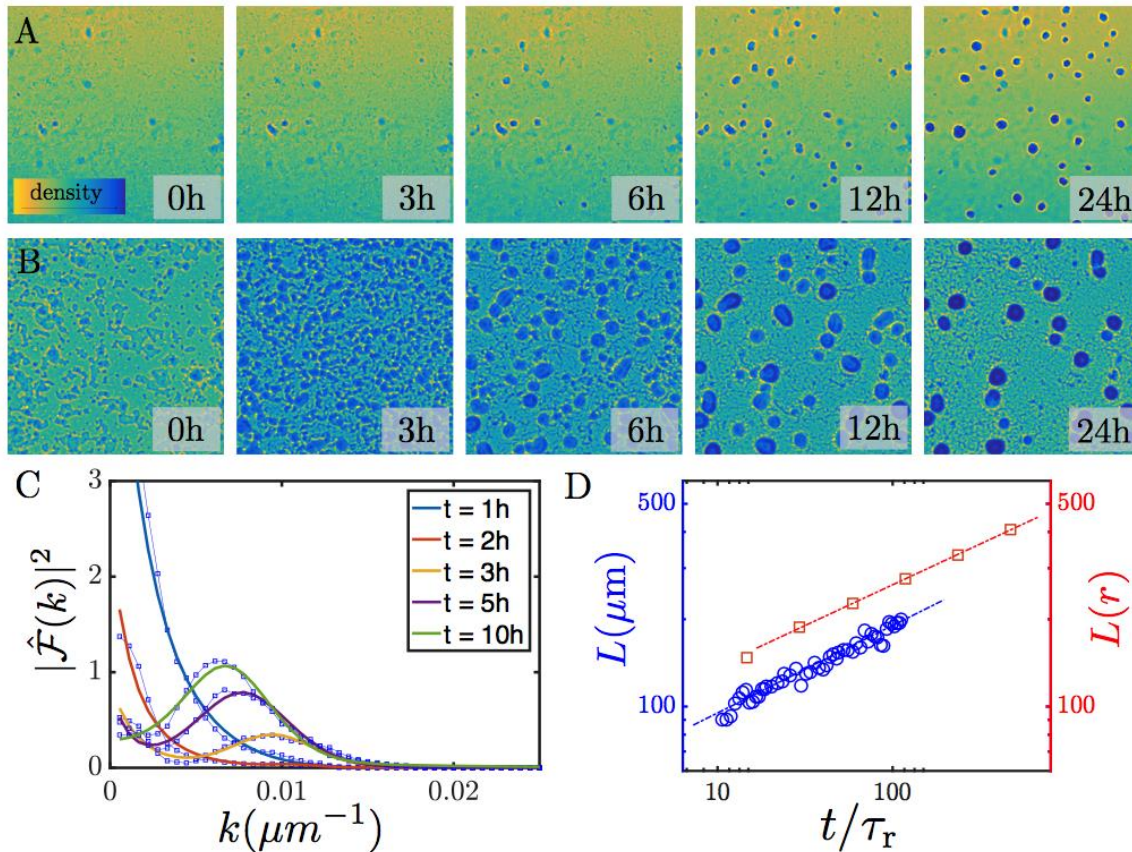


Figure 3-3. Aggregation in *M. xanthus* (A) Low cell densities of 3×10^9 cell/ml result in aggregation via a nucleation and growth process in *M. xanthus*. (B) Larger densities of 1×10^{10} cell/ml result in the formation of aggregates everywhere at the same time via spinodal decomposition in *M. xanthus*. (C) Radial component of the Fourier transform of images from *M. xanthus* aggregation at high density. Solid lines are fits to a Gaussian function added to a decaying

exponential for time $t = 1, 2, 3, 5,$ and 10h after starvation. (D) Growth of the dominant length scale with time for spinodal decomposition experiments. Times are written in units of the reversal time $\tau_r \approx 10$ min. The length scale of droplets coarsens as a power law in time with an exponent of $\alpha_{\text{experiment}} = 0.30 \pm 0.02$. Results from a simulation of reversing ABPs is shown in red, which result in an exponent of $\alpha_{\text{simulation}} = 0.281 \pm 0.002$

The later stages of coarsening involve significant flux between neighboring fruiting bodies. This can be seen directly in some movies and through dynamics similar to the Ostwald ripening seen in passive systems, a surface-tension driven phenomena that causes smaller aggregates to dissolve into nearby larger aggregates. Recent work by Bahar et al. used a model of Ostwald ripening to describe the later stages of *M. xanthus* aggregation and accurately predicted the disappearance and persistence of aggregates (Bahar, Pratt-Szeliga, Angus, Guo, & Welch, 2014).

3.4.3 A phase diagram for aggregation

To control the Pe_r^{-1} of *M. xanthus* cells experimentally, we took advantage of the non-reversing mutant ΔfrzE , which does not change its velocity over time even in starvation conditions. We then varied Pe_r^{-1} by altering the propulsion speed v_0 using the drug nigericin (Sun, Wartel, Cascales, Shaevitz, & Mignot, 2011). We prepared samples at different densities and nigericin concentrations and imaged their aggregation dynamics, determining for each experiment whether phase separation had occurred.

To calculate the inverse Péclet number for each experiment, we performed separate tracking experiments to probe D_r and cell speed for each nigericin concentration. We mixed a small number

of fluorescently-labeled cells with non-fluorescent cells at a ratio of 1:400 and tracked only the fluorescent cells to measure the speed. We estimated D_r by tracking the motion of cells at very low density such that cells do not physically interact with each other. The decay of the velocity temporal autocorrelation function indicates that $D_r = 0.04 \pm 0.02 \text{ min}^{-1}$. We note that the typical reversal frequency of Wild-Type *M. xanthus*, $f_{\text{rev}} \sim 0.05 - 0.17 \text{ min}^{-1}$, is of the same order of magnitude but slightly larger than the rotational diffusion coefficient. This implies that subtle changes to f_{rev} can have appreciable effects on Pe_r^{-1} . Had D_r been much larger, cellular control of f_{rev} would have been ineffective as a method to alter Pe_r^{-1} . We combine the measured speed and D_r with the average cell size of $\ell_c = 2.5 \text{ }\mu\text{m}$ (half a cell length) to calculate the Péclet number for each condition.

The experimentally derived phase diagram of *M. xanthus* aggregation is shown in Fig. 3-4A. As predicted, at low density or high inverse Péclet number, the system does not phase separate (black circles). At high density or low inverse Péclet number, the system phase separates via spinodal decomposition (red squares). The estimated spinodal line is denoted on the phase diagram. Interestingly, ΔfrzE did not always form stable fruiting bodies. While initially stable, aggregates sometimes fell apart at the end of 24 h towards the end of tradition fruiting body development. This potentially indicates that additional biological or chemical mechanisms may play a role in fruiting body stability over long times.

We have seen that ABPs and colonies of starved *M. xanthus* show similar aggregation patterns and that, in the phase-separated regime, aggregates grow with the same exponent. In order to demonstrate that *M. xanthus* aggregation is indeed an example of MIPS, we additionally need to show that the behavior is controlled entirely by density and by the effective inverse Péclet number:

$$Pe_r^{-1} = \ell_c D_r^{\text{eff}} / v_0 = \ell_c (D_r + 2f_{\text{rev}}) / v_0$$

The density Pe_r^{-1} phase diagram for ABPs has been obtained before by several authors (Patch, Yllanes, & Marchetti, 2017; Redner, Hagan, & Baskaran, 2013; Stenhammar et al., 2013). Here we construct the phase diagram for reversing ABPs by studying the probability distribution of local particle density (Fig. 3-4B).

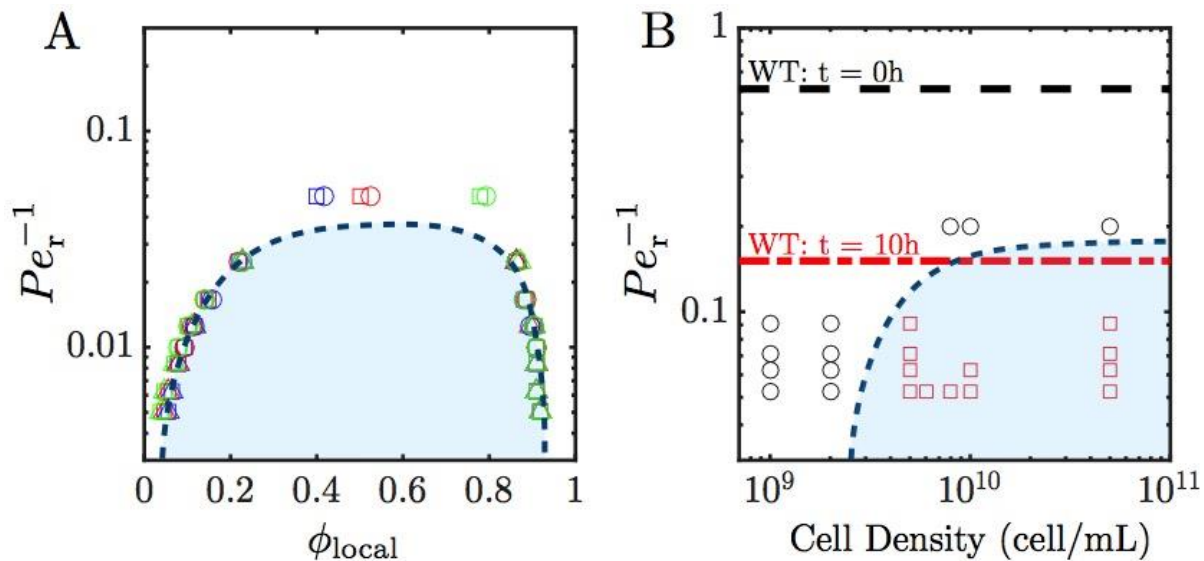


Figure 3-4. Phase Diagram of *M. xanthus* aggregation. (A) The phase diagram for reversing ABPs showing the spinodal boundary, obtained as described in the SM. The spinodal points correspond to the peaks of a bimodal distribution of local density in systems with different values off rev (different symbols) and different mean packing fraction (different colors). The dashed line is a guide to the eye. The horizontal axis is the particle packing fraction ϕ . (B) Experimental phase diagram for *M. xanthus* phase separation. For each experiment, we determined whether the system is phase separated (red squares) or homogeneous (black circles). The phase boundary is drawn by hand as a guide to the eye. Dashed horizontal lines represent Pe_r^{-1} for Wild-Type cells before (black) and after (red) starvation

In spatially homogeneous systems, this distribution is unimodal, with a peak at the total packing fraction ϕ . For phase-separated systems, the distribution is bimodal with peaks corresponding to the density of two coexisting phases. The phase diagram for reversing ABPs coincides with that of standard ABPs when plotted in terms of the effective inverse Péclet number (Berleman & Kirby, 2009).

3.4.4 Starving *Myxococcus xanthus* change velocity and reversal frequency to induce aggregation

The inverse Péclet number (Berleman & Kirby, 2009) contains four parameters, two of which *M. xanthus* potentially has the ability to control during fruiting body formation. Cells do not grow during aggregation due to the starvation conditions and D_r is presumably set by thermal fluctuations of the cell body and molecular noise in the motility process. However, both the cell speed v_0 and the reversal frequency f_{rev} are under cellular control.

We tracked individual fluorescent Wild-Type cells in an aggregating population of density 1×10^9 cell/ml for the first 11 h and found that when starved, Wild-Type cells change their gliding speed v_0 and reversal frequency f_{rev} . In the first 3 – 4 h, Wild-Type cells exhibited low gliding speed $v_0 \approx 1.5 \mu\text{m}/\text{min}$. Additionally, under 10% of cells are actively moving during this period, in agreement with previous reports of an initial “resting” phase (Jelsbak & Sørensen, 2002). After being starved for over 5 h, Wild-Type *M. xanthus* cells speed up to $v_0 \approx 2.5 \mu\text{m}/\text{min}$ (Fig. 3-5A), almost doubling their initial v_0 . At these times, over 90% of the cells are actively moving. $\Delta frzE$ cells, in contrast, do not change speed when starving, potentially indicating a link between the Frz molecular pathway and gliding speed. We also found that reversal frequency decreased significantly from 0.128 min^{-1} to 0.055 min^{-1} over the 11 h experiment (Fig. 3-5B). A

combination of increased v_0 and decreased f_{rev} together give rise to a reduction of the inverse Péclet number from 0.60 to 0.16 (Fig. 3-5C).

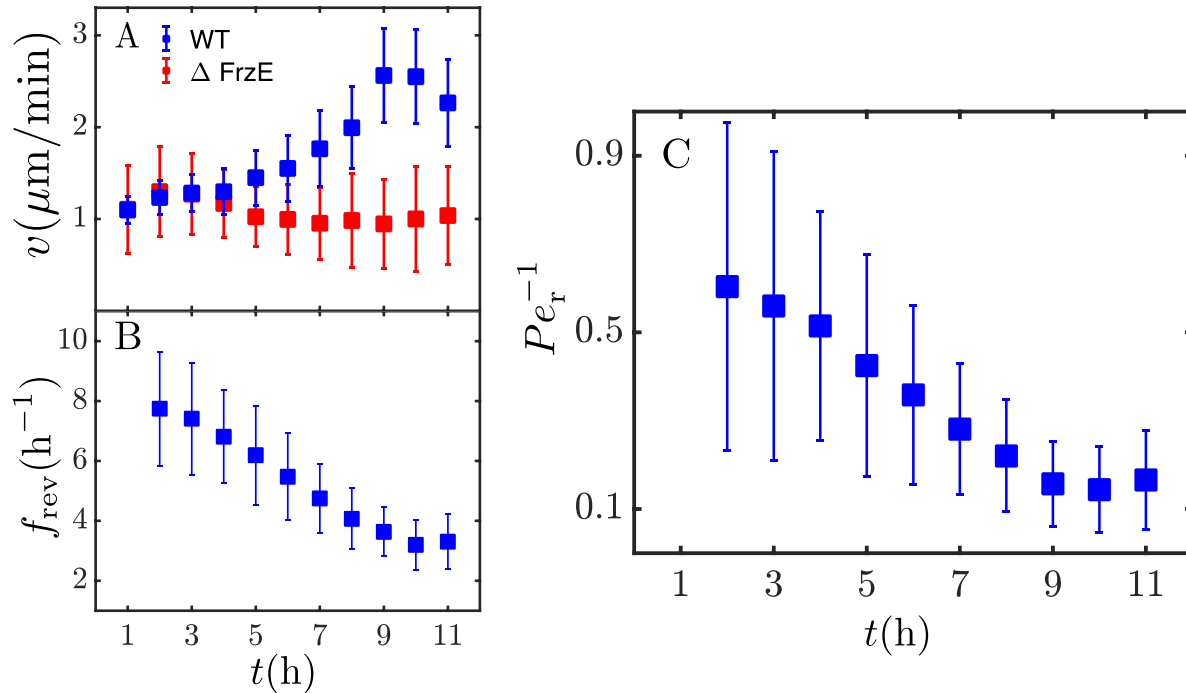


Figure 3-5. Cell tracking over time after starvation. (A) Speed, (B) reversal frequency, and (C) the resulting Pe_r^{-1} are shown for Wild-Type (blue) and $\Delta frzE$ cells (red)

This reduction in the inverse Péclet number is sufficient to drive aggregation and fruiting body formation. Before starvation, cells move slowly (or hardly at all) and reverse frequently, favoring a homogeneous population distributed throughout the surface (Fig. 3-5B black line). Upon starvation, Wild-Type cells speed up and reverse less often, producing a situation favorable for phase separation and fruiting body formation (Fig. 3-5B red line).

3.5 Discussion

In this paper, we considered *M. xanthus* fruiting body formation as a 2-dimensional phase separation process and compared experimental results at different densities, speeds, and reversal frequencies to an ABP model with reversals. We find that *M. xanthus* aggregation is driven, at least initially, by a MIPS process, a generic feature of active matter systems. Importantly, this can happen in the absence of complex signaling mechanisms and interactions between cells and requires very little real-time control at the cellular level. While the ability to actively change motility ultimately leads to a phase transition, cells do not have to implement a complicated feedback mechanism to alter motility in response to specific chemical or mechanical cues. Rather, cells need only speed up and suppress reversals upon starvation and the collective mechanics then naturally induces phase separation of the entire population.

We note that our simple ABP model is meant to capture the most basic underlying driving forces of aggregation. Many of the details that we purposely left out of our simulations most likely do play a role in the specific evolution and shape of the final fruiting bodies. These include cell-cell alignment, the effects of “slime following,” and cell-to-cell communication via C- and A-signaling mechanisms. More complicated models of *M. xanthus* aggregation may uncover the role of these additional parameters (Cotter, Schüttler, Igoshin, & Shimkets, 2017), however, we feel it is unlikely that they will change the basic features we have observed here.

Finally, our ABP simulations consider a 2-dimensional system of particles while developing *M. xanthus* cells form 3-dimensional aggregates. In simulations, aggregates form because particles impede each other’s motility and jam together. While this has also been observed in 3-dimensional simulations of swimming ABPs (Takatori & Brady, 2015), the 3-dimensional aggregation process

in *M. xanthus* is a dewetting phase transition where the population goes from a fully wetted phase, in which a liquid is evenly dispersed or spread across a surface, to a dewetted phase, in which individual droplets have separated from one another on that surface. In *M. xanthus*, the wetted phase is the pre-development swarm, which becomes “dewetted” as aggregates form and separate. The population forms droplets on the surface, similar to water on a hydrophobic surface. While we don’t expect this difference to change the very basic mechanism for phase transition we propose here, the details could prove important. Future work tracking cells and monitoring aggregate shape in 3-dimensions should lead to a more accurate, 3-dimensional theory of fruiting body formation.

3.6 Acknowledgment

We thank Suraj Shankar and Lisa Manning for useful discussions and Suraj Shankar for the calculation of the MSD for ABPs with reversals. MCM was supported by NSF-DMR-1609208 and by the Simons Foundation Targeted Grant in the Mathematical Modeling of Living Systems 342354. MCM and AP acknowledge support by the NSF IGERT program through award NSF-DGE- 1068780. MCM, AP and DY were additionally supported by the Soft Matter Program at Syracuse University. Our simulations were carried out on the Syracuse University HTC Campus Grid which is supported by NSF award ACI-1341006. DY acknowledges partial support by grant no. FIS2015-65078-C2-1-P, jointly funded by MINECO (Spain) and FEDER (European Union). JWS, ST, and GL were supported by NSF-PHY-1401506, NSF-PHY- 1521553, and a Human Frontier Science Program Cross Disciplinary Fellowship to ST. RDW and FB were supported by NSF-DBI-1244295. Part of this work was performed at the Aspen Center for Physics, which is supported by NSF-PHY-1607611.

3.7 References

- Bahar, F., Pratt-Szeliga, P. C., Angus, S., Guo, J., & Welch, R. D. (2014). Describing *Myxococcus xanthus* aggregation using Ostwald ripening equations for thin liquid films. *Scientific Reports*, 4.
- Balagam, R., Litwin, D. B., Czerwinski, F., Sun, M., Kaplan, H. B., Shaevitz, J. W., & Igoshin, O. A. (2014). *Myxococcus xanthus* Gliding Motors Are Elastically Coupled to the Substrate as Predicted by the Focal Adhesion Model of Gliding Motility. *PLoS Computational Biology*, 10(5).
- Banerjee, S., Utuje, K. J. C., & Marchetti, M. C. (2015). Propagating Stress Waves during Epithelial Expansion. *Physical Review Letters*, 114(22).
- Berleman, J. E., & Kirby, J. R. (2009). Deciphering the hunting strategy of a bacterial wolfpack. *FEMS Microbiology Reviews*.
- Blackhart, B. D., & Zusman, D. R. (1985). “Frizzy” genes of *Myxococcus xanthus* are involved in control of frequency of reversal of gliding motility. *Proceedings of the National Academy of Sciences*, 82(24), 8767–8770.
- Bray, A. J. (1994). Theory of phase-ordering kinetics. *Advances in Physics*, 43(3), 357–459.
- Bricard, A., Caussin, J. B., Desreumaux, N., Dauchot, O., & Bartolo, D. (2013). Emergence of macroscopic directed motion in populations of motile colloids. *Nature*, 503(7474), 95–98.
- Brugués, J., & Needleman, D. (2014). Physical basis of spindle self-organization. *Proceedings of the National Academy of Sciences*, 111(52), 18496–18500.
- Burchard, R. P. (1982). Trail following by gliding bacteria. *Journal of Bacteriology*, 152(1), 495–501.
- Cates, M. E., Marenduzzo, D., Pagonabarraga, I., & Tailleur, J. (2010). Arrested phase separation in reproducing bacteria creates a generic route to pattern formation. *Proceedings of the National Academy of Sciences*, 107(26), 11715–11720.
- Cates, M. E., & Tailleur, J. (2015). Motility-Induced Phase Separation. *Annual Review of Condensed Matter Physics*, 6(1), 219–244.
- Cavagna, A., & Giardina, I. (2014). Bird Flocks as Condensed Matter. *Annual Review of Condensed Matter Physics*, 5(1), 183–207.
- Cotter, C. R., Schüttler, H.-B., Igoshin, O. A., & Shimkets, L. J. (2017). Data-driven modeling reveals cell behaviors controlling self-organization during *Myxococcus xanthus* development. *Proceedings of the National Academy of Sciences*, 114(23), E4592–E4601.
- Crocker, J. C., & Grier, D. G. (1996). Methods of digital video microscopy for colloidal studies. *Journal of Colloid and Interface Science*, 179(1), 298–310.

- Curtis, P. D., Taylor, R. G., Welch, R. D., & Shimkets, L. J. (2007). Spatial organization of *Myxococcus xanthus* during fruiting body formation. *Journal of Bacteriology*, *189*(24), 9126–9130.
- Dormann, D., Vasiev, B., & Weijer, C. J. (2002). Becoming multicellular by aggregation; the morphogenesis of the social amoebae *Dicyostelium discoideum*. In *Journal of Biological Physics* (Vol. 28, pp. 765–780).
- Fily, Y., Henkes, S., & Marchetti, M. C. (2014). Freezing and phase separation of self-propelled disks. *Soft Matter*, *10*(13), 2132–2140.
- Fily, Y., & Marchetti, M. C. (2012). Athermal phase separation of self-propelled particles with no alignment. *Physical Review Letters*, *108*(23).
- Gasser, U., Weeks, E. R., Schofield, A., Pusey, P. N., & Weitz, D. A. (2001). Real-space imaging of nucleation and growth in colloidal crystallization. *Science*, *292*(5515), 258–262.
- Hodgkin, J., & Kaiser, D. (1979). Genetics of gliding motility in *Myxococcus xanthus* (Myxobacteriales): Two gene systems control movement. *MGG Molecular & General Genetics*, *171*(2), 177–191.
- Jelsbak, L., & Sørensen, L. (2002). Pattern formation by a cell surface-associated morphogen in *Myxococcus xanthus*. *Proceedings of the National Academy of Sciences of the United States of America*, *99*(Track II), 2032–2037.
- Konovalova, A., Petters, T., & Sørensen, L. (2010). Extracellular biology of *Myxococcus xanthus*. *FEMS Microbiology Reviews*.
- Kuspa, A., Plamann, L., & Kaiser, D. (1992). Identification of heat-stable A-factor from *Myxococcus xanthus*. *Journal of Bacteriology*, *174*(10), 3319–3326.
- Laub, M. T., & Loomis, W. F. (1998). A molecular network that produces spontaneous oscillations in excitable cells of *Dictyostelium*. *Molecular Biology of the Cell*, *9*(12), 3521–3532.
- Liu, Q. X., Doelman, A., Rottschäfer, V., de Jager, M., Herman, P. M., Rietkerk, M., & van de Koppel, J. (2013). Phase separation explains a new class of self-organized spatial patterns in ecological systems. *Proceedings of the National Academy of Sciences of the United States of America*, *110*(29), 11905–11910.
- Lobedanz, S., & Sørensen, L. (2003). Identification of the C-signal, a contact-dependent morphogen coordinating multiple developmental responses in *Myxococcus xanthus*. *Genes and Development*, *17*(17), 2151–2161.
- Marchetti, M. C., Fily, Y., Henkes, S., Patch, A., & Yllanes, D. (2016). Minimal model of active colloids highlights the role of mechanical interactions in controlling the emergent behavior of active matter. *Current Opinion in Colloid and Interface Science*.
- Marchetti, M. C., Joanny, J. F., Ramaswamy, S., Liverpool, T. B., Prost, J., Rao, M., & Simha, R. A. (2013). Hydrodynamics of soft active matter. *Reviews of Modern Physics*, *85*(3), 1143–1189.

- Patch, A., Yllanes, D., & Marchetti, M. C. (2017). Kinetics of motility-induced phase separation and swim pressure. *Physical Review E*, 95(1). Peruani, F., Starruß, J., Jakovljevic, V., Søgaaard-Andersen, L., Deutsch, A., & Bär, M. (2012). Collective motion and nonequilibrium cluster formation in colonies of gliding bacteria. *Physical Review Letters*, 108(9).
- Popović, M., Nandi, A., Merkel, M., Etournay, R., Eaton, S., Jülicher, F., & Salbreux, G. (2017). Active dynamics of tissue shear flow. *New Journal of Physics*, 19(3).
- Ramaswamy, S. (2010). The Mechanics and Statistics of Active Matter.
- Redner, G. S., Baskaran, A., & Hagan, M. F. (2013). Reentrant phase behavior in active colloids with attraction. *Physical Review E - Statistical, Nonlinear, and Soft Matter Physics*, 88(1).
- Redner, G. S., Hagan, M. F., & Baskaran, A. (2013). Structure and dynamics of a phase-separating active colloidal fluid. *Physical Review Letters*, 110(5).
- Shimkets, L. J. (1990). Social and developmental biology of the myxobacteria. *Microbiological Reviews*, 54(4), 473–501. Shimkets, L. J., & Rafiee, H. (1990). CsgA, an extracellular protein essential for *Myxococcus xanthus* development. *Journal of Bacteriology*, 172(9), 5299–5306.
- Stenhammar, J., Tiribocchi, A., Allen, R. J., Marenduzzo, D., & Cates, M. E. (2013). Continuum theory of phase separation kinetics for active brownian particles. *Physical Review Letters*, 111(14).
- Sun, M., Wartel, M., Cascales, E., Shaevitz, J. W., & Mignot, T. (2011). Motor-driven intracellular transport powers bacterial gliding motility. *Proceedings of the National Academy of Sciences*, 108(18), 7559–7564.
- Takatori, S. C., & Brady, J. F. (2015). Towards a thermodynamics of active matter. *Physical Review E - Statistical, Nonlinear, and Soft Matter Physics*, 91(3).
- Thutupalli, S., Sun, M., Bunyak, F., Palaniappan, K., & Shaevitz, J. W. (2015). Directional reversals enable *Myxococcus xanthus* cells to produce collective one-dimensional streams during fruiting-body formation. *Journal of the Royal Society Interface*, 12(109).
- Wu, Y., Kaiser, A. D., Jiang, Y., & Alber, M. S. (2009). Periodic reversal of direction allows *Myxobacteria* to swarm. *Proceedings of the National Academy of Sciences*, 106(4), 1222–
- Zusman, D. R., Scott, A. E., Yang, Z., & Kirby, J. R. (2007). Chemosensory pathways, motility and development in *Myxococcus xanthus*. *Nature Reviews Microbiology*.

Chapter 4: Describing *Myxococcus xanthus* Aggregation Using Ostwald Ripening Equations for Thin Liquid Film

This chapter has been published as below with minor modifications. Fatmagül Bahar, Philip C. Pratt-Szeliga, Stuart Angus, Jiaye Guo, and Roy D. Welch. Describing *Myxococcus xanthus* aggregation using Ostwald ripening equations for thin liquid films. Scientific Reports 2014, 4, 6376-8135.

4.1 Abstract

When starved, a swarm of millions of *Myxococcus xanthus* cells coordinate their movement from outward swarming to inward coalescence. The cells then execute a synchronous program of multicellular development, arranging themselves into dome shaped aggregates. Over the course of development, about half of the initial aggregates disappear, while others persist and mature into fruiting bodies. This work seeks to develop a quantitative model for aggregation that accurately simulates which will disappear and which will persist. We analyzed time-lapse movies of *M. xanthus* development, modeled aggregation using the equations that describe Ostwald ripening of droplets in thin liquid films and predicted the disappearance and persistence of aggregates with an average accuracy of 85%. We then experimentally validated a prediction that is fundamental to this model by tracking individual fluorescent cells as they moved between aggregates and demonstrating that cell movement towards and away from aggregates correlates with aggregate disappearance. Describing development through this model may limit the number and type of molecular genetic signals needed to complete *M. xanthus* development, and it provides numerous additional testable predictions.

4.2 Introduction

M. xanthus is a flexible rod-shaped bacterium that can move across a semi-solid surface in either direction along its long axis (Mignot, 2007) Under laboratory conditions, *M. xanthus* is grown either vegetatively in liquid culture or as a motile biofilm, called a swarm, on agar. A small swarm can be initiated by spotting a few microliters of liquid culture on an agar surface and letting it dry. If the agar is nutrient-rich, the swarm will expand outward in all directions across the surface through multicellular projections called flares (Zhang et al., 2011). If the agar is non-nutritive,

movement turns inward, and the swarm appears to contract. Within several hours, the millions of starving cells self-organize into several hundred dome shaped aggregates, each of which contains many thousands of cells. Following this period of aggregation, a subset of cells at the interior of each aggregate differentiates to become quiescent spores. When aggregation and sporulation are both completed, aggregates are considered to have matured into fruiting bodies. The entire developmental process can take less than 24 h (Curtis, Taylor, Welch, & Shimkets, 2007; Jelsbak & Søggaard-Andersen, 2003).

Prior research (Zhang et al., 2011) has reported that only about half the aggregates that appear at the beginning of the aggregation process will persist through maturation to become fruiting bodies, while the other half will shrink and disappear. Xie *et al.* (Xie, Zhang, Shimkets, & Igoshin, 2011) sought to identify differences between persisting and disappearing aggregates, and found that aggregate size was the only statistically reliable determinant: persisting aggregates were larger. This determinant can be used to accurately predict disappearing and persisting aggregates, but it provides no model to explain why or how this happens.

At present, the only models for *M. xanthus* aggregation are based on the “traffic jam” hypothesis, which states that during aggregation cells will clump together and become stuck, or jammed, at positions within the swarm when the concentration of cells is sufficiently high. Cells within these traffic jams undergo a transition from motile to non-motile, and in this way an aggregate is initiated. Additional motile cells encounter these initial aggregates, and they become jammed and undergo the same transition. Variations on this model based on a “capitalistic economic system” or reaction diffusion mechanism have been proposed for *Pseudomonas aeruginosa* (Zhao et al., 2013) and *Dictyostelium discoideum* (Vasiev, Hogeweg, & Panfilov, 1994) respectively. The

problem with these types of models in *M. xanthus* is incorporating a method for disappearance. Agent based models implementing the traffic jam hypothesis accurately predict aggregate formation, but have no disappearance component (Igoshin, Kaiser, & Oster, 2004; Igoshin, Welch, Kaiser, & Oster, 2004b; Igoshin, Goldbeter, Kaiser, & Oster, 2004; Sliusarenko, Zusman, & Oster, 2007; Sozinova, Jiang, Kaiser, & Alber, 2005).

In this report we propose a new hypothesis for controlling aggregate disappearance based on a model of Ostwald ripening in thin liquid films (Rump, 2008). We implement previously published 2-dimensional pairwise equations that describe Ostwald ripening in a simulator (o-simulator) that operates over an area large enough to cover dozens of aggregates. This o-simulator predicts the change in volume of each aggregate based on its current volume and the volume and relative proximity of its neighbors. We then test our hypothesis by experimentally deconstructing *M. xanthus* development, isolating the disappearance of aggregates, observing the transient swarm structures and the movements of individual cells, and then matching these observations to the results produced by the o-simulator.

A method similar to this was successfully applied in *M. xanthus* to provide a mechanism for describing the density waves, called ripples (Igoshin, Mogilner, Welch, Kaiser, & Oster, 2001; Shimkets & Kaiser, 1982; Welch & Kaiser, 2001), that sometimes travel across the surface of a swarm. Welch *et al* (Welch & Kaiser, 2001) were able to partially reveal the mechanism of rippling by isolating one set of opposing ripples, observing their behavior and the behavior of individual cells within ripples, and then matching these observations with a set of equations that describe non-zhabotinsky waves.

4.3 Material and methods

4.3.1 Growth and development culture conditions

Liquid cultures of *M. xanthus* were grown in agitating nutrient CTTYE (1.0% Casitone [Difco], 0.5% yeast extract [Difco], 10.0 mM Tris- HCl [pH 8.0], 1.0 mM KH₂PO₄, and 8.0 mM MgSO₄), and development assays were performed using starvation TPM agar (10.0 mM Tris-HCl (pH 7.6), 1.0 mM KH₂PO₄, 8.0 mM MgSO₄, and 1% agar). To prepare cells for development assays, growing cells were harvested from liquid culture at Klett 80–120 (log phase). Development assays were prepared as previously described (Zhang et al., 2011) with the following modifications: The gasket used to contain the agar was thicker (2.5 mm) than the gasket used to provide the airspace (0.5 mm); the initial spot had a concentration of 5.0×10^9 cells/mL. Microcinematography was performed at 30°C. Wild-Type DK1622 was used for development assays to record the behavior of aggregates, and a 1/150 mixture of DK1622 and fluorescent DK10547 (Welch & Kaiser, 2001) was used to record the behavior of individual cells.

4.3.2 Time lapse microcinematography and image processing

For aggregates: To obtain the data for aggregates, we created a custom C# application that allows identification to be performed semi-automatically. First, the image within the stack containing the highest number of aggregates is selected as a starting point (this is usually within 10 h after the initiation of development). The user of the application clicks on the image and a blue circle appears that can be moved by dragging or expanded/reduced in size by moving the mouse wheel. Once a frame is completely annotated, the designated aggregates (blue circles) in the frame are extended ten frames forward. The tenth frame is adjusted for changes by the user, and then the positions and

radii are interpolated within the ten frames range by the application. This process is repeated for the entire movie in ten frame batches. The positions and radii of each annotated aggregate in each frame are saved to a file format that can be read using the simulations written in Java.

For tracking individual cells: To obtain the data on the movement of individual cells, we performed microcinematography on developmental cultures using a 150:1 mixture of Wild-Type and GFP-expressing cells that develop as Wild-Type. At the period of development when disappearance is occurring, we identified individual aggregates as either growing or shrinking, increased magnification to 150 \times , moved the slide so that the aggregate was in the middle of the field-of-view, and then continued, acquiring time-lapse fluorescence images every minute. Using these images, we were able to identify and track individual cells moving around a growing or shrinking aggregate.

We manually recorded x/y coordinates of the cell at each time step and placed the coordinates into an excel spreadsheet. A Java program parsed the excel spreadsheet and visualized each trail relative to the center of the aggregate on an image. Then we manually determined whether each trail was moving towards, away or none, and inserted this new information into an updated spreadsheet. Another Java program then read the updated spreadsheet, colored the annotated trails, and placed them on composite images. We were then able to calculate the percentage moving towards/away when the aggregates were growing and shrinking.

4.3.3 Dynamical model to predict aggregate behavior

The o-simulator has a front end that can read the data files from the custom C# application which contain aggregate position and radii (first e-frame). The front end creates unique identifiers for each aggregate in the first e-frame and matches the closest aggregate in subsequent e-frames to associate aggregates by identifier throughout the image stack.

We seed the first o-frame of the o-simulation with the position and radii data from first e-frames as the only input (besides the free variables $\tau-1$ and $\tau-2$). For each subsequent o-frame, the discretized pairwise equations for Ostwald ripening are applied to each unique pair of simulated aggregates, and then changes in volume are accumulated in each hemisphere. Simulated aggregates whose volume is less than one are removed, and pairs of simulated aggregates whose edges touch are merged; the merged simulated aggregate has the combined volume of the two original simulated aggregates, and a center point that is the midpoint between the two. The e-frame aggregate movements are applied to the o-frame simulated aggregates so that movement and disappearance can be considered separately.

To determine the percent accuracy of the o-simulation, for each “o-frame::e-frame” pair we find the number of pairs where the simulated aggregate matches the experimental aggregate, and then divide this number by the initial number of aggregates at the first e-frame. A pair is scored as a match if it exists or does not exist in both the e-frame and corresponding o-frame. To control for boundary conditions, the simulation is run using all of the aggregates in the frame, but the accuracy is measured only for the aggregates inside of a border 250 pixels around the edge of the image (approximately the size of two large aggregates). This reduces the possibility that aggregates just outside the image will have a significant impact on the accuracy score.

To solve for the rate of mass transfer between droplets (τ -1 and τ -2) in the o-simulation, we attempted every value between 0 and 1500 using increments of 10. We determined which values for τ -1 and τ -2 are best for the 15 training replicates by trying every combination and selecting the pair that maximized the mean area under the accuracy plot. The decision to calculate two values for τ was made after observing a change in the collective behavior of the swarm in the middle of development. Evidence of this change appeared in the accuracy plots when a single value for τ was used. The single τ plots display an early drop in accuracy that recovers around the middle of the simulation. A single τ must represent the average rate of mass transfer for the entire o-simulation, so the drop in the accuracy plot means that the o-simulation is faster than the experiment in the beginning, and the experiment catches up by the end. These kinds of synchronous changes in behavior are not surprising for a multicellular bacterium like *M. xanthus* and may be the result of quorum sensing or some other cell signaling system. At this point, however, we have simply observed and noted the behavior and its effect but proposing a mechanism would be premature.

4.4 Results

4.4.1 A quantitative comparison between Ostwald ripening and *Myxococcus xanthus* aggregation

To observe and record swarm-scale dynamics of *M. xanthus* aggregation, we used bright field time-lapse microcinematography at $60\times$ magnification, 1 frame/min, covering an $\sim 50\text{ mm}^2$ area from an interior section of a 1 cm diameter swarm composed of 2.5×10^7 Wild-Type (DK1622) cells on starvation TPM agar (Fig. 4-1). A stack (movie) of 1440 sequential images (frames) were taken for each sample over of 24 h, beginning no later than 15 min after starvation.

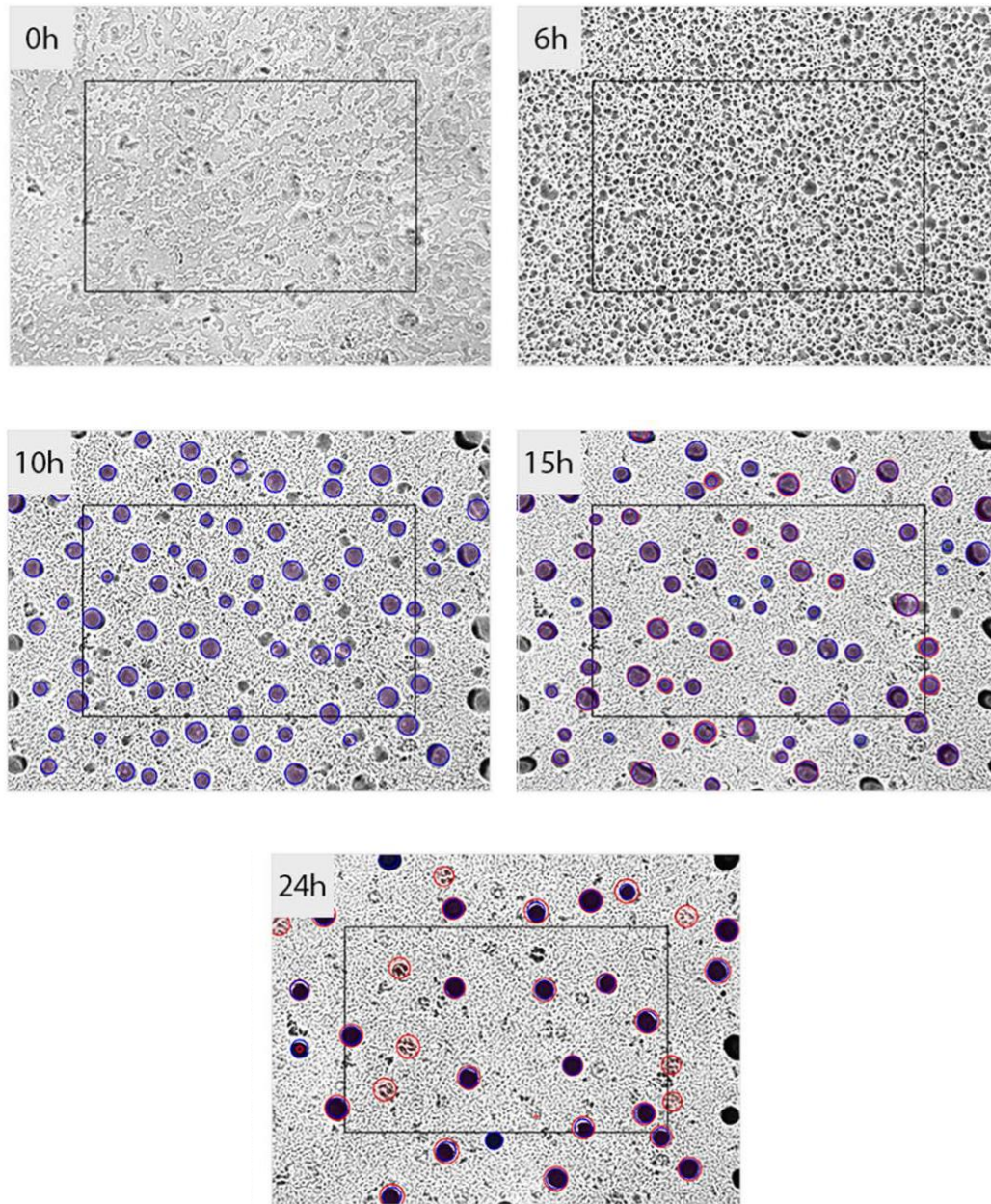


Figure 4-1. *M. xanthus* aggregation with time-lapse movie. Five microcinematography images selected from a time-lapse image stack that shows the progression of aggregation. Elapsed time is indicated in the upper left corner of each frame (0, 6, 10, 15 and 24 h). Blue circles with ID numbers represent the positions and volumes of aggregates, and red circles represent the positions and volumes of simulated aggregates (10, 15 and 24 h). Blue circles are not visible in frame 3, which is the first e-frame, because red circles exactly overlap blue circles on that frame

We independently repeated this procedure 20 times to produce 20 replicate experiments. Individual cells are not distinguishable under these conditions, but we can estimate from the cell concentration of the liquid culture, the volume spotted onto agar, the area of the initial swarm following liquid absorption and evaporation, and the area of the microscope field-of-view, that there are approximately 8.3×10^6 cells within the field-of-view at starvation onset (Fig. 4-1, Frame 1). Images recorded at starvation onset have a dappled appearance, with irregular variations in grayscale representing local differences in cell density. Initial aggregates begin to emerge as dark spots within the first 6 to 8 h (Fig. 4-1, compare frames 1 and 2). We define each microcinematography experiment frame (e-frame) as a data structure that contains the positions and radii of each aggregate in the frame. We begin the analysis of aggregate disappearance at the first e-frame (Fig. 4-1, frame 3), when initial aggregates are clearly visible and distinguishable from earlier and more transient fluctuations in grayscale.

To create the first e-frame, the position and size of each aggregate is manually determined, recorded, and then tracked for the rest of the image stack using a semi-automated method. Briefly, our method is to manually curate changes in the size and position of all aggregates every tenth image, record these changes and interpolate them over the intervening nine sequential images, manually check and adjust the interpolation and move on to the next set of ten images. Using this method, we tracked changes in the position and size of a total of 1,727 aggregates. Tracking data is visualized in Figure 4-1a as blue circles in frames 3, 4, and 5.

To synchronize the start of data collection and the start of the o-simulator, the size and location of aggregates in the first e-frame were used to construct the first o-simulator frame (o-frame). These data are visualized in Figure 4-1a as red circles in Figure 4-1a frames 3, 4, and 5. Because Figure

4-1a frame 3 represents both the first e-frame and first o-frame, the red circles and blue circles are identical and exactly overlap. The blue circles are rendered behind the red circles in the image, and so only the red circles are visible.

The simulation examines each pairwise set of circles in each o-frame, and adjusts their size according to the following equations

$$L^k = |X_1^k - X_2^k| \quad (1)$$

$$\Delta V = \tau \frac{4\pi^{4/3}}{\log(L^k / (V_1^k)^{1/3}) + \log(L^k / (V_2^k)^{1/3})} ((V_1^k)^{-1/3} - (V_2^k)^{-1/3}) \quad (2)$$

$$V_1^{k+1} = V_1^k - \Delta V \quad (3)$$

$$V_2^{k+1} = V_2^k - (V_1^{k+1} - V_1^k) \quad (4)$$

where X_1^k , X_2^k , V_1^k and V_2^k represents the positions and volumes at time k and V_1^{k+1} and V_2^{k+1} represents the volumes at time $k + 1$. The outcome from these pairwise equations is that the larger aggregate will increase in volume at the expense of the smaller aggregate, and the amount gained by the larger aggregate will be equal to the amount lost by the smaller aggregate. Distance between aggregates mediates the volume change, so that closer aggregates have more effect than distant aggregates. An aggregate will disappear when the volume drops below a minimum threshold and touching aggregates will merge into a single aggregate of their combined volume. For a detailed description of the o-simulation, see methods.

To measure the accuracy with which the o-simulation can predict the timing of aggregate disappearance, we first determined the appropriate rate of mass transfer between droplets, which is represented as tau (τ) in the volume equation (Eq. 2). The rate of mass transfer between cells appears to undergo a synchronous increase midway through development, and so τ was determined twice (τ -1 and τ -2); τ -1 was determined for the first half of the o-simulation, and τ -2 was determined for the second half (see methods). To calculate these values, we optimized τ for both halves using 15 randomly chosen replicates as training replicates with an advantage of evolutionary algorithms (Fig. 4-2), resulting in a τ -1 of 160 and a τ -2 of 700. We then determined the accuracy for the remaining 5 prediction replicates.

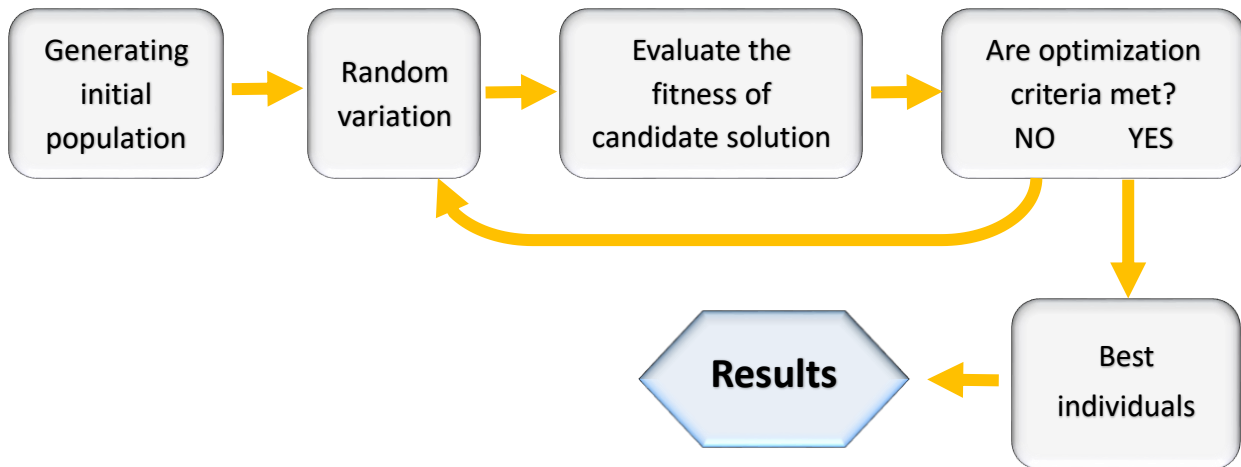


Figure 4-2. Evolutionary algorithm work flow for *M. xanthus* development. This algorithm is used to find the constant value in the Eq.2. First, initial aggregate population was collected from 15 Wild-Type time lapse movies and every value between 0 and 1500 using increment of 10 was tested to obtain τ

Specifically, we paired every aggregate to its corresponding o-simulated aggregate from each sequential e-frame and o-frame, and then employed a scoring mechanism that measured how

accurately the o-simulation matches experiment with respect to aggregate disappearance. The scoring starts at 100% accuracy because the first e-frames and first o-frames are identical. Sequential e-frames and o-frames were then examined, and if one half of an “e-frame::o-frame” aggregate pair disappeared while the other half persisted, the accuracy score would decrease accordingly for that frame and subsequent frames. If the other half of the pair disappeared in a later frame, the accuracy score for that pair would be restored for the remainder of frames. In this way the score represents the accuracy for each frame, so that changes in accuracy can be plotted as a function of time. Aggregate disappearance occurred during the entire period covered by the o-simulation, as seen in Fig. 4-3 (blue line).

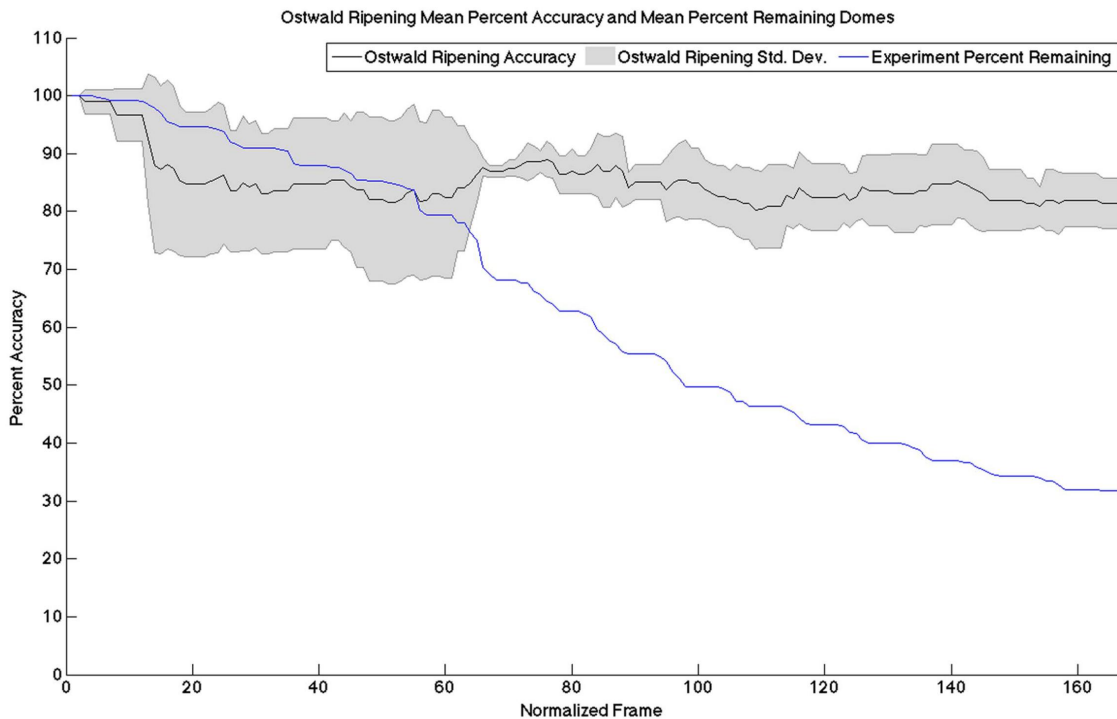


Figure 4-3. Accuracy of the o-simulation of *M. xanthus* aggregation. The black line displays the average accuracy (± 1 SD) of the disappearance model over 5 prediction replicates. The blue line represents the average percent aggregates remaining for the 20 replicates

The accuracy score initially fell to ~80% after the first 20 frames, remained relatively constant until 60 frames, and then increased slightly, reaching a final score of $81\% \pm 4.29\%SD$. The overall average accuracy score was $85.1\% \pm 7.09\%SD$ during the entire 10 to 14 simulated hours since the first e-frame. The relative consistency of the accuracy score indicates that the o-simulation was also able to match the timing of disappearance reasonably well.

To compare our results to previous research, we repeated this comparison using the only other proposed determinant to predict aggregate disappearance in *M. xanthus*, the size threshold hypothesis proposed by Xie *et al* (Xie et al., 2011). The size threshold hypothesis does not include a time component; small aggregates below a threshold simply disappear while the larger ones above the threshold persist. From this hypothesis we created a size simulation (s-simulation) that predicts aggregate disappearance if it is below a specified threshold size based on the first size frame (s-frame), which is also matched to the first e-frame. We determined the best size threshold for the same 15 training replicates that we used for the o-simulation, executed the s-simulation in same manner as the o-simulation, and then generated an accuracy score for the 5 prediction replicates. Because the size threshold hypothesis includes no time component, the rate of mass transfer (τ) is not a component of the s-simulation.

We compared the accuracy scores of the s- and o-simulations with respect to time (Fig. 4-4). The mean accuracy score of the o-simulation is always greater than 80%. In contrast, the mean accuracy score of the s-simulation is less than 40% after the first 20 frames, but this is due to the lack of a time component in the size simulation; between the first and second s-frames, everything below the threshold disappears, and all sequential s-frames are identical from the second to the last frame. In other words, the second s-frame is the last s-frame, and if the s-simulation is an accurate

predictor of which aggregates will disappear during development, then s-frames and e-frames should converge from the second to the last frames. We observed this effect; the mean accuracy score of the s-simulation increases steadily over the next 60 frames, reaching the average accuracy of the o-simulation by frame 100. After that, the accuracy of the two simulations remains similar. Therefore, we conclude that the Ostwald ripening hypothesis matches the accuracy of the size threshold hypothesis in predicting which aggregates will disappear and, because it includes a mechanism, it is also able to predict when they will disappear.

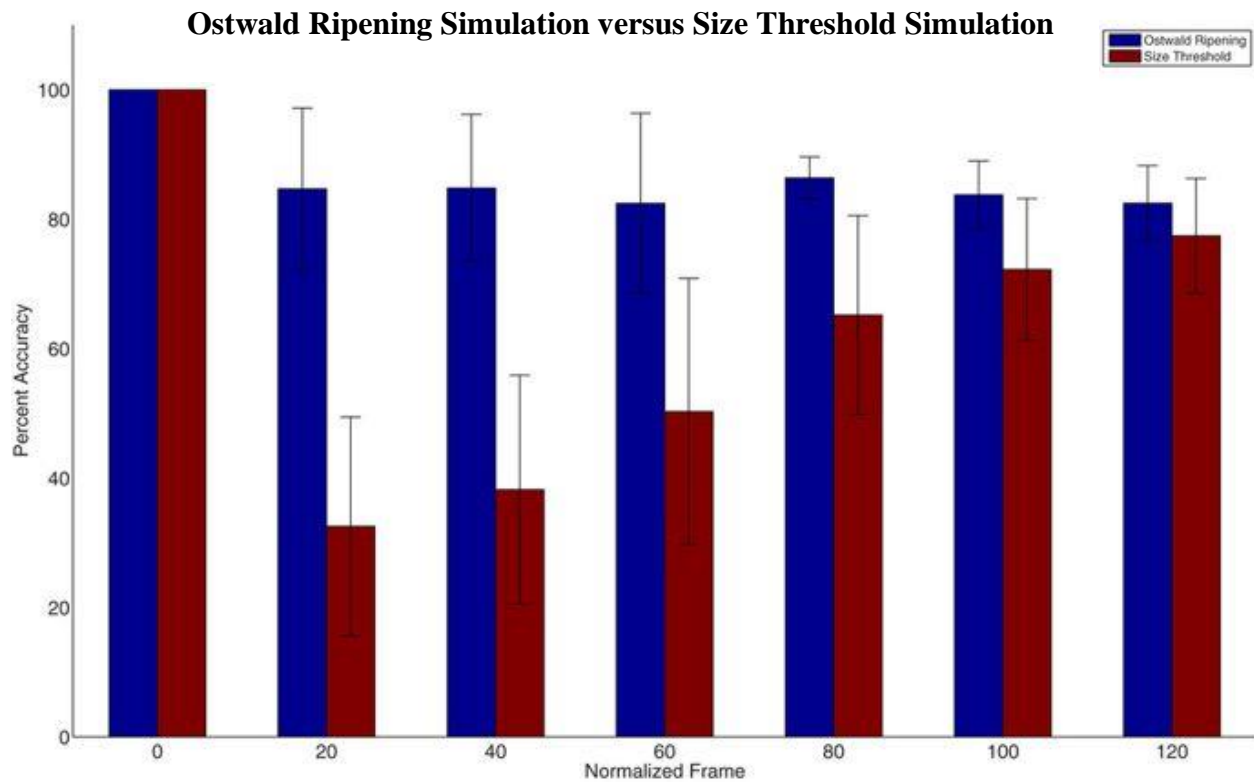


Figure 4-4. Ostwald ripening simulation versus size threshold simulation. A comparison of the average accuracy score between the o-simulator (blue bars) and s-simulator (red bars) with respect to predicting aggregate disappearance over time for 5 prediction replicates. Error bars report one standard deviation

4.4.2 Experimental validation of Ostwald ripening as the mechanism underlying aggregate disappearance

Ostwald ripening in a thin liquid film represents entropy minimization through the reduction in surface area. The surface area of a hemispherical droplet increases more slowly than its volume, and so the total surface area of the thin liquid film decreases as droplets become larger in size and fewer in number. Ostwald ripening also represents a zero-sum game, so shrinking droplets lose liquid to growing droplets (Rump, 2008). By analogy, in a developing *M. xanthus* swarm, shrinking aggregates must lose cells to growing aggregates. If aggregates shrink for a different reason, such as cell death, then the aggregation-as-Ostwald ripening analogy does not hold.

To test the analogy, we repeated the development microcinematography experiments using a 1:150 mixture of fluorescent *M. xanthus* cells. First, we used bright-field microcinematography at 60 × magnification to identify aggregates as either growing or shrinking, then we increased magnification to 150×, positioned the aggregate in the middle of the field-of-view, and used fluorescence microcinematography to track the movement of cells immediately outside the aggregate over 15-minute intervals.

To determine if the net migration of cells was toward or away from an aggregate, we examined the paths of fluorescent cells relative to the centered aggregate; if a cell moved closer to the aggregate, then the cell was designated “towards”, if it moved farther from the aggregate it was designated “away”, and if there was no net movement it was designated “none”. A total of 197 cells were tracked for 12 aggregates (7 growing and 5 shrinking) (Fig. 4-5).

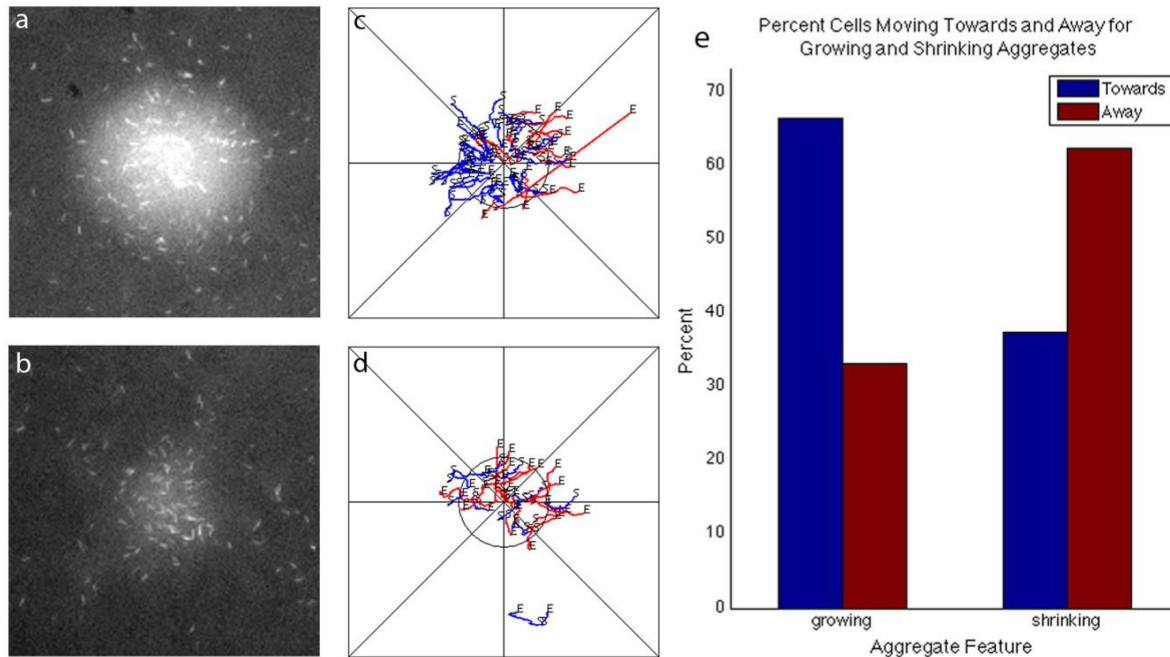


Figure 4-5. Towards/away comparison of fluorescent cells moving in and around growing and shrinking aggregates. (a) Fluorescent images of growing aggregates and (b) shrinking aggregates with fluorescent cells visible in and around them. (c) Total individual tracked cells on seven growing and (d) five shrinking aggregates. Blue lines represent cell tracks moving toward the aggregates, and red lines represent cell tracks moving away from the aggregates. The letters ‘E’ within the tracks indicates the endpoints of tracks, and the letters ‘S’ indicates the starting points of tracks. (e) The total number of cells tracked as moving ‘towards’ (blue bars) or ‘away’ (red bars) from growing and shrinking aggregates

Analysis of the comparison led us to think that the results are unambiguous. Cells near a growing aggregate (Fig. 4-5a) are more likely to be moving toward it (Fig. 4-5c), and cells near a shrinking aggregate (Fig. 4-5b) are more likely to be moving away from it (Fig. 4-5d). The overall difference is two-fold (Fig. 4-5e), which strongly supports the idea that disappearing aggregates shrink

because they are losing cells to growing aggregates that persist. Therefore, these data support the aggregation-as-Ostwald ripening analogy.

4.4.3 Characterizing phenotypic boundaries for an aggregation-as-Ostwald ripening analogy

Ostwald ripening is only one of two behaviors that describe the dynamics of entropy minimization in a thin liquid film. The second behavior is called migration, which describes how droplets move across a thin liquid film. Ostwald ripening and migration can be represented by separate sets of equations, but they are mechanistically linked, and collectively they are called coarsening.

Migration is caused by asymmetries in the density of particles around a droplet as a function of Ostwald ripening by neighboring droplets. *M. xanthus* aggregates sometimes move across the swarm in a manner that appears similar to migration, but the speed and direction of aggregate movement is highly variable. Equations that describe droplet migration on thin liquid films fail to predict aggregate movement any better than equations that describe random movement.

We note two phenotypic features clearly visible in image stacks from the 20 replicates that may partly explain why aggregate movement is not comparable to droplet migration. We refer to these two features as “snakes” and “scars”. Neither snakes nor scars are predicted by a coarsening model, and they may indicate important ways in which coarsening and aggregation are dissimilar. We discuss snakes and scars separately.

Snakes sometimes occur when an aggregate disappears (Fig. 4-6a, also stack 20 inset within frames 800–1000). They can be observed in the image stacks as elongated slightly darker regions that

travel quickly away from the disappearing aggregate, usually in two opposing directions. Often a snake will seem to travel directly toward a nearby aggregate.

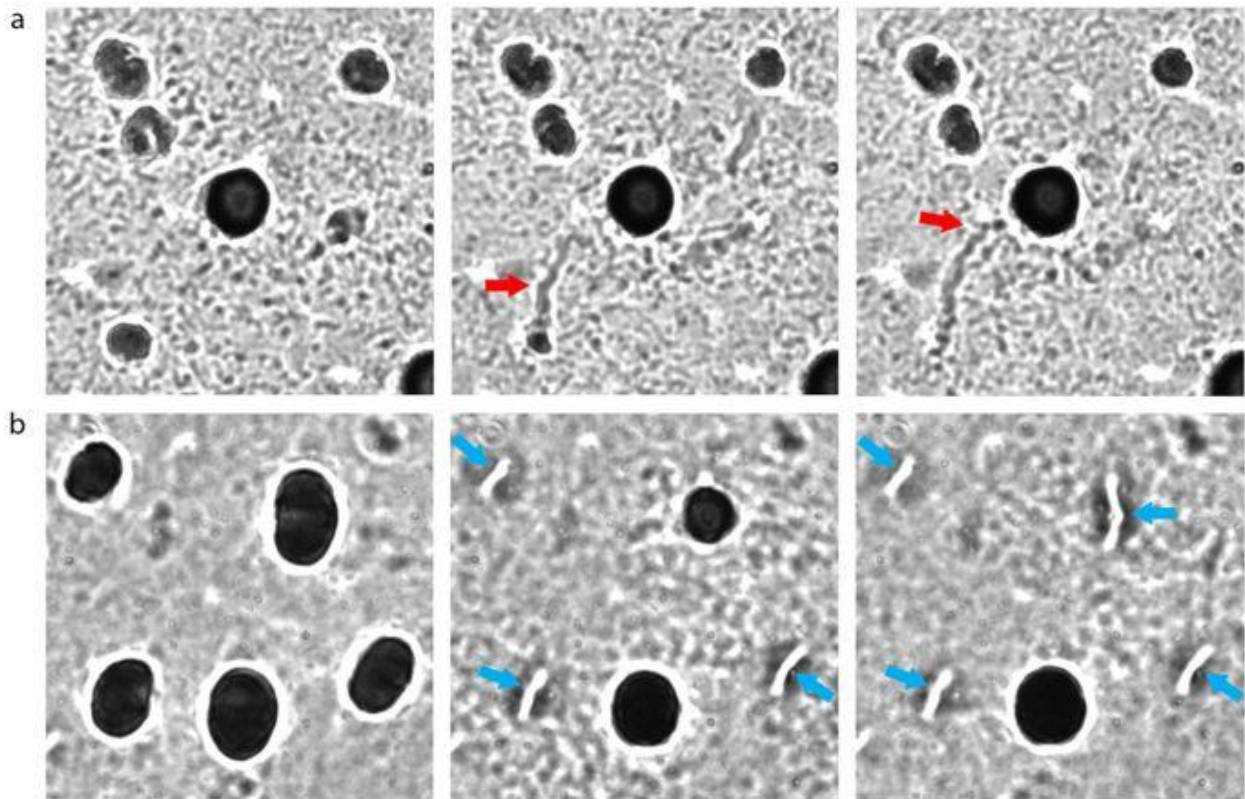


Figure 4-6. Representative examples of snakes and scars. (a) A snake (red arrow) traveling from a disappearing aggregate to a growing aggregate. (b) Scars remaining (blue arrows) where aggregates have disappeared

We hypothesize that snakes represent the transfer of large quantities of cells from one aggregate to another through structures called slime trails. *M. xanthus* cells deposit trails of a polysaccharide matrix, called slime, as they move across agar, and cells encountering previously deposited slime trails tend to follow them (Wolgemuth, Hoiczyk, Kaiser, & Oster, 2002). This effect of slime trails functions together with other forces, such as surface tension, to cause the formation of parallel

lines of cells, called streams (Jelsbak & Sørensen, 2002). Our observation that snakes frequently travel in opposing directions may indicate where slime trails have formed, and our observation that snakes frequently travel to nearby aggregates may indicate that slime trails cause a preferential transfer of cells between aggregate pairs.

Scars also sometimes occur when an aggregate disappears (Fig. 4-6b). Scars seem residual, as though the disappeared aggregate had caused a change in the substrate that permanently altered the structure of the swarm in that region. Cell movement is observed within and around scars, but the scars do not move across a swarm. The overwhelming majority of disappearing aggregates that leave scars also do not move, but even in the few cases where the disappearing aggregates do move, the scars they leave behind do not. We hypothesize that scars represent the aborted maturation of an aggregate to a fruiting body. Perhaps they are the beginnings of mucoid stalks that would have suspended the bolus of spores.

We further hypothesize that snakes and scars are phenotypic features that indicate two aspects of aggregation that make it unlike coarsening. Snakes indicate that cells leaving a disappearing aggregate do not diffuse evenly into a swarm, but preferentially follow slime trails. This would cause coarsening and aggregation to deviate with respect to both movement and disappearance, since the asymmetry of cell density would be greatly increased, and cell transfer between pairs of aggregates would depend on more than size and proximity. Scars indicate that aggregate movement may be disconnected from disappearance. In coarsening, Ostwald ripening and migration are linked by the same underlying mechanism. In contrast, if aggregates can anchor themselves to the substrate so that they don't move, but they still exchange cells and may disappear, then aggregate movement and disappearance have been mechanistically uncoupled. Perhaps

snakes and scars are some visible manifestations of why our predictions for movement are not accurate, and why the accuracy of the o-simulations top out at ~85%.

4.5 Discussion

We have demonstrated that a model simulating *M. xanthus* aggregation based on equations that describe Ostwald ripening in thin liquid films is able to predict which aggregates will persist and which will disappear with ~85% accuracy. We also tested and validated one of the central predictions of such a model: that aggregates grow because of cell accumulation and shrink and disappear because of cell loss. This provides a mechanism for the size threshold determinant (Xie et al., 2011), and is the first alternative to the traffic jam model that includes aggregate disappearance.

Our argument from analogy is not to claim that *M. xanthus* aggregation is coarsening in thin liquid films; enough is known about *M. xanthus* genetics, cellular behavior, and multicellular self-organization to refrain from making this much stronger claim. For example, we know that *M. xanthus* synchrony and symmetry breaking is under genetic control by molecular signals and pathways that coordinate swarm cell movement (Jelsbak & Sørensen, 2002; Zhang et al., 2011). We also know that *M. xanthus* cells are active (Mauriello, Mignot, Yang, & Zusman, 2010; Mignot, 2007; Nan et al., 2011), they move along a semi-rigid axis with a genetically controlled reversal frequency (Blackhart & Zusman, 1985; Spormann & Kaiser, 1999), and they form streams that steer them over long distances (Jelsbak & Sørensen, 2000; Sager & Kaiser, 1993). Finally, we know that the shape and structure of an *M. xanthus* fruiting body requires the coordination of thousands of cells because it is much more than a droplet, with a cell-free mucoid stalk and a bolus of myxospores at the center (Dao, Kessin, & Ennis, 2000).

Instead, our argument is that Ostwald ripening is similar enough to *M. xanthus* aggregation that it can provide testable genetic and behavioral hypotheses and a mechanistic model consistent with Occam's Razor. An Ostwald ripening aggregation model reduces the number of developmental decisions that must be assigned to quorum sensing and cell-to-cell contact mediated mechanisms. It also provides a hypothesis that links individual cell movements to an important aspect of swarm self-organization.

4.6 Acknowledgements

This research was made possible by a National Science Foundation Career award (MCB-0746066, Characterization of Transcriptional Activators that Regulate Emergent Behavior) to R.D.W., and National Science Foundation EFRI-MIKS award (EFRI-1106933, Deciphering and Controlling the Signal Processes in Bacterial Multicellular Systems and Bacteria-Host Interactions) to R.D.W. (co-PI). We would like to thank Joshua Shaevitz and Shashi Thutupalli (Princeton University) for help with interpreting the discretized 2-dimensional migration equations from Vasiev, B. et al. (1994) (Vasiev et al., 1994). We would also like to thank Laura Welch for editing the manuscript.

4.7 References

- Blackhart, B. D., & Zusman, D. R. (1985). “Frizzy” genes of *Myxococcus xanthus* are involved in control of frequency of reversal of gliding motility. *Proceedings of the National Academy of Sciences*, 82(24), 8767–8770.
- Curtis, P. D., Taylor, R. G., Welch, R. D., & Shimkets, L. J. (2007). Spatial organization of *Myxococcus xanthus* during fruiting body formation. *Journal of Bacteriology*, 189(24), 9126–9130.
- Dao, D. N., Kessin, R. H., & Ennis, H. L. (2000). Developmental cheating and the evolutionary biology of Dictyostelium and Myxococcus. *Microbiology*, 146(7), 1505–1512.
- Igoshin, O. A., Kaiser, D., & Oster, G. (2004). Breaking symmetry in myxobacteria. *Current Biology*, 14(12), R459–R462.
- Igoshin, O. A., Mogilner, A., Welch, R. D., Kaiser, D., & Oster, G. (2001). Pattern formation and traveling waves in myxobacteria : Theory and modeling, 98(26), 14913–14918.
- Igoshin, O. A., Welch, R., Kaiser, D., & Oster, G. (2004). Waves and aggregation patterns in myxobacteria.
- Igoshin, O. a, Goldbeter, A., Kaiser, D., & Oster, G. (2004). A biochemical oscillator explains several aspects of *Myxococcus xanthus* behavior during development. *Proceedings of the National Academy of Sciences of the United States of America*, 101(44), 15760–15765.
- Jelsbak, L., & Søgaard-Andersen, L. (2000). Pattern formation: Fruiting body morphogenesis in *Myxococcus xanthus*. *Current Opinion in Microbiology*, 3(6), 637–642.
- Jelsbak, L., & Søgaard-Andersen, L. (2002). Pattern formation by a cell surface-associated morphogen in *Myxococcus xanthus*. *Proceedings of the National Academy of Sciences of the United States of America*, 99(Track II), 2032–2037.
- Jelsbak, L., & Søgaard-Andersen, L. (2003). Cell behavior and cell-cell communication during fruiting body morphogenesis in *Myxococcus xanthus*. In *Journal of Microbiological Methods* (Vol. 55, pp. 829–839).
- Mauriello, E. M. F., Mignot, T., Yang, Z., & Zusman, D. R. (2010). Gliding Motility Revisited: How Do the Myxobacteria Move without Flagella? *Microbiology and Molecular Biology Reviews*, 74(2), 229–249.
- Mignot, T. (2007). The elusive engine in *Myxococcus xanthus* gliding motility. *Cellular and Molecular Life Sciences*.
- Nan, B., Chen, J., Neu, J. C., Berry, R. M., Oster, G., & Zusman, D. R. (2011). Myxobacteria gliding motility requires cytoskeleton rotation powered by proton motive force. *Proceedings of the National Academy of Sciences*, 108(6), 2498–2503.

- Rump, T. (2008). Coarsening processes in thin liquid films: Analysis and numerics, 143.
- Sager, B., & Kaiser, D. (1993). Two cell-density domains within the *Myxococcus xanthus* fruiting body. *Proceedings of the National Academy of Sciences of the United States of America*, 90(8), 3690–3694.
- Shimkets, L. J., & Kaiser, D. (1982). Induction of coordinated movement of *Myxococcus xanthus* cells. *Journal of Bacteriology*, 152(1), 451–461.
- Sliusarenko, O., Zusman, D. R., & Oster, G. (2007). Aggregation during Fruiting Body Formation in *Myxococcus xanthus* Is Driven by Reducing Cell Movement $\square \dagger$, 189(2), 611–619.
- Sozinova, O., Jiang, Y., Kaiser, D., & Alber, M. (2005). A three-dimensional model of myxobacterial aggregation by contact-mediated interactions. *Proceedings of the National Academy of Sciences of the United States of America*, 102(32), 11308–11312.
- Spormann, A. M., & Kaiser, D. (1999). Gliding mutants of *Myxococcus xanthus* with high reversal frequencies and small displacements. *Journal of Bacteriology*, 181(8), 2593–2601.
- Vasiev, B. N., Hogeweg, P., & Panfilov, A. V. (1994). Simulation of dictyostelium discoideum aggregation via reaction-diffusion model. *Physical Review Letters*, 73(23), 3173–3176.
- Welch, R., & Kaiser, D. (2001). Cell behavior in traveling wave patterns of myxobacteria.
- Wolgemuth, C., Hoiczyk, E., Kaiser, D., & Oster, G. (2002). How myxobacteria glide. *Current Biology*, 12(5), 369–377.
- Xie, C., Zhang, H., Shimkets, L. J., & Igoshin, O. A. (2011). Statistical image analysis reveals features affecting fates of *Myxococcus xanthus* developmental aggregates. *Proceedings of the National Academy of Sciences*, 108(14), 5915–5920.
- Zhang, H., Angus, S., Tran, M., Xie, C., Igoshin, O. a, & Welch, R. D. (2011). Quantifying aggregation dynamics during *Myxococcus xanthus* development. *Journal of Bacteriology*, 193(19), 5164–5170.
- Zhao, K., Tseng, B. S., Beckerman, B., Jin, F., Gibiansky, M. L., Harrison, J. J., ... Wong, G. C. L. (2013). Psl trails guide exploration and microcolony formation in *Pseudomonas aeruginosa* biofilms. *Nature*, 497(7449), 388–391.

**Chapter 5: Establishing A Correlation between Dynamical Changes
in Developmental Phenotype and Single Gene Disruptions within
Paralogous Gene Families in *Myxococcus xanthus***

5.1 Introduction

In the laboratory, Wild-Type *M. xanthus* cells are defined by their ability to both swarm and develop into several hundred fruiting bodies over a period of 24 - 48 h. This is how the Wild-Type phenotype is defined and studied in *M. xanthus*, and any deviation from this expected pattern is considered a deviation from Wild-Type. For example, development is delayed if the formation of aggregates does not start for more than 48 h, and fruiting bodies are abnormal if they are elongated or have no clearly defined boundary. Over time, a set of phenotypic variables (number, timing, shape, etc.,) has come to define *M. xanthus* development, with Wild-Type falling within an acceptable range of values. These standard variables are used in the laboratory to measure phenotypic differences between Wild-Type and mutant strains.

There is no reason to believe that laboratory assay results designed to measure the standard set of variables provide a comprehensive description of the *M. xanthus* phenotype. Even with the standard set of assays, there is limited consensus on the range that should be used to define Wild-Type. In many cases, these standard assays will fail to identify subtle phenotypic manifestations of any given mutation. Therefore, it is difficult to make accurate comparisons between the *M. xanthus* genome and phenome since the impact of many mutations might be lost.

M. xanthus, a delta-proteobacterium, has a large genome of over 9Mbp compared to many other bacteria; approximately 90% of the genome contains protein coding sequences (Goldman et al., 2006). Other delta-proteobacteria have smaller genomes, ranging from 3.66 to 5.01 Mbp (Karlin, Brocchieri, Mrazek, & Kaiser, 2006). Gene duplications are one of the primary reasons for the comparative size of the *M. xanthus* genome. Bioinformatic analysis indicated that almost 50% of

its proteome covers 872 paralogous gene families and most of them are dedicated to cell-to-cell signaling and small molecule sensing (Goldman et al., 2006).

Genes with signaling functions make up 8.7% of *M. xanthus* genome, forming the largest functional group (Unpublished data from Anthony Garza's lab) (Fig. 5-1).

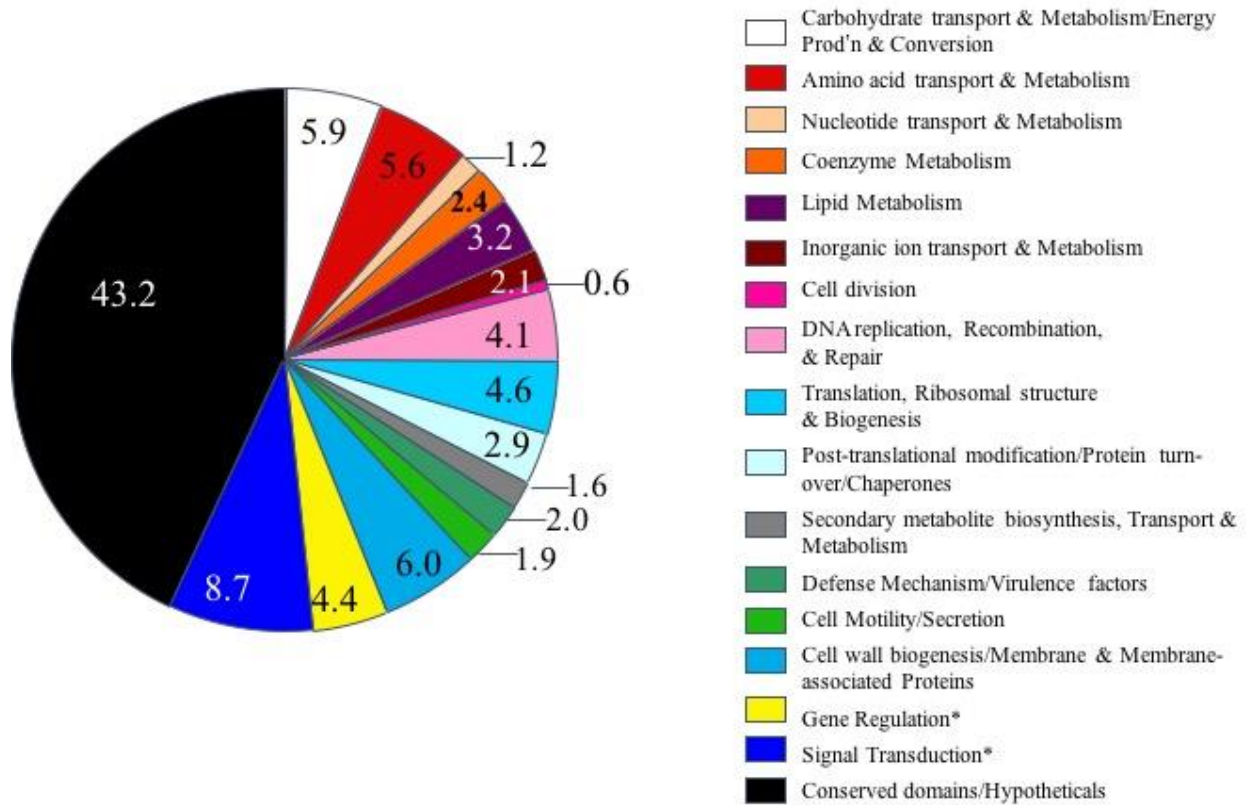


Figure 5-1. Pie chart representing annotation of 9.6 Mb *M. xanthus* genome (Unpublished data from Anthony Garza's lab)

The *M. xanthus* genome is predicted to encode 97 serine/threonine protein kinases (STPK), 137 sensor and hybrid histidine protein kinases (HPK) (far more than any other delta-proteobacteria), 53 NtrC-like activators, and 38 ECF sigma 70 factors (Goldman et al., 2006). The large number of DNA-binding transcription regulators in the *M. xanthus* genome indicates a clear divergence

from other prokaryotes. However, *M. xanthus* has a surprisingly low number of one-component transcriptional regulators, with only 310. Other soil bacteria have more, e.g., *Streptomyces coelicolor* with 584, and *S. avermitilis* with 530 (Romero et al., 2014). TetR, LuxR, and AraC protein family members are examples of these regulators. On the other hand, the *M. xanthus* genome encodes a high number of two-component transcriptional regulators, more than five times the number found in other delta-proteobacteria (Goldman et al., 2006). This may indicate that *M. xanthus* has a better signal transduction system, which is able to receive more signals from external stimuli and regulate inner metabolism to optimize survival.

One of the challenges we face in annotating bacterial genomes is that the function of only about half the genes can be predicted with a reasonable degree of confidence based on sequence homology (Bork, 2000). The remaining genes are either “conserved hypotheticals” (homologous to other genes of unknown function) or “hypotheticals” (with no known homologous genes). In other words, in the average annotated bacterial genome, one out of three proteins has an unknown function (Sivashankari & Shanmughavel, 2006). This is true of *M. xanthus* as well. As shown in the above bioinformatics analysis (Fig. 5-1), almost half of the genome, 43.2%, contains both conserved hypotheticals and hypotheticals and the role of these gene products during fruiting body formation has not been yet to be studied (Goldman et al., 2006).

To address the effects of paralogous gene groups on *M. xanthus* development, the entire family of NtrC-like activators and ABC transporters have been studied, and several genes have been found to be important for different stages of fruiting body formation (Caberoy et al., 2003; Giglio et al., 2011; Giglio et al., 2010; Lancero et al., 2004; Sarwar & Garza, 2015; Yan, Bradley, Friedman, & Welch, 2014).

In this study, we aimed to identify new variables for aggregates and carefully characterize the existing ones in a more efficient way. To accomplish this, we generated the biggest library of phenotypic data on *M. xanthus* development so far by recording the behavior of Wild-Type and 392 mutant strains using time-lapse microcinematography.

These mutant strains generated in our lab were selected to represent the above-mentioned ABC transporters and NtrC-like regulators, along with two other important gene families, the ECF sigma factors and One-component regulators, as well as a small set of hypotheticals. The data set is composed of 1608 image stacks representing at least three replicates of each mutant strain. We hypothesize that (i) phenotypes would cluster according to homologous families and (ii) there is a finite number of ways that mutation can impact phenotype.

5.2 Material and methods

Cultivation and Development: Liquid cultures for vegetative growth and development assays of *M. xanthus* were prepared as explained in Chapter 4.3.1.

Identification of paralogous gene families: A sequence-level characterization of ABC transporters has been done as explained by Yan, Bradley, Friedman, & Welch, 2014. NtrC-like activators were identified as reported by Jakobsen et al., 2004. ECF sigma factors, One Components and hypotheticals were reviewed and identified using pfam (Finn et al., 2014; Sonnhammer, Eddy, & Durbin, 1997) and the MIST method (Ulrich & Zhulin, 2007). BLAST analysis (Altschul, Gish, Miller, Myers, & Lipman, 1990) over GenBank (Benson et al., 2013) was used as an additional tool to confirm the alignment and selection.

Mutant library generation: Web-based primer3 software (<http://sourceforge.net/projects/primer3/>) was used to generate primers to amplify inner fragments among chosen *M. xanthus* ORFs. These primers were then used for mutant creation through homologous recombination by plasmid insertion as described previously (Caberoy et al., 2003; Yan et al., 2014). In brief, amplified fragments, with a length of 400-600bp, were ligated into pCR®2.1-TOPO (Invitrogen) plasmid. These plasmids were cloned into *E. coli* DH5- α cells with antibiotic marker, kanamycin. Isolated plasmid particles were then cloned into *M. xanthus* cells by electroporation (650V). Inner fragments of *M. xanthus* ORFs on plasmids were incorporated into *M. xanthus* genome by homologous recombination (Caberoy et al., 2003). Successful clones with desired locations of inner fragments were confirmed with PCR by targeting upstream of each target gene loci and TOPO vector part. The amplicons around 1.2Kbp in length were taken as successful clones. Wild-Type DK162 was used as a negative control.

5.3 Results and Discussion

The analysis of this massive movie library is still ongoing, but we have already made four important observations so far: (i) more than half of the mutant strains were found to display a developmental phenotype that is distinguishable from Wild-Type, (ii) a new common periodic multicellular behavior, which we call “pulsatile,” was also detected, (iii) all observed phenotypes were found to be consistent with the “aggregation-as-phase-change” model of development, and (iv) some mutant phenotypes were overrepresented in particular gene families.

5.3.1 Identification of paralogous gene families in *Myxococcus xanthus*

Annotation of ABC transporters (192) (Yan et al., 2014), NtrC-like activators (53) (Jakobsen et al., 2004), ECF sigma factors (38) and One Components (96) has been performed using a combination of pfam (Finn et al., 2014; Sonnhammer et al., 1997), MIST (Ulrich & Zhulin, 2007), and BLAST (Altschul et al., 1990) using previously submitted genomes on GenBank (Benson et al., 2013) as the reference data pool for each genetic element. The distribution of each gene family we studied is demonstrated in Fig. 5-2 compared to the entire genome of *M. xanthus*.

5.3.2 Characterization of *Myxococcus xanthus* developmental phenotype

Development is a dynamic process that begins when cells are placed on agar and continues to the point when they aggregate to form multicellular fruiting bodies. In order to understand the function of a given gene product on aggregation, we analyzed the development process as a whole. First, 5×10^9 cell/ml were spotted on starvation agar, and time-lapse microcinematography was started, recording an image at 1 min intervals for 24 h. For reproducibility, every experimental condition was kept the same for all movie setups. A gasket-slide complex was prepared daily to minimize variation in the stiffness properties of agar, and at least three replicates were generated for each mutant.

Movies were carefully analyzed in comparison with the Wild-Type phenotype, including: (i) timing: Wild-Type cells aggregate between 7h to 11h in our experimental conditions; (ii) behavior: after elongated aggregates form, they continuously mature into fruiting bodies by becoming circular and darker, and the transition pattern is uninterrupted; and (iii) mature fruiting bodies: Wild-Type aggregates become dark, circular, stable, immobile fruiting bodies at the end of 24h.

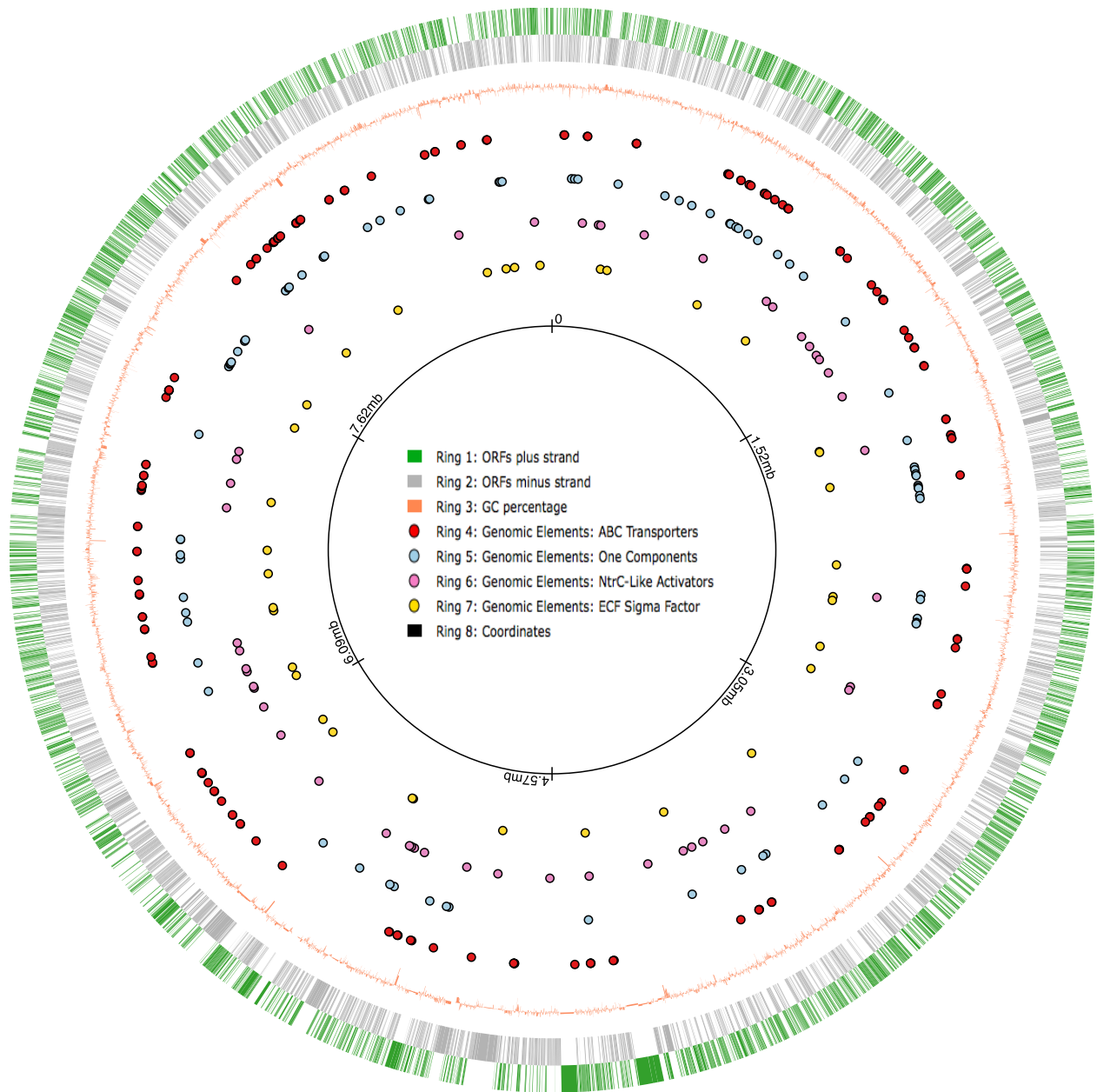


Figure 5-2. Distribution of paralogous gene families in *M. xanthus* genome. Green bars in the outer ring represent the genes transcribed in the clockwise direction while gray bars represent the genes transcribed on a negative strand. Orange frequencies indicate GC percentages and red colored dots show coding genes for ABC transporters. Light-blue, pink, yellow colored dots represent One Components, NtrC-like activators and ECF sigma factors respectively

Based on these parameters, we found that phenotypes fall into 9 different categories (Fig. 5-3). The majority of the genes we tested demonstrated different phenotypes compared to Wild-Type, while only 41% of studied genes showed Wild-Type-like phenotype.

The most abundant non-Wild-Type phenotype we analyzed was pulsatile aggregation, which was detected in 20% of the mutants. In this phenotype, aggregates were formed around 7 h, but then demonstrated a unique transition pattern different than Wild-Type development. The pulsatile aggregates partially dissolve and reform several times between 7 h and 24 h periodically, appearing as “pulses” on the time-lapse video. These “pulses” were found to be directional, meaning they start at one point of the swarm and move to another point, and this process repeats several times. While some of the pulses last for 15 h, some only persist for 2 h. Phenotypic variation in some mutant strains was observed. For example, ABC transport MXAN_0721 only demonstrates a pulsatile phenotype occasionally. This could be due to a sub-phenotype of the pulsatile phenotype. Preliminary cell tracking data shows that cells within a pulsing aggregate regulate their movement in a way which increases their net movement and may create pulses in return.

The second type of common mutant phenotype, approximately 10% of strains tested, is “no aggregation.” This confirms estimates from previous studies (Kuner & Kaiser, 1981). Some of them show no movement at all and some show accumulation of cells that do not go on to form defined structures. 8% of the all phenotypes show late aggregation and abnormal aggregates, meaning they aggregate later than 13 h and do not become mature fruiting bodies. Some have elongated aggregates, but some of them do not progress beyond a couple of layers of cells. If aggregation takes place after 13 h and aggregates quickly mature into fruiting bodies, these are

Type		Description	Example Images		
1	Like Wild Type	Indistinguishable from WT aggregation	7h	12h	24h
2	Early Aggregation	Aggregates appear early	4.5h	12h	24h
3	Pulsatile Aggregation	Aggregates repeatedly form & re-form in synchrony	8h	14h	24h
4	Aggregation and re-aggregation	Aggregates form, dissipate, and form again	10h	15h	24h
5	Aggregation & Disintegration	Aggregates form and dissipate	9h	15h	24h
6	Late aggregation, normal aggregates	Aggregates like WT but appear later	13h	18h	24h
7	Late aggregation, abnormal aggregates	Aggregates abnormal & appear later	13h	18h	24h
8	Abnormal	Aggregates form but remain immature	7h	11h	24h
9	No aggregation	Movement in swarm, but no aggregation	9h	15h	24h

Figure 5-3. Phenotype categories of *M. xanthus* development. The second column represents the type of phenotype. The third column represents the definition of corresponding phenotype and last column shows example images of phenotypes taken from time-lapse movies. The time point for each image is indicated in the middle upper part of the images. Numbers from 1 to 9 were added to the table as a visual aid

called late aggregation and normal aggregates, which occurs in 5% of strains studied. If aggregates are formed around 7 h and do not mature into fruiting bodies within 24 h, then it is called abnormal aggregate, 5% of strains. There are other rare phenotypes in which aggregation and disintegration occur, with tiny aggregates forming around 7 h and persisting for 2 h at most before disintegrating. Another rare phenotype is aggregation and re-aggregation, in which formed aggregates begin to dissipate and reform again later towards 15 h. The percentage distribution of these mutant phenotypes is shown in Fig. 5-4.

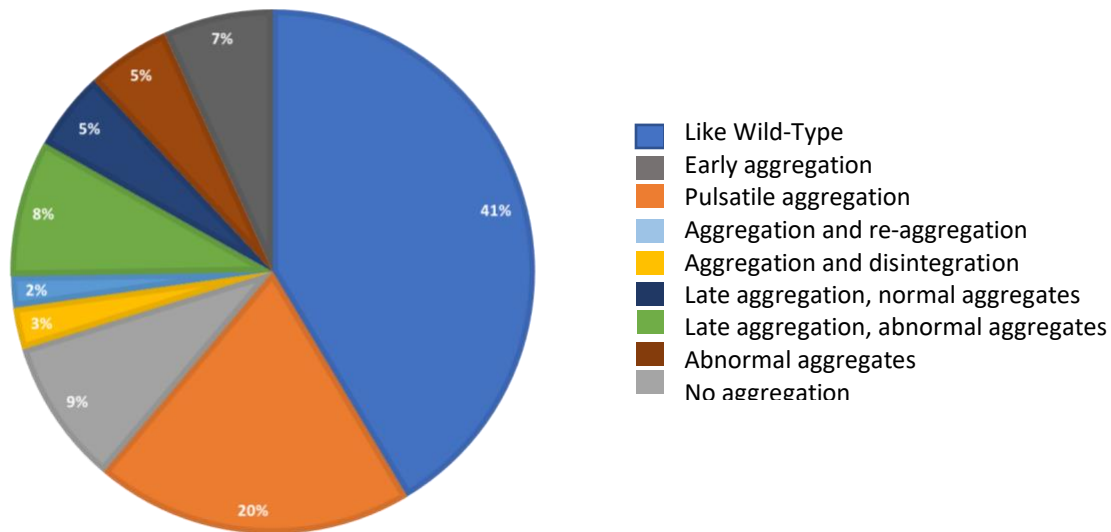


Figure 5-4. Pie chart of phenotype category analysis of *M. xanthus* mutant library

5.3.3 Correlation between gene families and phenotype

Next, we investigated phenotype frequencies within the homologous gene families. Even though members of gene families have different individual functions or regulate the transcription of a variety of different genes, they may play a collective role to contribute to some aspect of development. If that is the case, we should be able to see correlation between phenotype and

functional gene groups. Statistical analysis showed that ABC transporters do in fact correlate with pulsatile phenotype. Almost 35% of the ABC transporter mutant phenotypes exhibit pulses during development (Fig 5-5). Other phenotypes are observed in fewer than 8% and some phenotypes are not observed in ABC transporters in a 24 h time course, e.g., aggregation and reaggregation.

NtrC-like activators play a very important role during early development and later in the development process (Caberoy et al., 2003; Krista M. Giglio et al., 2010). This group carries the lowest number of mutants that exhibit Wild-Type-like phenotype. Mutants of One Component signal transduction systems appear to have little impact on phenotype. However, these exhibit the largest number of no aggregation phenotypes. 12 out of 96 could be potentially lethal, because their knockouts were not successfully grown (data plots from these trials were not included in total calculations). On the other hand, none of the ECF sigma factor mutants showed the no aggregation phenotype. These also exhibited more early aggregation phenotypes than any other phenotype. Mutants of the 20 hypothetical genes tested also diverged from Wild-Type, manifesting an array of phenotypes. This suggests that there are many other genes with no known function that may in fact play a role in *M. xanthus* development.

In order to understand the transition from autonomous individual cells to multicellularity, it is important to analyze each step of the development process in detail. Thus, we studied multiple entire transcriptional regulator families that include over 400 knockout mutant strains (including those strains that failed to grow) to reveal the role of 4 entire homologous gene families to enable us to understand *M. xanthus* development better. To do this, we employed time-lapse microcinematography to closely investigate the self-organization that characterizes *M. xanthus* development. Analysis of over 1200 movies uncovered that fruiting body formation can be

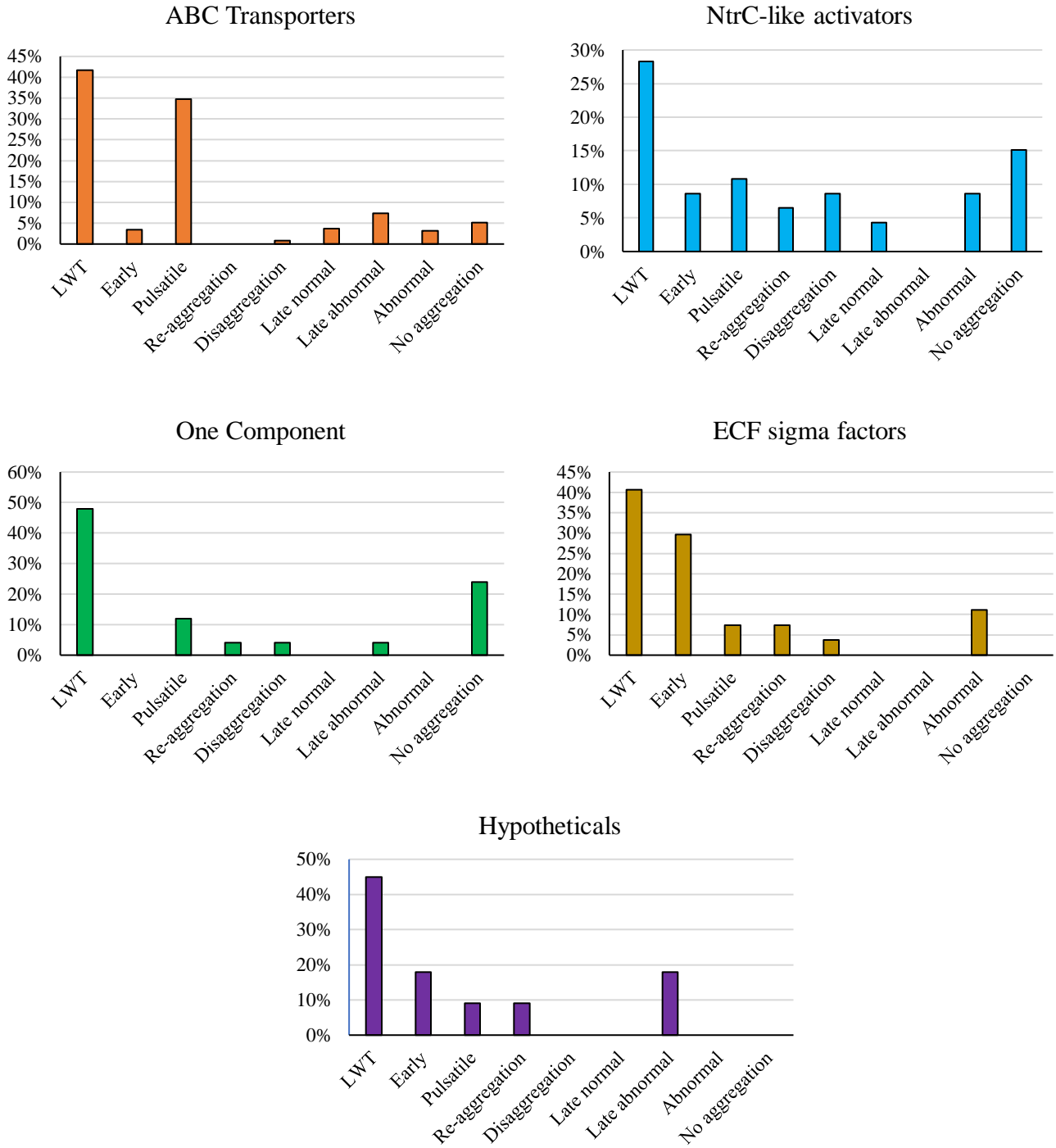


Figure 5-5. Distribution of developmental phenotypes based on paralogous gene families. The x-axis on each graph represent 9 phenotype categories and the y-axis represents their percentage distribution

grouped into one of nine unique patterns. Further, we were able to identify phenotypic impact in over 50% of the mutant strains studied, a much higher percentage than is typically identified using standard assays. One of these phenotypic categories, which we call pulsatile, was enriched in ABC transporters. Moreover, within the phenotypic categories, some developmental dynamic features were more likely to appear together. This might show a close relation between gene groups critical for those phenotypic categories. This study has generated a substantial developmental movie library for each of four major gene families: ABC transporters, NtrC-like regulators, ECF sigma factors, and One-component regulators.

5.4 References

- Altschul, S. F., Gish, W., Miller, W., Myers, E. W., & Lipman, D. J. (1990). Basic local alignment search tool. *Journal of Molecular Biology*.
- Benson, D. A., Cavanaugh, M., Clark, K., Karsch-Mizrachi, I., Lipman, D. J., Ostell, J., & Sayers, E. W. (2013). GenBank. *Nucleic Acids Research*.
- Bork, P. (2000). Powers and pitfalls in sequence analysis: The 70% hurdle. *Genome Research*.
- Caberoy, N. B., Welch, R. D., Jakobsen, J. S., Slater, S. C., & Garza, A. G. (2003). Global Mutational Analysis of NtrC-Like Activators in *Myxococcus xanthus* : Identifying Activator Mutants Defective for Motility and Fruiting Body Development, *185*(20), 6083–6094.
- Finn, R. D., Bateman, A., Clements, J., Coggill, P., Eberhardt, R. Y., Eddy, S. R., ... Punta, M. (2014). Pfam: The protein families database. *Nucleic Acids Research*.
- Giglio, K. M., Caberoy, N., Suen, G., Kaiser, D., & Garza, A. G. (2011). A cascade of coregulating enhancer binding proteins initiates and propagates a multicellular developmental program. *Proceedings of the National Academy of Sciences*, *108*(32), E431–E439.
- Giglio, K. M., Eisenstatt, J., & Garza, A. G. (2010). Identification of enhancer binding proteins important for *Myxococcus xanthus* development. *Journal of Bacteriology*.
- Goldman, B. S., Nierman, W. C., Kaiser, D., Slater, S. C., Durkin, A. S., Eisen, J. A., ... Kaplan, H. B. (2006). Evolution of sensory complexity recorded in a myxobacterial genome. *Proceedings of the National Academy of Sciences*, *103*(41), 15200–15205.
- Jakobsen, J. S., Jelsbak, L., Jelsbak, L., Welch, R. D., Cummings, C., Goldman, B., ... Kaiser, D. (2004). σ 54 enhancer binding proteins and *Myxococcus xanthus* fruiting body development. *Journal of Bacteriology*, *186*(13), 4361–4368.
- Karlin, S., Brocchieri, L., Mrazek, J., & Kaiser, D. (2006). Distinguishing features of γ -proteobacterial genomes. *Proceedings of the National Academy of Sciences*, *103*(30), 11352–11357.
- Kuner, J. M., & Kaiser, D. (1981). Introduction of transposon Tn5 into *Myxococcus* for analysis of developmental and other nonselectable mutants. *Proceedings of the National Academy of Sciences*, *78*(1), 425–429.
- Lancero, H., Caberoy, N. B., Castaneda, S., Li, Y., Lu, A., Dutton, D., ... Garza, A. G. (2004). Characterization of a *Myxococcus xanthus* mutant that is defective for adventurous motility and social motility. *Microbiology*, *150*(12), 4085–4093.
- Romero, D. A., Hasan, A. H., Lin, Y. fei, Kime, L., Ruiz-Larrabeiti, O., Urem, M., ... Mcdowall, K. J. (2014). A comparison of key aspects of gene regulation in *Streptomyces coelicolor* and *Escherichia coli* using nucleotide-resolution transcription maps produced in parallel by global and differential RNA sequencing. *Molecular Microbiology*.

- Sarwar, Z., & Garza, A. G. (2015). Two-component signal transduction systems that regulate the temporal and spatial expression of *Myxococcus xanthus* sporulation genes. *Journal of Bacteriology*.
- Sivashankari, S., & Shanmughavel, P. (2006). Functional annotation of hypothetical proteins - A review. *Bioinformation*.
- Sonnhammer, E. L. L., Eddy, S. R., & Durbin, R. (1997). Pfam: A comprehensive database of protein domain families based on seed alignments. *Proteins: Structure, Function and Genetics*.
- Ulrich, L. E., & Zhulin, I. B. (2007). MiST: A microbial signal transduction database. *Nucleic Acids Research*.
- Yan, J., Bradley, M. D., Friedman, J., & Welch, R. D. (2014). Phenotypic profiling of ABC transporter coding genes in *Myxococcus xanthus*. *Frontiers in Microbiology*, 5(JULY).

Chapter 6: Conclusions and Future Directions

6.1 Introduction

The life cycle of *M. xanthus* features many self-organizing multicellular behaviors, including swarming, hunting, rippling, and fruiting body formation. Each of these is beneficial and improves the fitness of the *M. xanthus* swarm (Cao, Dey, Vassallo, & Wall, 2015). In this research, we focused on one of the most sophisticated and unique (for a bacterium) behaviors of *M. xanthus*: starvation induced development. The onset of starvation stress forces cells to completely switch gears to survive, from predatory spreading to defensive consolidation. This consolidation produces 3-dimensional fruiting bodies filled with spores. A preponderance of experimental data supports the idea that *M. xanthus* development is under genetic control, and the complexity of that control is evident in the stepwise changes in expression of hundreds of genes throughout the process. However, the developmental dynamics (*i.e.*, what happens to the cells within the swarm when the genetic rules are applied) are constrained by physical laws. It is entirely consistent, and perhaps somewhat obvious, to say that *M. xanthus* development is controlled both by genetics and physical laws.

Most of the existing aggregation models are built on the idea of contact-dependent signaling and cells changing after collisions. Any of the observed swarm characteristics, such as streams, slime trails, or cell alignments are considered essential; it is assumed that, without one or all of them, aggregation would not be possible. Perhaps these assumptions should be revisited. Studies have shown that, 2 h after the onset of starvation, A-signaling, (p)ppGpp accumulation, and C-signal expression increases after 6 h together with many other genes. Aggregates are first visible after approximately 7 h (Søgaard-Andersen, Slack, Kimsey, & Kaiser, 1996). However, many of the connections between these functional genetics, swarm characteristics, and self-organization are

correlative and the mechanisms that actually drive the cells to act and form multicellular patterns between 0 to 7h are not really known completely and still stay as a “black box”.

As development proceeds, aggregates continue to change, and each may have a different fate. This dynamic rearrangement from 7 h to around 18 h, when aggregates mature into fruiting bodies, could be considered a second and somewhat independent black box. The research presented in this thesis attempted to address some questions in each of these boxes; (i) whether all the prerequisites are really necessary for development, and (ii) what determines the fate of an aggregate.

Standard development assays for identifying the function of a given gene are based on broad analysis of development and usually result in little or no discernible phenotypic affect. However, development is a continuous dynamic process from the initiation of starvation to the formation of spore-filled fruiting bodies. Defining fruiting body formation and analyzing the role of a protein in that process is still a challenge in biological systems. In this thesis, we aimed to further address the relationship between genome and phenome and the breaking points of development that can improve our understanding of *M. xanthus* self-organization in the context of a single gene mutation.

6.2 A mechanism for early aggregation

We explored early development in *M. xanthus* by comparing aggregation and phase separation. These population behaviors are known as important processes for many living systems, such as the aggregation of mussels in coastal regions (Liu et al., 2013), the formation of membrane-less organelles in a cell (Alberti, 2017), and the aggregation of proteins *in vitro* or *in vivo* (Hyman, Weber, & Jülicher, 2014).

Phase separation is a concept in physics used to explain the transition from ‘out of thermodynamic equilibrium’ (each molecule consumes energy from the environment) to ‘thermodynamic equilibrium’ (no net energy or matter flow in the system). The separation of ingredients in vinaigrette salad dressing is a simple example of this phenomenon. Soon after the ingredients are mixed together, each ‘oil particle’ will start to align with other oil molecules and each ‘vinegar particle’ will start to align with other vinegar particles to reduce the free energy of the system. This leads the system toward a state of thermodynamic equilibrium which, when achieved, results in two distinct phases (*i.e.*, phase separation). After spotting cells on starvation agar, they first form a homogenous swarm (nonequilibrium), followed by the separation into dome-shaped aggregates that mature into fruiting bodies when they reach a stable, non-mobile state (equilibrium).

In order to test whether the early stage of aggregation is driven by phase separation, we conducted the experiments in Chapter 3: (i) changed the initial cell density, (ii) tracked individual cells for 11 h from onset of starvation to the time when aggregates become visible, (iii) modified the velocity of non-reversing mutant, and (iv) simulated aggregation by incorporating our empirical findings to an ABM.

We first showed that aggregation depends on cell density using time lapse microcinematography. At very low densities, no aggregates were observed regardless of time, whereas aggregates formed via nucleation and growth at medium cell densities as tiny spots that grow with time. At even higher cell densities, spontaneous emergence becomes clear over the entire field of view, which is similar to the spinodal decomposition process in passive systems. We then demonstrated that cells actively regulate their movement during aggregation. Starving cells have a constant velocity during the first 2 - 3 h, an accelerated velocity after 4 h, and a reduced reversal frequency at time periods over 11 h.

In passive systems, a phase separation diagram can be drawn based on density and temperature to predict the phase boundaries of the system. Since *M. xanthus* behaves as a self-propelled system, the inverse Péclet number is used instead of temperature. The dimensionless inverse Péclet number is defined as rotational diffusion coefficient and reversal frequency with respect to active motion. According to the definition, high speed and low reversal, along with longer directed movement, results in a low Péclet number. High density with a low Péclet number drives the system to phase separation, while high density with high Péclet number does not. To generate data points for an aggregation phase separation graph, we took advantage of a mutant strain of *frzE*, that does not regulate its movement during development. Since these cells do not actively regulate their speed, we chemically manipulated the sample to see if we could drag it into the phase separated region. A change in the velocity of *frzE* non-reversing mutant cells at the same density demonstrated that cells with a higher Péclet number (low velocity) failed to aggregate, while cells with lower Péclet number (higher speed) formed aggregates. This is a clear example where changing only the speed can cause aggregation to occur at a density at which it would otherwise be impossible.

Finally, using data-driven motility parameters, we modeled aggregation according to active Brownian particles, where each particle velocity is calculated based on self-propulsion and steric interactions. The direction of self-propulsion is updated stochastically according to a random torque of unit variance without including any complicated signaling mechanisms or slime trails. We showed that an increase in velocity and a decrease in reversal frequency are sufficient to drive self-organization in a density-dependent manner. These findings are consistent with the hypothesis that *M. xanthus* employs a dynamic process very similar to MIPS to achieve aggregation. A MIPS-based model of development is also consistent with the idea of coarsening.

Recently it has been shown that polymertropism (bacterial directional movement in response to the orientation of the polymers on agar surfaces) and the slime trails produced by individual cells play a role in the alignment of *M. xanthus* cells (Lemon, Yang, Srivastava, Luk, & Garza, 2017). There is limited data on the composition of slime, and studies to identify mutants which are defective in slime production and/or secretion have been inconclusive (Mauriello et al., 2010; Yu & Kaiser, 2007). Slime secretion and slime trail following were suggested to be important population behaviors during development based on observations and algorithmic models (Burchard, 1982; Holmes, Kalvala, & Whitworth, 2010; Lemon et al., 2017; Sozinova, Jiang, Kaiser, & Alber, 2005, 2006). Slime production is assumed to be essential to *M. xanthus* movement as it is observed during development and can also be observed during swarm expansion. Cells tend to follow slime trails in response to starvation rather than exploring the environment as they would in a nutrient rich environment (Thutupalli, Sun, Bunyak, Palaniappan, & Shaevitz, 2015). However, there is no evidence that slime secretion increases during development or that slime trail following is specific to development. Therefore, we suggest that slime trail following may not be required for self-organization of *M. xanthus*, but it may contribute the timing and final shape of aggregates.

6.3 A model to predict aggregate fate

After the initial aggregation phase, aggregates actively rearrange between 8h and 20h, as shown by Zhang et al. (Zhang et al., 2011). The random distribution of initial aggregates becomes ordered by the end of 24 h. During this rearrangement, about half of the aggregates persist and mature into fruiting bodies, while the other half disappear. Xie et al showed that only aggregates smaller than ~6000 μm disappear (Xie, Zhang, Shimkets, & Igoshin, 2011). In this study, we proposed a

mechanism to explain how the fate of aggregates is determined across the entire swarm, based on a model of Ostwald ripening in the liquid films. This is consistent with the MIPS model of initial aggregation, and also enables us to suggest testable hypotheses.

Ostwald ripening is a physical process that occurs during a phase separation in which smaller droplets of a condensing liquid shrink and larger droplets grow at the expenses of smaller ones to reach a thermodynamically stable state (Gratton & Shearer, 2008). 2-dimensional equations that describe Ostwald ripening are built on (i) current volume of a droplet, (ii) current volume of its neighbors, and (iii) relative distance to its neighbors. We generated 20 Wild-Type time-lapse movies and semi-automatically tracked each aggregate's size and position from the time when the number of the aggregates is the greatest to 24 h, which is the end of the movie. By incorporating the size and position of each aggregate into the simulation, and calculating the volume change based on the equations, we were not only able to predict which aggregates would disappear with average accuracy of 85%, but also when they would disappear.

We then tracked individual cells around growing and shrinking aggregates. The results showed that there are more cells moving toward a growing aggregate than moving away from it, and more cells moving away from a shrinking aggregate than moving towards it. This implies that smaller aggregates disappear because cells leave them and move to larger aggregates. Therefore, our result demonstrates that Ostwald ripening equations can predict aggregate fate with high accuracy, and that something similar to Ostwald ripening may be occurring during the later stages of aggregation.

Phenotypic analysis of approximately 400 single gene disruptions, which included four homologous gene families, revealed that phenotypic changes resulting from mutations can be grouped into nine different categories. Previously, members of two important gene families, ABC

Transporters and NtrC-like activators, had been studied for their role in fruiting body formation (Caberoy et al., 2003; Giglio et al., 2011; Giglio et al., 2010; Lancero et al., 2004; Sarwar & Garza, 2015; Yan, Bradley, Friedman, & Welch, 2014). In this study, we also discovered two other gene families that have important impact on fruiting body formation: ECF sigma factors and One-component regulators. We also discovered that some hypothetical genes that may play a role in the *M. xanthus* development process. Therefore, we concluded that ORFs with hypothetical or conserved hypothetical annotations, which make up 43.2% of the *M. xanthus* genome, might in fact be important for development.

The studies described in Chapters 3, 4 and 5 significantly improved our understanding of aggregation in 2-dimensions. There are still many questions that must be addressed, such as “how initial aggregation points are determined”; “how cells move within an aggregate to define its final shape”; “why and how aggregates in some mutant strains do not move or disappear at all, while in other mutant strains they move much more than Wild-Type”. Future work involving the tracking of individual Wild-Type and mutant cells that show deviations from Wild-Type aggregation would bring us a step closer to answering those questions.

In her review, Eva K. Paluch provides an important insight regarding the purpose of models in living systems. She states that “the aim of a model is not to describe the cell in all its complexity but to strike the appropriate level of simplification to use the power of mathematical formalism to make quantitative predictions” (Paluch, 2015). This holds true for the importance of the models we propose: while they do not yield a complete understanding of development in *M. xanthus*, their ability to predict some aspects of the system help us to begin to elucidate the underlying mechanisms. These approaches based on above mentioned models will be able to help to increase our understanding of both *M. xanthus* in particular, and biofilms in general.

6.4 Final conclusion

Models can provide perspective regarding how emergent behavior takes place on a multicellular level, as well as a framework to propose testable hypotheses. We proposed two models, one that examines the initiation of aggregation, and another that explores aggregate dynamics without complex signaling. These two models support one another in that the MIPS model in Chapter 3 can also be part of the Ostwald Ripening model in Chapter 4. We proposed a mechanism that not only explains initial aggregation as a phase separation, but also explains how these aggregates rearrange themselves. This yields a consistent picture of how fruiting body formation proceeds in *M. xanthus*. Biofilms are a critical field of study because they are interesting from a fundamental science perspective, and also pose a serious threat to human health and hygiene. Improving our understanding of biofilm dynamics may well have important future applications in medicine and beyond.

6.5 References

- Alberti, S. (2017). Phase separation in biology. *Current Biology*.
- Burchard, R. P. (1982). Trail following by gliding bacteria. *Journal of Bacteriology*, *152*(1), 495–501.
- Cao, P., Dey, A., Vassallo, C. N., & Wall, D. (2015). How Myxobacteria Cooperate. *Journal of Molecular Biology*.
- Gratton, M. B., & Shearer, M. (2008). Coarsening of Thin Fluid Films by by.
- Holmes, A. B., Kalvala, S., & Whitworth, D. E. (2010). Spatial Simulations of Myxobacterial Development, *6*(2).
- Hyman, A. A., Weber, C. A., & Jülicher, F. (2014). Liquid-Liquid Phase Separation in Biology. *Annual Review of Cell and Developmental Biology*.
- Lemon, D. J., Yang, X., Srivastava, P., Luk, Y.-Y., & Garza, A. G. (2017). Polymertropism of rod-shaped bacteria: movement along aligned polysaccharide fibers. *Scientific Reports*, *7*(1), 7643.
- Liu, Q. X., Doelman, A., Rottschäfer, V., de Jager, M., Herman, P. M., Rietkerk, M., & van de Koppel, J. (2013). Phase separation explains a new class of self-organized spatial patterns in ecological systems. *Proceedings of the National Academy of Sciences of the United States of America*, *110*(29), 11905–11910.
- Mauriello, E. M. F., Mignot, T., Yang, Z., & Zusman, D. R. (2010). Gliding Motility Revisited: How Do the Myxobacteria Move without Flagella? *Microbiology and Molecular Biology Reviews*, *74*(2), 229–249.
- Paluch, E. K. (2015). After the Greeting: Realizing the Potential of Physical Models in Cell Biology. *Trends in Cell Biology*.

- Søgaard-Andersen, L., Slack, F. J., Kimsey, H., & Kaiser, D. (1996). Intercellular C-signaling in *Myxococcus xanthus* involves a branched signal transduction pathway. *Genes and Development*, *10*(6), 740–754.
- Sozinova, O., Jiang, Y., Kaiser, D., & Alber, M. (2005). A three-dimensional model of myxobacterial aggregation by contact-mediated interactions. *Proceedings of the National Academy of Sciences of the United States of America*, *102*(32), 11308–11312.
- Sozinova, O., Jiang, Y., Kaiser, D., & Alber, M. (2006). A three-dimensional model of myxobacterial fruiting-body formation. *Proceedings of the National Academy of Sciences of the United States of America*, *103*(46), 17255–17259.
- Thutupalli, S., Sun, M., Bunyak, F., Palaniappan, K., & Shaeviz, J. W. (2015). Directional reversals enable *Myxococcus xanthus* cells to produce collective one-dimensional streams during fruiting-body formation. *Journal of the Royal Society Interface*, *12*(109).
- Xie, C., Zhang, H., Shimkets, L. J., & Igoshin, O. A. (2011). Statistical image analysis reveals features affecting fates of *Myxococcus xanthus* developmental aggregates. *Proceedings of the National Academy of Sciences*, *108*(14), 5915–5920.
- Yu, R., & Kaiser, D. (2007). Gliding motility and polarized slime secretion. *Molecular Microbiology*, *63*(2), 454–467.
- Zhang, H., Angus, S., Tran, M., Xie, C., Igoshin, O. A., & Welch, R. D. (2011). Quantifying aggregation dynamics during *Myxococcus xanthus* development. *Journal of Bacteriology*, *193*(19), 5164–5170.

VITA

NAME OF THE AUTHOR: Fatmagül Bahar

PLACE OF BIRTH: Akcaabat, Trabzon, Turkey

DATE OF BIRTH: October 15, 1984

UNDERGRADUATE SCHOOLS ATTENDED: Karadeniz Technical University, Turkey

DEGREES AWARDED:

Bachelor of Science in Biology, 2008, Karadeniz Technical University

MPhil in Biology, 2018, Syracuse University

AWARDS AND HONORS:

Syracuse University: Teaching Assistantship 2016-2018

Ministry of National Education, Republic of Turkey: Dissertation Fellowship 2012-2016

Ministry of National Education, Republic of Turkey: Master Fellowship 2010-2012

Ministry of National Education, Republic of Turkey: Language Fellowship 2009-2010

PUBLICATIONS:

Liu G, Patch A, **Bahar F**, Yllanes D, Thutupalli S, Marchette M C, Welch R D, and Shaevitz J, (2018) A self-driven phase transition drives *Myxococcus xanthus* fruiting body formation. *PLR (in press)*

Bradley M, Neu D, **Bahar F**, Welch R D, (2016) Inter-laboratory evolution of a model organism and its epistatic effects on mutagenesis screens. *Scientific Reports 6:38001*

Bahar F, Pratt-Szeliga P C, Angus S, Guo J, Welch R D (2014) Describing *Myxococcus xanthus* Aggregation Using Ostwald Ripening Equations for Thin Liquid Films. *Scientific Reports 4:6376*

Canakci S, Cevher Z, Bektas K, Tokgoz M, **Bahar F**, Kacagan M, Sal F, Belduz A O (2012) Cloning, purification and characterization of an alkali-stable endoxylanase from thermophilic *Geobacillus sp.* 7. *World Journal of Microbiology and Biotechnology 28(5):1981-8*